

UNCLASSIFIED

AD NUMBER

ADB019126

LIMITATION CHANGES

TO:

Approved for public release; distribution is unlimited.

FROM:

Distribution authorized to U.S. Gov't. agencies only; Test and Evaluation; MAY 1976. Other requests shall be referred to Air Force Flight Dynamics Laboratory, ATTN: AFFDL/FGL, Wright-Patterson AFB, OH 45433.

AUTHORITY

AFFDL ltr dtd 29 Dec 1978

THIS PAGE IS UNCLASSIFIED

THIS REPORT HAS BEEN DELIMITED
AND CLEARED FOR PUBLIC RELEASE
UNDER DOD DIRECTIVE 5200.20 AND
NO RESTRICTIONS ARE IMPOSED UPON
ITS USE AND DISCLOSURE.

DISTRIBUTION STATEMENT A

APPROVED FOR PUBLIC RELEASE;
DISTRIBUTION UNLIMITED.

✓

AFFDL-TR-76-122

2

H

AD B019126

BI-DIRECTIONAL MULTI-STATION COMMAND/INFORMATION BUS

IIT Research Institute
10 West 35th Street
Chicago, Illinois 60616

November 1976

FINAL REPORT APRIL 1975—MAY 1976

Distribution limited to U. S. Government agencies only;
Test and Evaluation, May 1976. Other requests for this
document must be referred to the Air Force Flight Dynamics
Laboratory/FGL Wright-Patterson AFB, Ohio 45433.

AU NO. _____
DDC FILE COPY

AIR FORCE FLIGHT DYNAMICS LABORATORY
AIR FORCE WRIGHT AERONAUTICAL LABORATORIES
Air Force Systems Command
Wright-Patterson Air Force Base, Ohio 45433

DDC
RECEIVED
JUN 30 1977
RECEIVED
NA

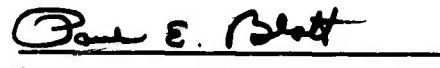
NOTICE

When Government drawings, specifications, or other data are used for any purpose other than in connection with a definitely related Government procurement operation, the United States Government thereby incurs no responsibility not any obligation whatsoever; and the fact that the government may have formulated, furnished, or in any way supplied the said drawings, specifications, or other data, is not to be regarded by implication or otherwise as in any manner licensing the holder or any other person or corporation, or conveying any rights or permission to manufacture, use, or sell any patented invention that may in any way be related thereto.

Copies of this report should not be returned, unless return is required by security considerations, contractual obligations, or notice on a specific document.

This technical report has been reviewed and is approved for publication.


Dong G. Kim
Project Engineer


PAUL E. BLATT
Chief
Control Systems Development Branch
Flight Control Division
AF Flight Dynamics Laboratory

UNCLASSIFIED

SECURITY CLASSIFICATION OF THIS PAGE (When Data Entered)

19 REPORT DOCUMENTATION PAGE		READ INSTRUCTIONS BEFORE COMPLETING FORM
18 REPORT NUMBER AFFDL-TR-76-122 ✓	2. GOVT ACCESSION NO.	3. RECIPIENT'S CATALOG NUMBER
6 4. TITLE (and Subtitle) BI-DIRECTIONAL MULTI-STATION COMMAND/INFORMATION BUS	9 5. TYPE OF REPORT & PERIOD COVERED Final Report, Apr 75 - May 76	8. PERFORMING ORG. REPORT NUMBER E6328
10 7. AUTHOR(s) Allan R. Kaurs, James E. Kietzer, Narayan P. Murarka	13 8. CONTRACT OR GRANT NUMBER(s) F33615-75-C-3100 New	10. PROGRAM ELEMENT, PROJECT, TASK AREA & WORK UNIT NUMBERS 19870256
9. PERFORMING ORGANIZATION NAME AND ADDRESS IIT Research Institute 10 West 35th Street Chicago, Illinois 60616	11 11. CONTROLLING OFFICE NAME AND ADDRESS Air Force Flight Dynamics Laboratory (FGL) Air Force Systems Command Wright-Patterson AFB, Ohio 45433	12. REPORT DATE November 1976
14 14. MONITORING AGENCY NAME & ADDRESS (if different from Controlling Office) 12 122p.	13. NUMBER OF PAGES 120	15. SECURITY CLASS. (of this report) Unclassified
16. DISTRIBUTION STATEMENT (of this Report) Distribution limited to U.S. Government agencies only; Test and Evaluation, May 1976. Other requests for this document must be referred to the Air Force Flight Dynamics Laboratory/FGL Wright-Patterson AFB, Ohio 45433.		
17. DISTRIBUTION STATEMENT (of the abstract entered in Block 20, if different from Report) 14 IITRI-FR-E6328 (16 1987 (
18. SUPPLEMENTARY NOTES 17 42		
19. KEY WORDS (Continue on reverse side if necessary and identify by block number) Data Bus, Dielectric Waveguide, Flight Control Signals, Frequency-Selective Coupler, Millimeter-Wave Integrated Image Line Technology (MILIC), Tunable Coupler, Tunable Filter, YF-16.		
20. ABSTRACT (Continue on reverse side if necessary and identify by block number) The suitability of dielectric waveguide as a transmission medium in data bus applications has been presented in this report. The feasibility of the concepts has been demonstrated through a Model 400 Dielectric Waveguide Data Bus System. The system operates at millimeter-wave fre- quencies (22 to 30 GHz) and has two frequency division multiplexed (FDM) data channels, each of which can carry data at rates of up to about 10 Mb/s. (continued...)		

DD FORM 1 JAN 73 1473 EDITION OF 1 NOV 65 IS OBSOLETE

UNCLASSIFIED
SECURITY CLASSIFICATION OF THIS PAGE (When Data Entered)

145350

YB

UNCLASSIFIED

SECURITY CLASSIFICATION OF THIS PAGE(When Data Entered)

The system demonstrates multi-channel bi-directional data transfer capabilities over a 100 ft dielectric cable.

In this report the design features and test results of a tunable bandpass ring coupler are also presented. These couplers are used in the Model 400 System for coupling signals to and from the data bus.

In addition to hardware demonstration of dielectric waveguide systems, their concepts have been used to obtain a data bus configuration for a specific aircraft. For this purpose, flight control signals of the YF-16 aircraft were chosen as an illustration. The data bus configuration for this aircraft has been presented in a block diagram form. It shows that the dielectric waveguide system can fully accommodate all the signal flow requirements.

Handwritten mark: *✓*

BY		
DISTRIBUTION/AVAILABILITY CODES		
N.S. AVAIL. CODE/SPECIAL		
B		

UNCLASSIFIED

SECURITY CLASSIFICATION OF THIS PAGE(When Data Entered)

FOREWORD

This is the Final Report for Contract F33615-75-C-3100, "Bi-Directional Multi-Station Command/Information Bus," performed for the Air Force Flight Dynamics Laboratory, Wright-Patterson AFB, Ohio, by IIT Research Institute, Chicago, Illinois.

Program participants included Allan R. Kaurs, James E. Kietzer, Narayan P. Murarka, B. J. Levin, and R. F. Heidelmeier. The program was monitored by Mr. Dong Kim of the Air Force Flight Dynamics Laboratory.

TABLE OF CONTENTS

<u>Section</u>	<u>Page</u>
I. INTRODUCTION	1
1. Background	1
2. Objectives	3
3. Scope of the Report	4
II. PART I - FREQUENCY SELECTIVE BANDPASS RING COUPLERS	7
1. Introduction	7
2. Theory and Experimental Data	7
a. Single-Pole Bandpass Filter Theory	7
b. Simulation Approach	17
c. Experimental Filter Data	18
3. Tunable Bandpass Ring Filter	24
a. Introduction	24
b. Ring Filter Tuning Considerations	24
c. An Experimental Tunable Bandpass Filter	29
4. Conclusions and Extensions	33
III. PART II - MODEL 400 DATA BUS SYSTEM	37
1. General System Description	37
2. Description of 23.5 GHz Channel	50
3. Description of 23 GHz Channel	53
4. Component Description	53
a. Oscillator Design	53
b. Mixer Design	58
c. IF/Video System	58
d. Data Bus Cable	61
e. MILIC Main Bus	64
5. Test Results	64
6. Conclusions and Extensions	69
IV. PART III - DATA BUS SYSTEM DESIGN APPLICABLE TO YF-16 FLIGHT CONTROL SIGNALS	71
1. Introduction	71
2. Dielectric Waveguide Data Bus Concepts	71
a. Generalized Block Diagram	71
b. Duplex Operation	74
c. Coupling Considerations	74
d. Interchannel Interference Considerations	81

TABLE OF CONTENTS (con't.)

<u>Section</u>	<u>Page</u>
3. YF-16 Data Bus System Configuration	83
a. Introduction	83
b. YF-16 Flight Control Signal Flow Requirements	83
c. YF-16 Data Bus Configuration	92
d. Redundancy Considerations	101
4. Conclusions	101
V. CONCLUSIONS AND RECOMMENDATIONS	103
APPENDIX --- Millimeter Image Line Integrated Circuits (MILIC) Technology	105
REFERENCES	119

LIST OF ILLUSTRATIONS

<u>Figure</u>	<u>Page</u>
1. Generalized Data Bus Architecture	2
2. Image Line Bandpass Directional Filter	8
3. Schematic Diagram of Single-Ring Directional Coupler	8
4. Typical Bandpass Ring Filter Response for a Loosely Coupled Ring	19
5. Three Experimental Fixed Tuned Bandpass Ring Filters	20
6. Bandpass Ring Filter Response for the Three Different Radii Rings	21
7. Bandpass Ring Filter Responses for Various Equal Coupling Gaps	23
8. Dispersion Characteristics of Insular Guide (TE_{11} Mode).	25
9. Free Space to Guide Wavelength Ratio Versus t/b	26
10. Ring Filter Configuration for Theoretical Analysis	27
11. The Effects of an Air Gap on a Bandpass Ring Filter	28
12. Cross Section of Tunable MILIC Bandpass Filter	30
13. K-Band Tunable MILIC Bandpass Filter	31
14. Insertion Loss and Tuning Characteristics of Experimental MILIC Filter	32
15. Theoretical and Experimental Center Frequencies for the Laboratory Prototype Filter	34
16. Double Ring Bandpass Coupler	35
17. Block Diagram of a Three Terminal Dielectric Waveguide Microwave Data Bus System	38
18. Rack Mounted MODEM Units	39
19. A Terminal of the Model 400 Data System	40
20. Model 400 Data Bus System Layout	42
21. Terminal No. 1 Top View	43
22. Terminal No. 2 Top View	44
23. Terminal No. 3 Top View	45

LIST OF ILLUSTRATIONS (con't.)

<u>Figure</u>	<u>Page</u>
24. Terminal No. 1 Bottom View	46
25. Terminal No. 2 Bottom View	47
26. Terminal No. 3 Bottom View	48
27a. Transmitter Module Block Diagram	49
27b. Receiver Module Block Diagram	49
28. Transmitter Module (23.5 GHz Channel)	51
29. Receiver Module (23.5 GHz Channel)	52
30. Direct Coupled Oscillator Cavity with Post Mounted Gunn Device	54
31. Tuning Curve for Typical 23 GHz Transmitter Oscillator (Measured)	56
32. Mechanical Tuning Curve for Typical 23 GHz Transmitter Oscillator (Measured)	57
33. Transmitter Schematic	59
34. Cross Section of K-Band Mixer Mount	60
35. Receiver Schematic	62
36. Construction of the Dielectric Waveguide Bus	63
37. Attenuation Characteristics of the Three Data Bus Cables	65
38. Insertion Loss of the MILIC Main Bus Inside the MODEMs	66
39. Input Data Waveforms	67
40. Output Data Waveforms	67
41. FDM Data Bus System Block Diagram	72
42a. Unidirectional Coupling Arrangement	75
42b. Bidirectional Coupling Arrangement	75
43. Power Distribution Along a Bus	76
44. Optimum Coupling Ratio	80
45. Adjacent Channel Interference Example	82
46. Flight Control System (YF-16)	84
47. YF-16 Flight Control Signals Flow Diagram	87
48. Data Bus Layout	93
49. YF-16 Data Bus System Design	95
50. YF-16 Data Bus System Design	99

LIST OF TABLES

<u>Table</u>	<u>Page</u>
1. Transmitter Oscillator Data	55
2. Signal Margin Test Results	68
3. Optimum Coupling Ratio	79
4. Insertion Loss for Couplers	79
5. Signal Flow Requirements	89
6. Signal Flow Requirements	90
7. Signal Characteristics	91

SECTION I

INTRODUCTION

1. Background

In many new airframes, there is a trend towards using multiplexing and data bus techniques for on-board information transfer between several subsystems. In such techniques, point-to-point wiring is replaced by a single transmission line which carries the information. To achieve this, both time division and frequency division multiplexing can be used. A generalized architecture of a data bus system is shown in Figure 1. In the figure, two Remote Terminals (RTs) and one Data Bus Controller are shown connected to the main bus. Additional RTs can be connected where necessary. The RT consists of a modulator/demodulator (MODEM) and a Multiplex Terminal Unit (MTU) which interfaces the subsystems and the data bus.

The MTU performs all necessary functions to make the subsystem data input/output compatible with the data bus operational mode. These functions might include A/D or D/A conversion, multiplexing, demultiplexing, signal conditioning, etc. The nature of the MODEM depends on the type of the transmission line itself. It basically converts the MTD input/output into data bus compatible signals. The Data Bus Controller performs the function of controlling signal flow between various RTs. Some concepts for bus control are given in MIL-STD-1553.

Over the last five years or so, major efforts have been underway at various DoD agencies regarding development and determination of the capabilities and limitations of several transmission lines for data bus applications. The following three types have emerged as potential candidates for future applications:

- Twisted Shielded Pair (TSP)
- Dielectric Waveguide (DWG)
- Fiber Optic Cable.

The twisted shielded pair operates at baseband frequencies and carries data at rates of up to about 2 Mb/s. The dielectric waveguide operates at microwave frequencies and offers large bandwidths on the order of a few GHz. The fiber optic cable operates at optical wavelengths and also offers large bandwidths. In choosing a transmission line for any given application, considerations have to be given not only to their bandwidth capabilities, but also to their immunity against EMP and lightning flash. These requirements are becoming increasingly important due to a trend towards use of low metallic content skins for outer shells of aircraft. Both dielectric waveguide and fiber optic cables can offer this immunity.

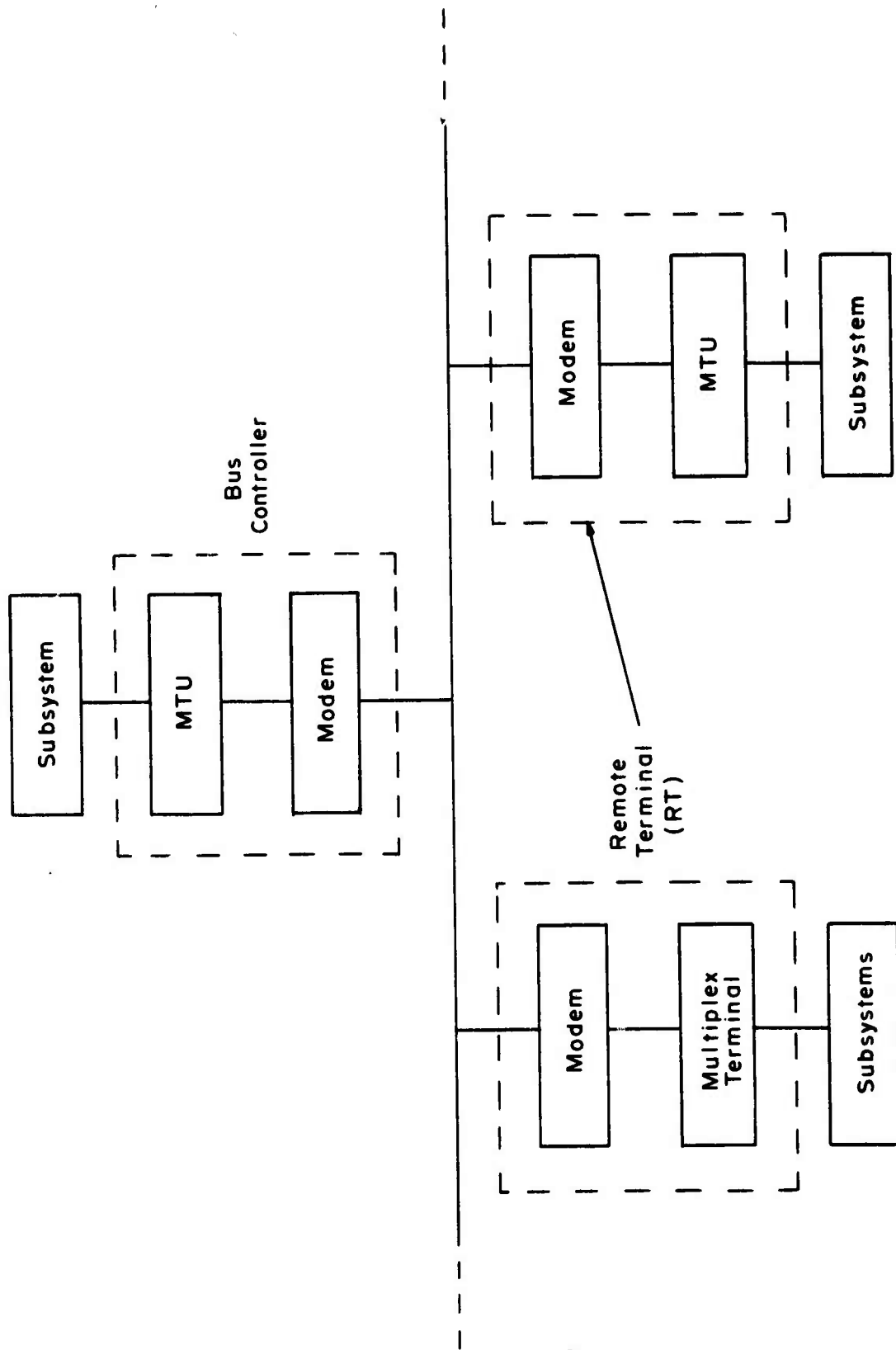


Fig. 1 GENERALIZED DATA BUS ARCHITECTURE

During the present program, dielectric waveguide has been pursued in an effort to improve the technology base in this area. Dielectric waveguides offer several advantages for data bus applications. They include:

- Immunity against EMP and lightning flash
- Immunity against internal electromagnetic interference (EMI)
- Ease of coupling signals in and out of the bus
- Availability of wide bandwidths
- Ease of simultaneous multichannel operation
- Suitability for simultaneous bi-directional signal flow on one cable.

The feasibility of using dielectric waveguide for data bus applications was demonstrated previously under Contract F33615-73-C-2063. A Model 400 Data Bus System was developed under that contract. The system consisted of three MODEM terminals and operated with one channel. Data transfer was achieved over 100 ft of dielectric waveguide. The MODEM terminals used Millimeter-wave Image Line Integrated Circuit (MILIC) technology. This technology was used due to its compatibility with dielectric waveguides. A brief description of the MILIC technology is presented in the Appendix.

2. Objectives

The objectives of the present program were threefold. First, it was desired that the previous Model 400 System be expanded to accommodate greater capacity. In order to increase the capacity, it was desired to employ frequency division multiplexing techniques which would permit non-interfering concurrent transmission of information among selected stations while employing common lengths of dielectric waveguide over portions of the communication path. This objective has resulted in incorporation of an additional Frequency Division Multiplexed (FDM) data channel. The expanded Model 400 System now has two data channels. During the course of this expansion, it was also the objective to improve the stability and reliability of the old channel in the Model 400 System. This was achieved by redesigning the MILIC components of the previous system and replacing them with new designs. In particular, all the old oscillators have been replaced with new oscillators of a new design developed under the present program. This effect has resulted in improved stability and reliability of both channels of the expanded Model 400 System.

In order to meet the first objective of incorporating an additional FDM channel into the Model 400 System, it was necessary to develop frequency selective tunable ring couplers. The second objective was to design and develop such couplers for eventual use with the Model 400 System. Such couplers, when incorporated into a data bus system for coupling signals to or extracting them from the bus, offer considerable advantages over wide-band couplers. In particular, the frequency selective coupler will extract signals from the bus only at that frequency to which it is tuned. Signals at other frequencies flowing through the bus will not be significantly affected. In other words, the insertion loss through such a coupler will be minimal. This feature is explained further in detail in Part III of this report. This is in sharp contrast to wide-band couplers which will extract signals out of the bus at all frequencies. Consequently, the insertion loss through the coupler will be significantly increased. The function of the frequency selective couplers can also be viewed by considering them as channel dropping filters, in that only signals at one frequency are taken out from the bus without significantly affecting other signals.

Finally, the third objective was to conduct a study to relate the development of the dielectric data bus concepts to a realistic example. For this purpose, the flight control signals of the YF-16 aircraft were examined in detail in order to come up with a possible data bus configuration fulfilling all its signal flow requirements. In particular, it was intended to examine the flight control system data/command flow requirements of the YF-16 through aircraft manuals and other available sources. The areas to be considered included:

- Control surface position, movement
- Engine status, operational change
- Altitude
- Attitude, including angles of attack, sideslip, yaw
- Aircraft motion/acceleration rate
- High data rate, e.g., TV.

The complete aircraft information flow scheme was to be presented in the form of an aircraft information flow model. This model was then to be used to obtain a dielectric data bus configuration using frequency selective couplers.

3. Scope of the Report

This report is divided into three major parts. In Part I, all the theoretical discussions and experimental results of the frequency selective bandpass ring couplers are presented. It also describes the design features of a tunable ring coupler,

invented under this program. The tunable coupler was eventually used in the Model 400 System. A detailed description of the expanded version of the Model 400 System is presented in Part II. It describes the system block diagram, two FDM data channels and design features of various elements of the system. In Part III, the results of the study program of the data bus configuration incorporating the YF-16 flight control signals are presented. The model of the signal flow requirements is presented both schematically and in tabular form. From this model, a possible data bus configuration is obtained. Finally, overall conclusions and extensions are presented.

SECTION II

PART I

FREQUENCY SELECTIVE BANDPASS RING COUPLERS

1. Introduction

Bandpass couplers in the Millimeter-wave Image Line Integrated Circuit (MILIC) technology have been successfully constructed at IITRI through the use of a resonant ring structure. These couplers consist of a ceramic ring which is proximity coupled to two dielectric waveguides which form the input and output lines of this four-port device. Furthermore, during this program a new design concept was developed and implemented whereby the frequency response of bandpass couplers can be mechanically tuned. This capability enhances the usefulness of such couplers, not only in data bus systems, but also other communication and radar systems.

As mentioned earlier, the primary purpose for developing ring couplers was to demonstrate their usefulness in data bus applications. It may be recalled that due to their channel dropping feature, such couplers cause minimal insertion loss of signals flowing on a data bus. Consequently, they are preferred over wide-band couplers.

In this section, an analysis of this device is presented along with supporting experimental data for both fixed frequency and tunable couplers. This device has actually been incorporated in the Model 400 Data Bus System as described in Part II. Due to the similarity of the characteristics of a coupler and a filter, these two terms are used interchangeably in the rest of this section.

2. Theory and Experimental Data

a. Single-Pole Bandpass Filter Theory

This section presents an analysis of a single-pole traveling-wave loop directional filter assuming that a pure traveling-wave exists on the loop (see Figure 2). This assumption enables calculation of such quantities as loaded Q_L and insertion loss in terms of the coupling coefficients of the directional couplers and the length and attenuation of the loop image guide. Specifically, the following assumptions are made:

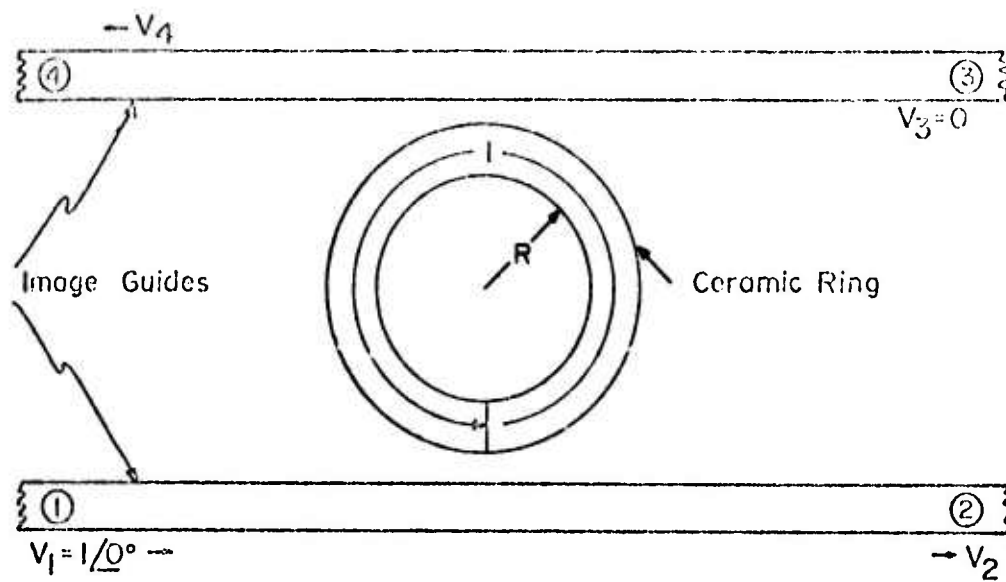


Fig. 2 IMAGE LINE, BANDPASS DIRECTIONAL FILTER

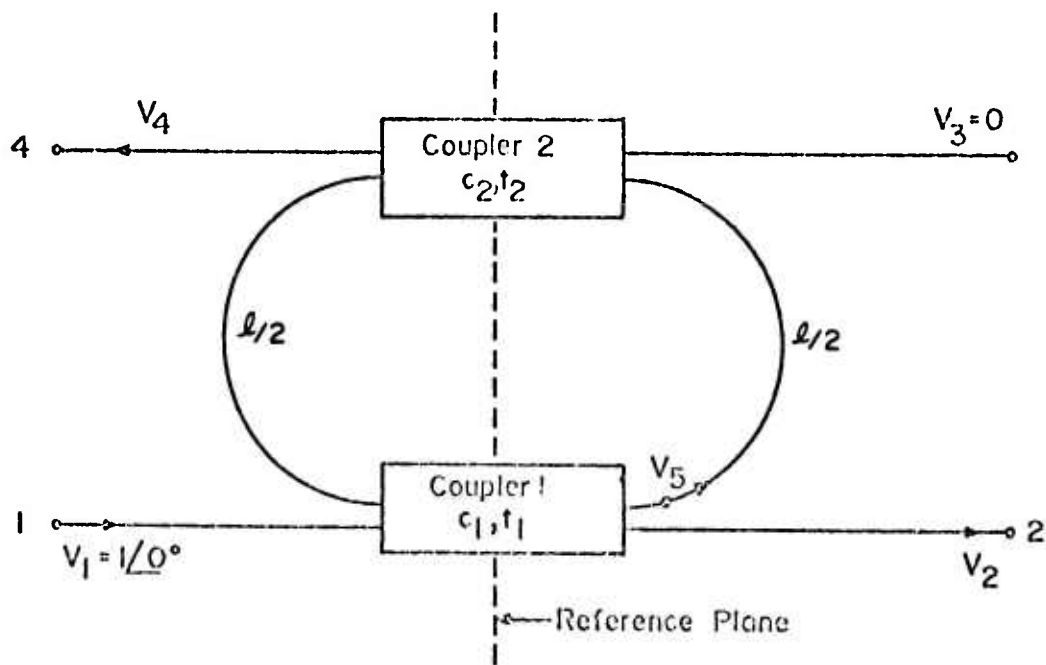


Fig. 3 SCHEMATIC DIAGRAM OF SINGLE-RING DIRECTIONAL COUPLER

- a) All image guides have identical characteristic impedances,
- b) Both directional couplers are perfectly matched and have infinite directivity, and
- c) No points of reflection exist in the loop and thus a pure traveling wave exists.

A schematic diagram of the filter is shown in Figure 3, where the voltages V_1 , V_2 , V_3 , and V_4 at its four ports are also marked. For convenience, the phases of the voltages shown at the terminals of the directional couplers are referred to the symmetrical planes of the couplers, whereas the voltage magnitudes apply at the coupler terminals. From Figure 3, it is seen that

$$V_5 = c_1 + V_5 t_1 t_2 e^{-\gamma \ell}$$

or

$$V_5 = \frac{c_1}{1 - t_1 t_2 e^{-\gamma \ell}} \quad (1)$$

Similarly,

$$V_2 = t_1 + c_1 t_2 V_5 e^{-\gamma \ell}$$

Substituting for V_5 from Equation (1), we obtain

$$V_2 = \frac{t_1 - t_2 e^{-\gamma \ell} (t_1^2 - c_1^2)}{1 - t_1 t_2 e^{-\gamma \ell}} \quad (2)$$

Also,

$$V_3 = 0$$

and

$$V_4 = c_2 V_5 e^{-\gamma \ell / 2}$$

Substituting for V_5 from Equation (1), we obtain

$$V_4 = \frac{c_1 c_2 e^{-\gamma \ell / 2}}{1 - t_1 t_2 e^{-\gamma \ell}} \quad (3)$$

where

c_1, t_1 = complex voltage coupling and transmission coefficients of coupler 1, respectively. These coefficients vary with distance between the main line and the ring.

c_2, t_2 = complex voltage coupling and transmission coefficients of coupler 2, respectively. These coefficients vary with distance between the main line and the ring.

γ = $\alpha + j\beta_g$, complex propagation constant in the ring

α = attenuation constant in the ring

β_g = $2\pi/\lambda_g$, phase constant

λ_g = guide wavelength in the ring

ℓ = mean ring circumference.

It is to be noted that for a loss-less coupler

$$|c_1|^2 + |t_1|^2 = 1 \quad (4a)$$

$$|c_2|^2 + |t_2|^2 = 1 \quad (4b)$$

Furthermore, for symmetrical couplers,

$$t_1 = t_2 = t$$

$$c_1 = c_2 = c$$

Therefore,

$$t^2 - c^2 = 1 \quad (5a)$$

$$\frac{c}{t} = \left| \frac{c}{t} \right| \angle -90^\circ. \quad (5b)$$

The condition for perfect rejection between ports 1 and 2 may be obtained by setting $|V_2| = 0$, which at resonance yields

$$e^{\alpha \ell} = \frac{|t_2|}{|t_1|} = \left\{ \frac{1 - |c_2|^2}{1 - |c_1|^2} \right\}^{\frac{1}{2}} \quad (6)$$

when

$$\ell = n\lambda_{g0} \quad (n = 1, 2, \dots)$$

$$\lambda_{g0} = \text{guide wavelength at } f_0.$$

Thus, for perfect rejection Equation (6) requires that

$$|c_2| < |c_1| \quad \text{for } \alpha > 0, \text{ or}$$

$$|c_2| = \sqrt{1 - (1 - |c_1|^2)e^{2\alpha \ell}} \quad (7)$$

The above condition should be applied if the filter is to be used as a band rejection filter. However, the condition for maximum output voltage, V_4 , for a given bandwidth, can be shown to be $c_1 = c_2 = c$. Thus, when attenuation of the ring is considered, the conditions are different for obtaining $|V_2| = 0$ and $|V_4| = \text{maximum}$. The conditions of equal coupling and thus maximum $|V_4|$ are to be employed when a low-insertion loss, bandpass response between ports 1 and 4 is required, or when the filter is to be used as a channel-dropping filter.

The resonant condition of the ring filter, given as $\ell = n\lambda_{g0}$ above, is only approximate, since the guide wavelength, λ_{g0} , of the uncoupled portion of the loop is different, in general, from that of the coupled portion. However, in most practical cases, the filter Q under loaded condition is rather high (i.e., $Q_L \geq 100$) resulting in a low voltage coupling coefficient (i.e., $|c| \ll 1$). As a result, the resonant wavelength would be nearly uniform all around the loop and $\ell = n\lambda_{g0}$ condition can be used.

The loaded Q_L of the filter may now be calculated under the conditions $c_1 = c_2 = c$ and $t_1 = t_2 = t$. At resonance, the output voltage is

$$V_4(f_0) = \frac{|c|^2 e^{-\alpha \ell / 2}}{1 - (1 - |c|^2)e^{-\alpha \ell}} \quad (8)$$

At a different frequency within the filter bandwidth which corresponds to an electrical length around the ring equal to $2\pi n + 0$, the output voltage is

$$V_4 = \frac{|c|^2 e^{-\alpha l/2}}{|1 - (1 - |c|^2)e^{-(\alpha l + j\theta)}|} \quad (9)$$

where it is assumed that, for narrow-band filters,

$$c(f) \approx c(f_0) \quad (10a)$$

$$\alpha(f) \approx \alpha(f_0). \quad (10b)$$

Define the filter loaded Q_L as

$$Q_L \equiv \frac{f_0}{\Delta f} = \frac{f_0}{2(f_2 - f_0)} = \frac{f_0}{2(f_0 - f_1)} \quad (11)$$

where

f_0 = frequency of resonance

Δf = filter 3 db bandwidth

f_2 = upper 3 db frequency

f_1 = lower 3 db frequency.

At the upper half-power point, f_2 or θ_2 , $|V_4|$ is obtained from Equation (9). The value of $|V_4|$ is also equal to $1/\sqrt{2} V_4(f_0)$ given in Equation (8). This equivalency is shown below.

$$\begin{aligned} |V_4| &= \frac{|c|^2 e^{-\alpha l/2}}{|1 - (1 - |c|^2)e^{-(\alpha l + j\theta_2)}|} \\ &= \frac{1}{\sqrt{2}} \frac{|c|^2 e^{-\alpha l/2}}{1 - (1 - |c|^2)e^{-\alpha l}} \end{aligned} \quad (12)$$

which yields

$$\cos \theta_2 = 1 - \frac{\{1 - (1 - |c|^2)e^{-\alpha l}\}^2}{2(1 - |c|^2)e^{-\alpha l}} \quad (13)$$

Since θ_2 is small for narrow-band filters, $\cos \theta_2$ may be replaced by

$$\cos \theta_2 \approx 1 - \frac{1}{2} \theta_2^2$$

and

$$\theta_2 \approx \frac{1 - (1 - |c|^2)e^{-\alpha\ell}}{(1 - |c|^2)^{\frac{1}{2}} e^{-\alpha\ell/2}} \quad (14)$$

but

$$\theta_2 = (\beta_{g2} - \beta_{g0})\ell$$

and therefore

$$(\beta_{g2} - \beta_{g0})\ell = \frac{1 - (1 - |c|^2)e^{-\alpha\ell}}{(1 - |c|^2)^{\frac{1}{2}} e^{-\alpha\ell/2}} \quad (15)$$

where

$$\beta_{g0} = \beta_g |_{f=f_0} = \frac{2\pi}{\lambda_{g0}}$$

$$\beta_{g2} = \beta_g |_{f=f_2} = \frac{2\pi}{\lambda_{g2}}$$

$$\lambda_{g0} = \lambda_g \text{ at } f_0$$

$$\lambda_{g2} = \lambda_g \text{ at } f_2.$$

In order to obtain an expression for Q_L in terms of $|c|$ and α , it would be necessary to relate $\Delta\beta_g$ of Equation (15) to the filter bandwidth, Δf or $\Delta\omega$. Thus, for narrow bandwidths,

$$\begin{aligned} \Delta\beta_g &= \frac{\beta_g(\omega_0 + \frac{\Delta\omega}{2}) - \beta_g(\omega_0)}{\Delta\omega/2} \cdot \frac{\Delta\omega}{2} \\ &\approx \frac{(\Delta\omega)}{2} \frac{d\beta_{g0}}{d\omega_0} \\ &\approx \frac{\beta_0}{2Q_L} \frac{d\beta_{g0}}{d\beta_0} \end{aligned} \quad (16)$$

where

$$\frac{d\beta_{g0}}{d\beta_0} = \left. \frac{d\beta_g}{d\beta} \right|_{\beta=\beta_0}$$

$$\beta_g = 2\pi/\lambda_g$$

$$\beta_0 = 2\pi/\lambda_0$$

$$\lambda_0 = \text{freespace wavelength at } f_0.$$

It can be shown that (see Reference 1):

$$\frac{d\beta_{g0}}{d\beta_0} = \lambda_0/\lambda_{g0} + B_0 M_0 \quad (17)$$

where

$$B_0 = \frac{4b}{\lambda} \sqrt{\epsilon_r - 1} \quad (\text{normalized height of image guide})$$

$$M_0 = \frac{d(\lambda_0/\lambda_{g0})}{dB_0} \quad (\text{slope of image guide dispersion curve for the } E_{11} \text{ mode at } B_0).$$

$$\epsilon_r = \text{dielectric constant.}$$

Combining Equations (15), (16), and (17) yields

$$\begin{aligned} Q_L &= \frac{\beta_0}{2\Delta\beta_g} (\lambda_0/\lambda_{g0} + M_0 B_0) \\ &= \left(\frac{\beta_0 \ell}{2} \right) \frac{(\lambda_0/\lambda_{g0} + M_0 B_0) (1 - |c|^2)^{\frac{1}{2}} e^{-\alpha\ell/2}}{1 - (1 - |c|^2) e^{-\alpha\ell}} \end{aligned} \quad (18)$$

where

$$\ell = n\lambda_{g0}.$$

It should be noted that this expression gives the true loaded Q_L of the resonator as it would be measured and takes into account the external loading due to both couplers combined with the losses in the transmission line of the ring.

For $|c| = 0$, Equation (18) gives the resonator unloaded Q_u as:

$$Q_u = \frac{(\beta_o \ell)}{4} \frac{\{\lambda_o / \lambda_{go} + M_o B_o\}}{\{\sinh(\alpha \ell / 2)\}} \quad (19)$$

In addition, for a low-loss ($\alpha \ell \ll 1$) ring resonator, Equation (18) and (19) may be further simplified as

$$Q_L = \left[\frac{\beta_o \ell}{2} \right] (\lambda_o / \lambda_{go} + M_o B_o) \frac{\{\sqrt{1 - |c|^2}\}}{\{\alpha \ell + |c|^2\}} \quad (20)$$

$$Q_u = \left[\frac{\beta_o}{2\alpha} \right] (\lambda_o / \lambda_{go} + M_o B_o) \quad (21)$$

for $\alpha \ell \ll 1$.

Considering now the case of weak coupling or narrow-band filters (i.e., $|c| \ll 1$), Equation (20) becomes

$$Q_L \approx \left[\frac{\beta_o}{2\alpha} \right] \frac{\{\lambda_o / \lambda_{go} + M_o B_o\}}{\{1 + |c|^2 / \alpha \ell\}} \quad (22)$$

$$(|c|^2 \ll 1)$$

and

$$\frac{Q_L}{Q_u} \approx \frac{1}{1 + |c|^2 / \alpha \ell} \quad (23)$$

$$(\alpha \ell \ll 1, |c|^2 \ll 1).$$

The insertion loss at resonance is given by

$$L = 20 \log_{10} |V_1 / V_2| \text{ db}$$

and since $V_1 = 1 / \underline{0^0}$, one has, from Equation (2):

$$L = 20 \log_{10} \frac{\{1 - (1 - |c|^2)e^{-\alpha l}\}}{|c|^2 e^{-\alpha l/2}} \quad (24a)$$

or

$$L \approx 20 \log_{10} \left(1 + \frac{\alpha l}{|c|^2} \right) \text{ db} \quad (24b)$$

for $\alpha l \ll 1$ and $|c|^2 \ll 1$.

Using Equation (23) in Equation (24) yields

$$L \approx 20 \log_{10} \frac{\{1\}}{\{1 - Q_L/Q_U\}} \quad (25)$$

Consider the following example:

$$2a = 0.200 \text{ in.}$$

$$b = 0.100 \text{ in.}$$

$$R/2a = 3.815$$

$$\epsilon_r = 9.8$$

$$f_o = 13.874 \text{ GHz}$$

$$\alpha = 0.027 \text{ np/in.}$$

$$l = 4.794 \text{ in.}$$

$$|c| = 6.71 \times 10^{-2} \text{ at } f_o.$$

For this example,

$$Q_L/Q_U = 0.6586$$

and from Equation (25):

$$L = 9.33 \text{ db}$$

whereas the exact expression, Equation (24a), gives

$$L = 9.15 \text{ db}$$

indicating that Equation (25) is accurate for low-loss rings and weak coupling.

Measurements performed on the above Ku-band ring filter have shown the following results:

$$f_o = 13.896 \text{ GHz}$$

$$Q_L = 397$$

compared with

$$f_o = 13.974 \text{ GHz}$$

$$Q_L = 408$$

calculated on the basis of the above theory. Thus, considering the close correlation between theory and experiment, it should be possible to accurately design single-ring channel dropping filters to given specifications.

b. Simulation Approach

The simulation model has been shown in Figure 3. In order to calculate the bandpass response of a ring filter it is necessary to evaluate the expression obtained from Equation (3) by substituting $c_1 = c_2 = c$ and $t_1 = t_2 = t$.

$$V_4 = \frac{c^2 e^{-\frac{(\alpha + j\beta_g)\ell}{2}}}{1 - t^2 e^{-(\alpha + j\beta_g)\ell}} \quad (26)$$

This requires the calculation of the complex voltage coupling and transmission coefficients of the two directional couplers shown in Figure 3. Since we are interested in the maximum bandpass response, this requires the two couplers to be identical so that $c_1 = c_2 = c$. The basic theory for calculation of the coupling and transmission parameters for parallel coupled dielectric image lines can be found in Reference [1]. In order to model the curved sections of the ring, a piecewise-linear approach was taken using small stepped sections of parallel coupled lines. A superposition of the parameters was then performed to obtain composite coupling, transmission, and phase terms. The end result was a means of calculating the theoretical filter response given the physical parameters of the ring. It is this simulation approach which was used to calculate resonant frequencies for various ring structures which are described in later sections.

c. Experimental Filter Data

An experimental effort was conducted to evaluate the performance of various ring filter structures. The main purpose of this work was to determine the effects of the various physical parameters, and aid in the proper choice of a ring filter for the data bus application. A fixture was fabricated which permitted the testing of various size rings with different coupling gaps.

The ring test plate is a three port device consisting of three K-band waveguide-to-dielectric image guide launchers. Two of the launchers are connected to a straight section of dielectric line forming the main line of the device. The coupled part launcher is fed by a dielectric line which is at a slight angle to the main one. The angle on the coupled part line permits the positioning of rings with various coupling gaps on the input and output sides of the filter structure.

A typical bandpass ring response for a loosely coupled ring is shown in Figure 4. This ring has a cross section of 0.106×0.106 in. and an outer radius of 0.339 in. The coupling gap was set at 0.106 in. which implies loose coupling. The general characteristics of a bandpass ring filter are demonstrated in Figure 4, and are stated as follows:

- Multiple bandpass responses occur at frequencies where the circumference is approximately $n\lambda g$.
- Coupling decreases as frequency increases.

Ring filters with three different size radii were fabricated from Custom Materials 707-L plastic with a dielectric constant of $\epsilon_r = 9.8$. These rings were designed to be compatible with the existing data bus dielectric waveguide lines, i.e., they have the 0.010 in. air gap beneath and 0.106×0.106 in. overall cross sections. A drawing of these rings is shown in Figure 5. The following experimental data will be presented to demonstrate the bandpass response obtainable as a function of the ring radius and coupling gap. Only equal coupling gaps ($c = c_1 = c_2$) on the input and output sides of the ring will be considered since this was the condition stated for the maximum bandpass response.

Typical K-band responses for the three rings of different radius are shown in Figure 6. Both of the coupling gaps were set at 0.040 in. for all of the cases shown. The ring radius is therefore a means for varying the position of the bandpass

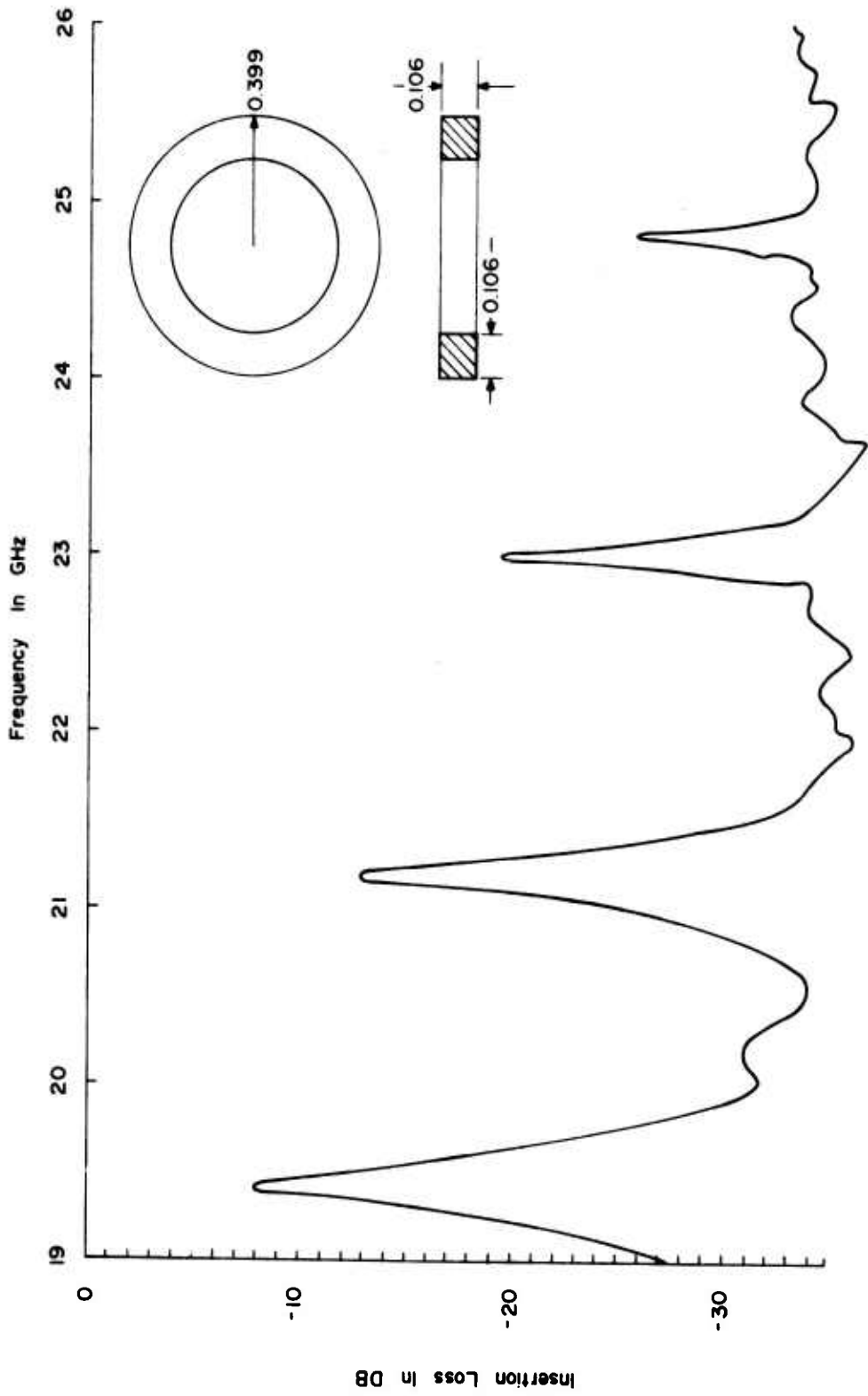
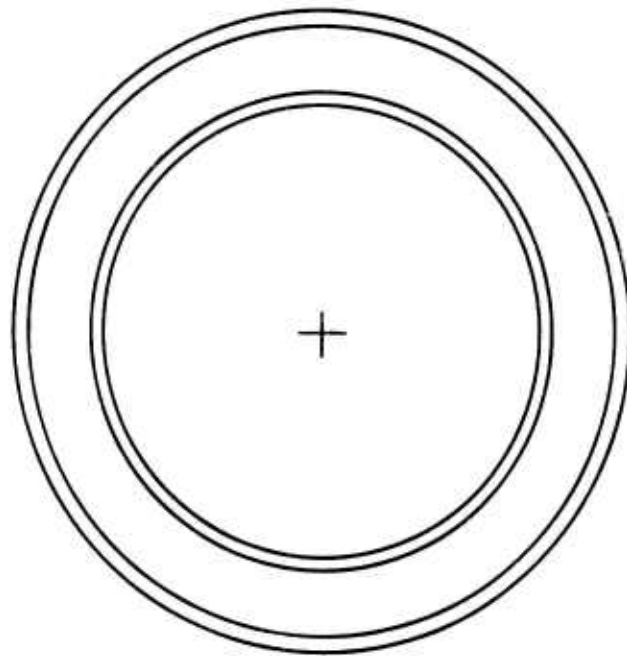
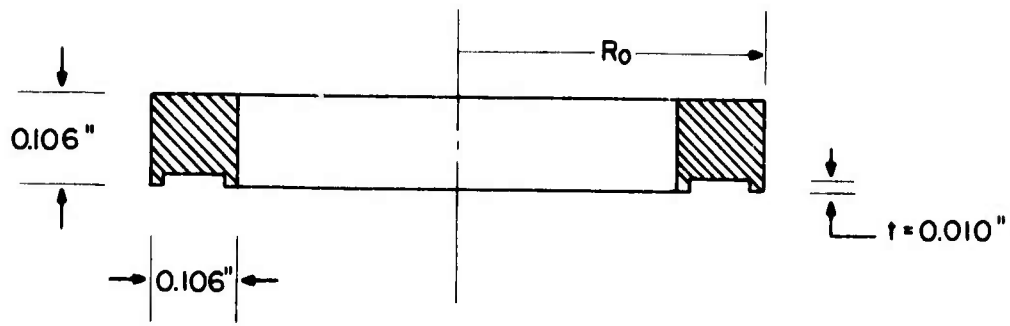


Fig. 4 TYPICAL BANDPASS RING FILTER RESPONSE FOR A LOOSELY COUPLED RING



RING	R_0 Inches
Small	0.308
Medium	0.339
Large	0.363

Fig. 5 THREE EXPERIMENTAL FIXED TUNED BAND PASS RING FILTERS

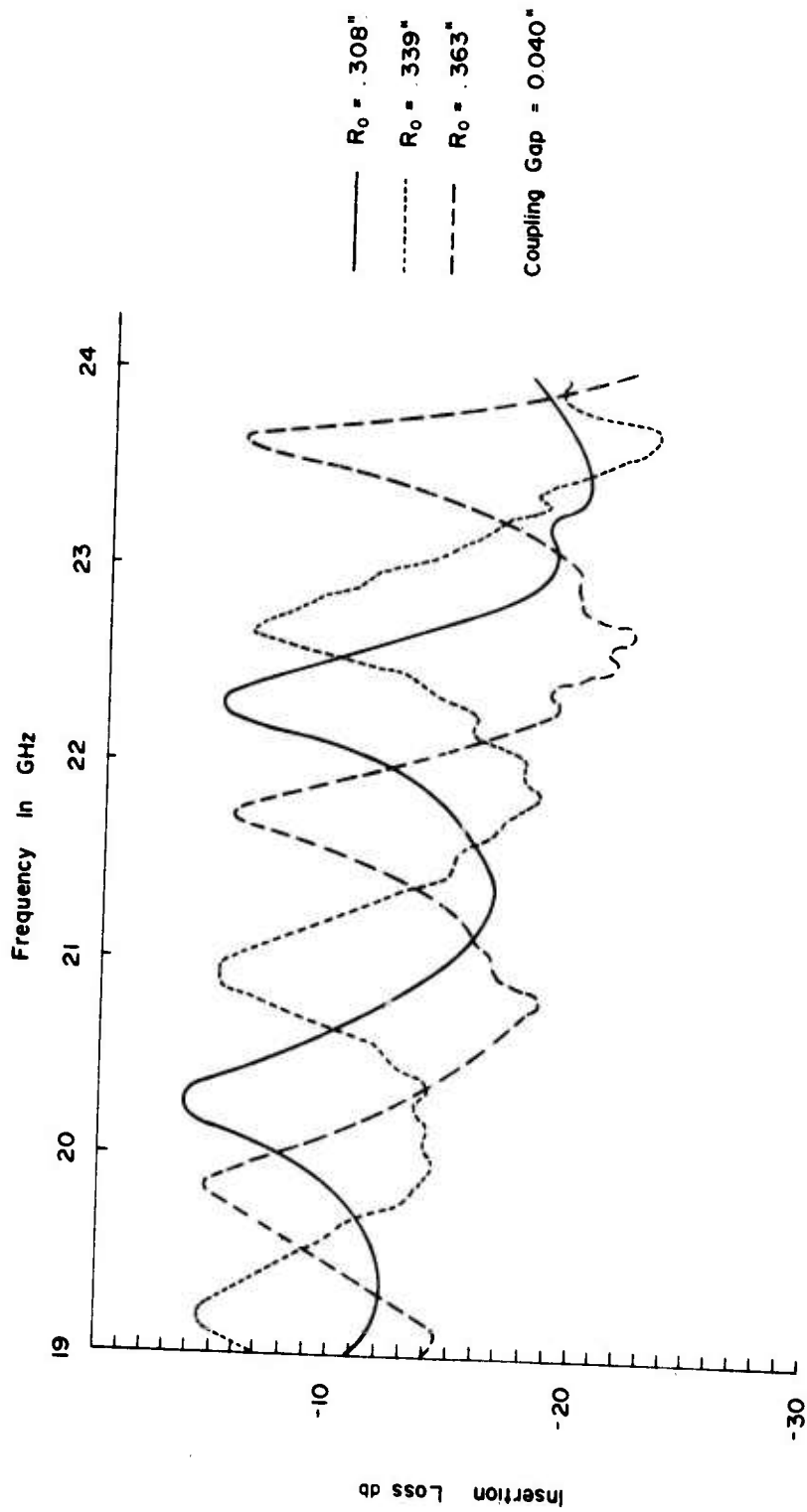


Fig. 6 BANDPASS RING FILTER RESPONSE FOR THE THREE DIFFERENT RADII RINGS

response in the frequency domain. As the radius of curvature of the ring is decreased, radiation losses due to the excess bending increase. It has been previously determined (in Reference [1]) that a practical minimum normalized circuit bend (R_0 /guide width) is on the order of three. Smaller bends will operate as a filter, but with increased radiation loss.

The effects of changing the coupling gap between the ring structure and the feed lines is demonstrated in Figure 7. The experimental data was taken for equal coupling gaps on both sides of the ring. The radius of the ring was 0.363 in., and coupling gaps of 0.025, 0.050, and 0.070 in. were used. An increase in the coupling gap caused increased insertion loss and decreased the loading of the ring. The loaded Q of the filter increased as the coupling was decreased. One other effect of varying the coupling gap is a downward shifting of the center frequency of the responses as the gap is increased. This change in center frequency can be attributed to the change in the dispersion characteristics of the coupled sections of the ring.

To summarize, the ring filter is a multiple resonant structure which can be used to transfer a maximum possible microwave signal between dielectric waveguide lines at discrete frequencies. This multiple resonant effect may be viewed as a disadvantage, therefore a method for eliminating some of the spurious responses will be presented in a later section.

The use of this filter as an in-line bandpass device required maximum signal transmission with minimum loss. This requires tighter coupling between the ring and feed lines for a specific frequency in order to minimize coupling losses. Also, low-loss dielectric material such as alumina is required for the construction of an optimal device. The radius of curvature of the ring must be kept large enough so that energy is not lost through radiation.

The ring filter can also be used as a sampling device to couple discrete signals from a main bus line. In this case, the amount of coupling necessary is governed by the amount of loading that can be tolerated on the main line and sensitivity of any detection devices connected to the coupled part of the filter. The design in this case is dependent on the application.

The frequency response of the ring filter has been shown to be a function of various parameters. In the following section this dependence will be investigated further and a means of controlling the response discussed.

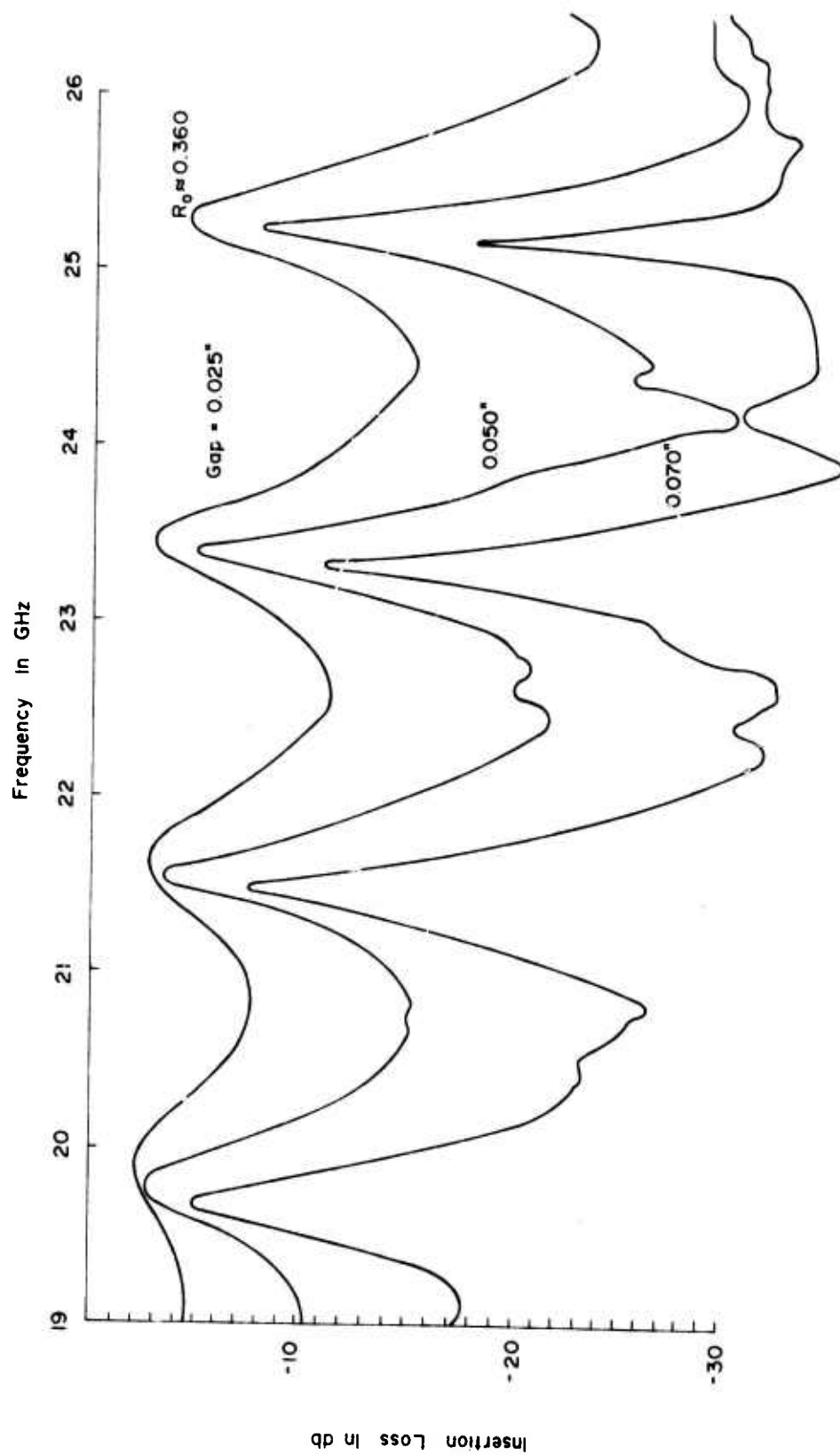


Fig. 7 BANDPASS RING FILTER RESPONSES FOR VARIOUS EQUAL COUPLING GAPS

3. Tunable Bandpass Ring Filter

a. Introduction

In a previous section it was stated that the ring filter has a resonant frequency response when its length is some $n\lambda$ ($n = 1, 2, 3, \dots$). This condition was said to be approximate because the guide wavelength in the ring filter is different in the coupled and uncoupled portions of the filter. The guide wavelength around the ring is therefore a function of position along the ring. If a method existed for controlling or changing the effective guide wavelength around the ring, the frequency response of the filter could also be changed.

b. Ring Filter Tuning Considerations

It is known that the dispersion characteristics of insulated image guide (insulator guide) are a function of the thickness of the low permittivity dielectric layer used to suspend the high dielectric constant waveguide off the metal ground plane. The theoretical dispersion characteristics for a V-band insular waveguide dominant E_{r1}^y mode are shown in Figure 8 for various t/b ratios [2]. Figure 8 clearly shows the variations in dispersion curves that occur for a fixed waveguide structure as the dielectric substrate varies in thickness. To demonstrate this dependence more clearly, Figure 9 shows an example in which the frequency is held constant at 60 GHz, and the ratio λ/λ_g is plotted as a function of t/b . From Figure 9 it is seen that there may be significant variation in the guide wavelength on the thickness of the substrate layer for a fixed waveguide height, b , that is proposed for tuning of the ring filter.

To demonstrate the feasibility of tuning a ring filter by varying the gap beneath the ring, a computer simulation was performed for a filter at K-band. The resonant frequency responses of a ring filter in the bandpass configuration were calculated as the gap beneath the ring was increased from 0.010 in. to 0.080 in.

The dielectric or insular layer in this simulated filter was assumed to be an air gap, therefore $\epsilon_{rg} = 1.0$. The theoretical ring filter used in this K-band simulation is shown in Figure 10. The simulation was accomplished using a computer program combining the ring filter analysis and insulated image guide analysis.

The results of the simulation are summarized in Figure 11. From the frequency versus gap curve, it is seen that the resonant frequency changes as the gap beneath the ring changes, with the greatest variation being seen for small values of the gap. The second curve in Figure 11 is a plot of λ/λ_g versus

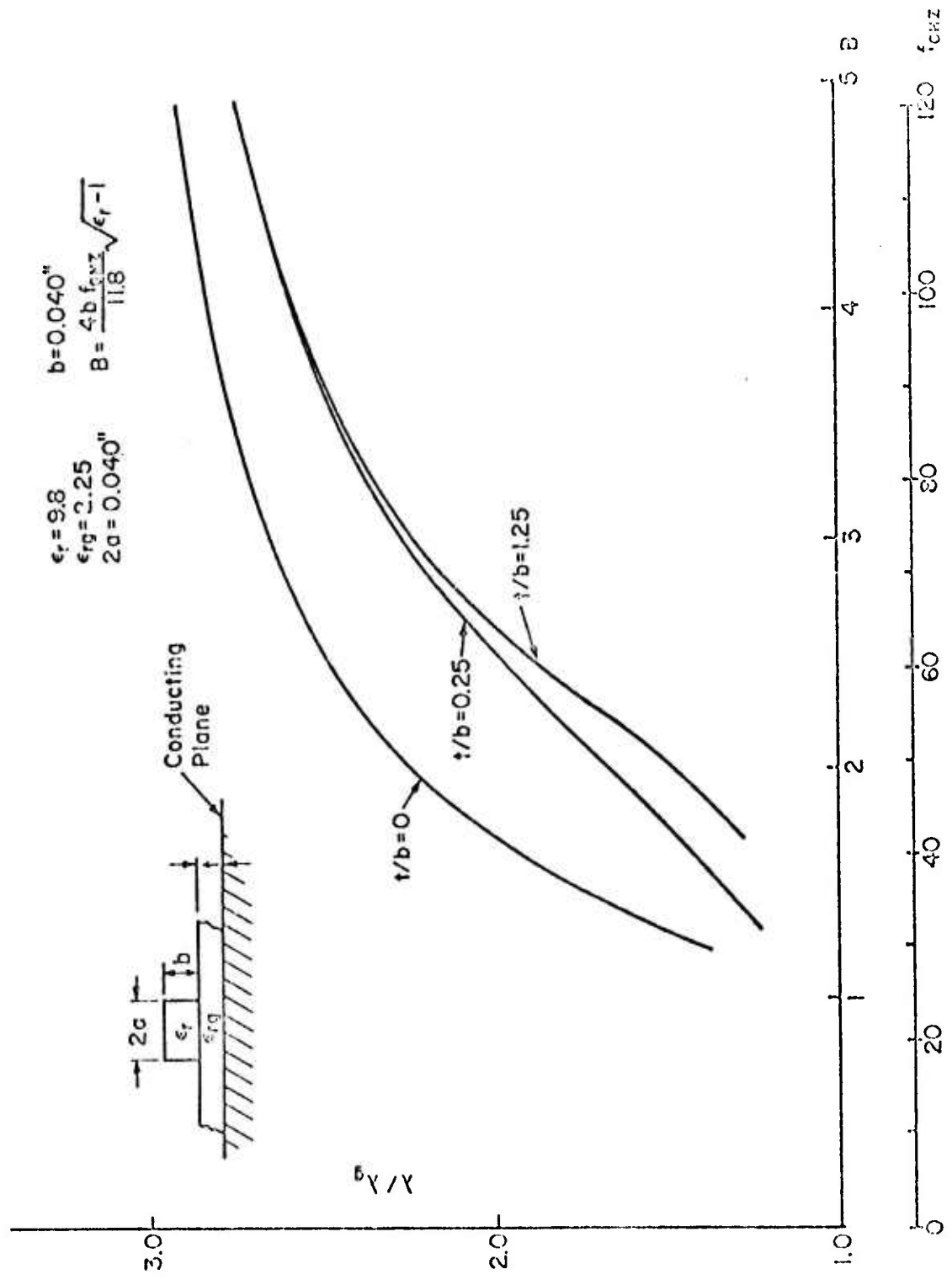


Fig. 8 DISPERSION CHARACTERISTICS OF INSULAR GUIDE (TE₁₀ MODE)

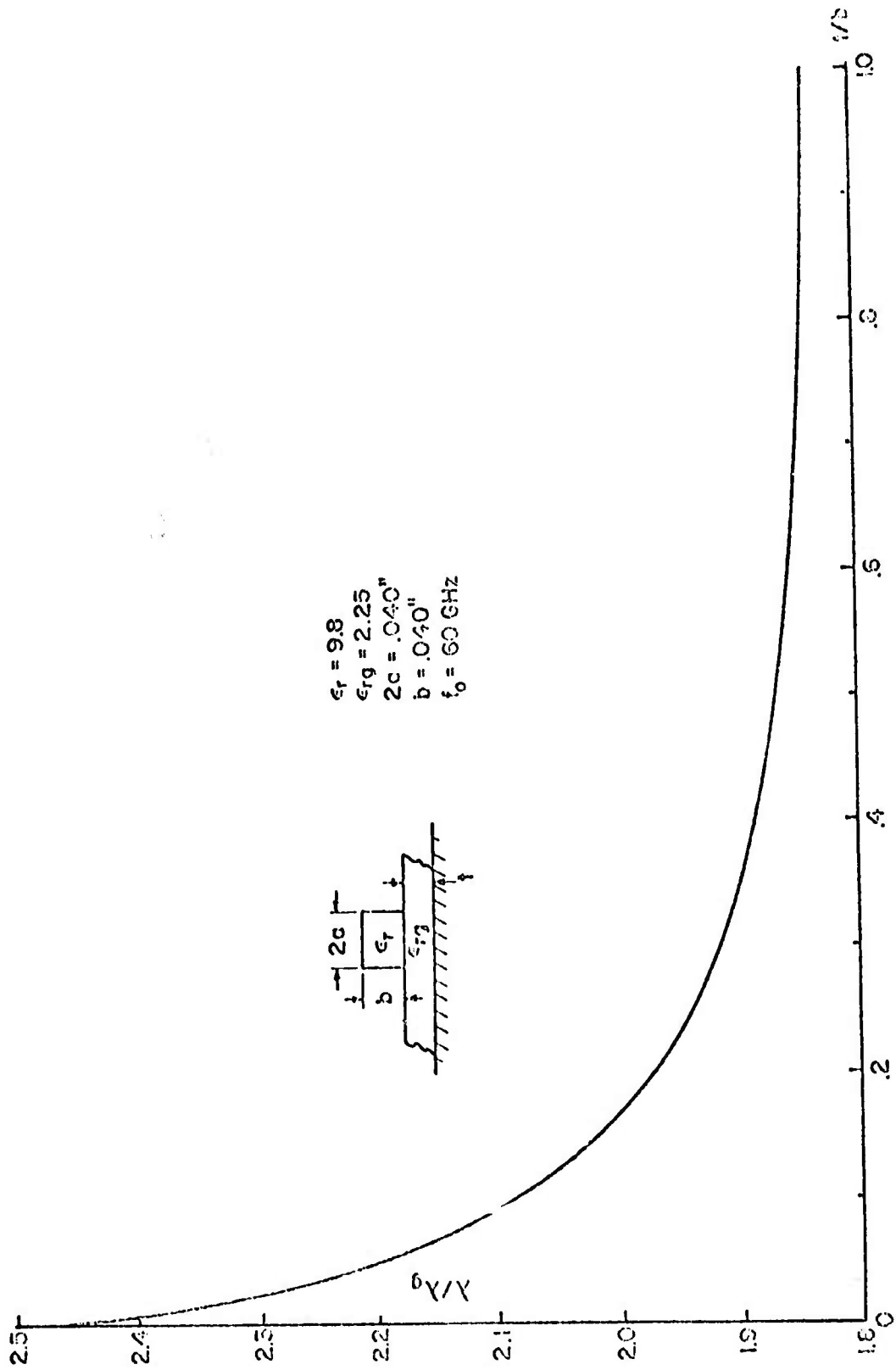


Fig. 9 FREE SPACE TO GUIDE WAVELENGTH RATIO VERSUS λ/b

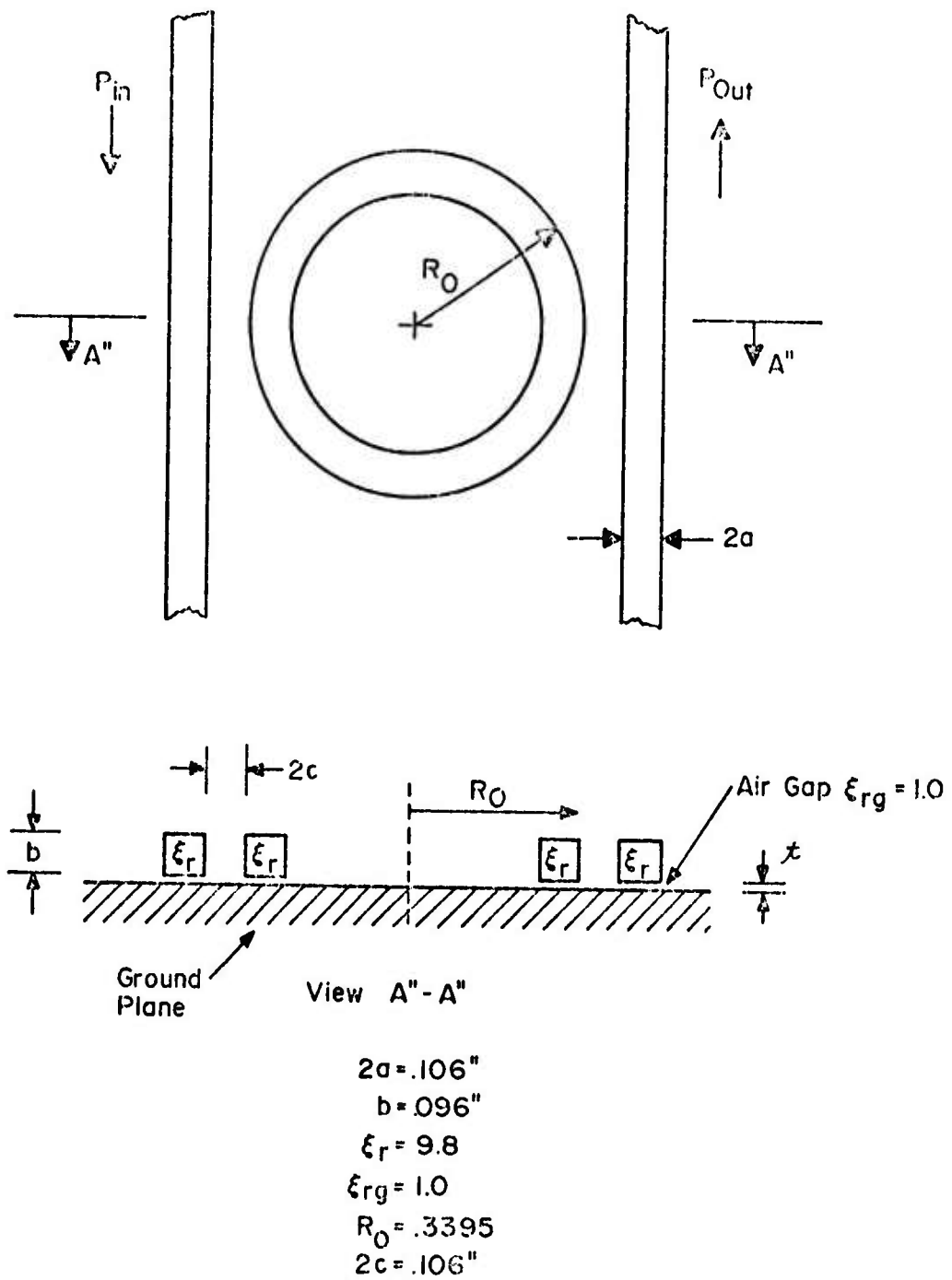


Fig. 10 RING FILTER CONFIGURATION FOR THEORETICAL ANALYSIS

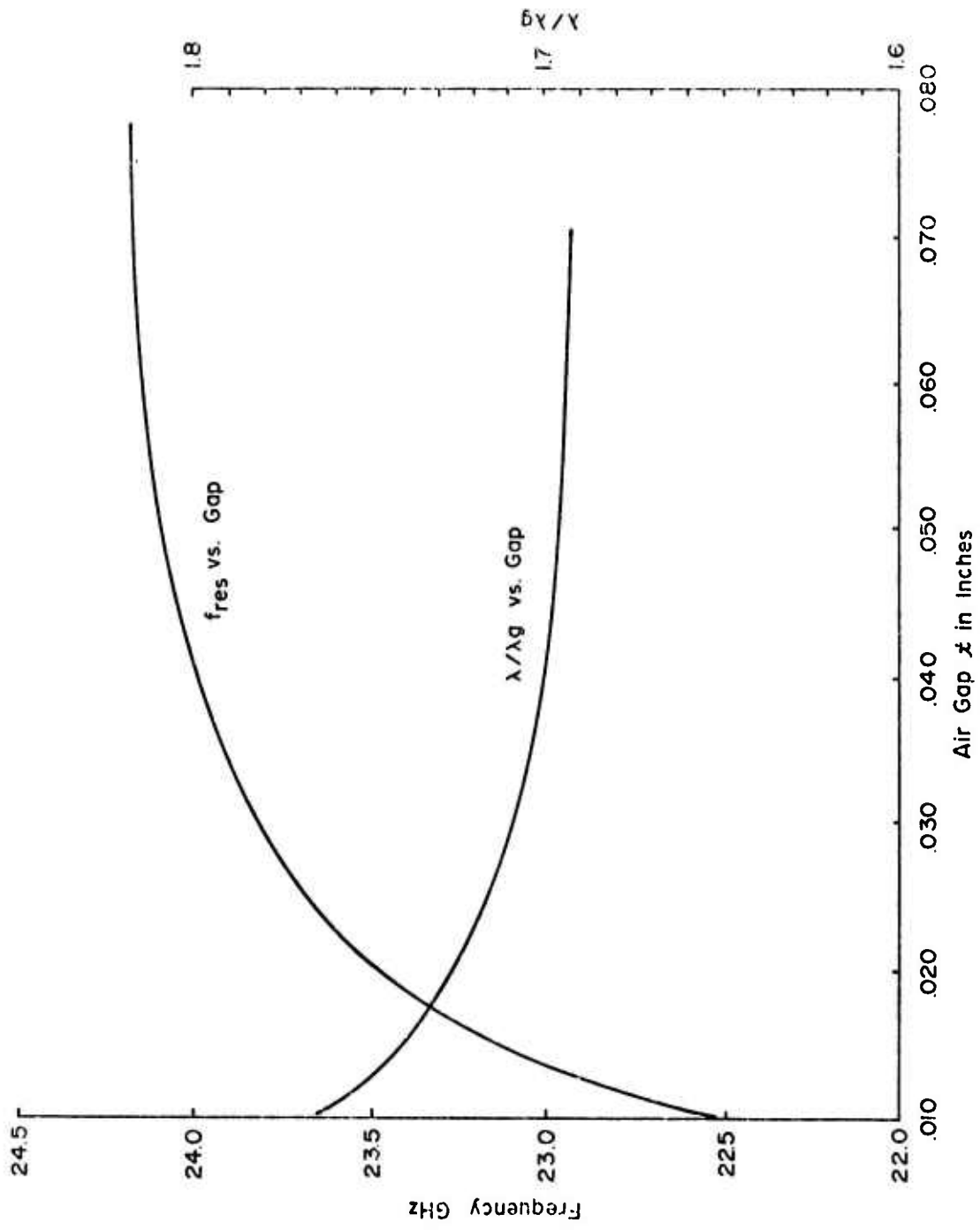


Fig. 11 THE EFFECTS OF AN AIR GAP ON A BANDPASS RING FILTER

gap for an uncoupled section of image guide with the same cross section as the ring. A comparison of the two curves of Figure 11 shows that as the guide wavelength becomes less sensitive to the gap effect, the change in the resonant frequency of the ring also becomes less sensitive.

Figure 11 demonstrates the theoretical feasibility of tuning a ring by varying the air gap beneath it. In the following section, an actual device which implements this tuning procedure is described.

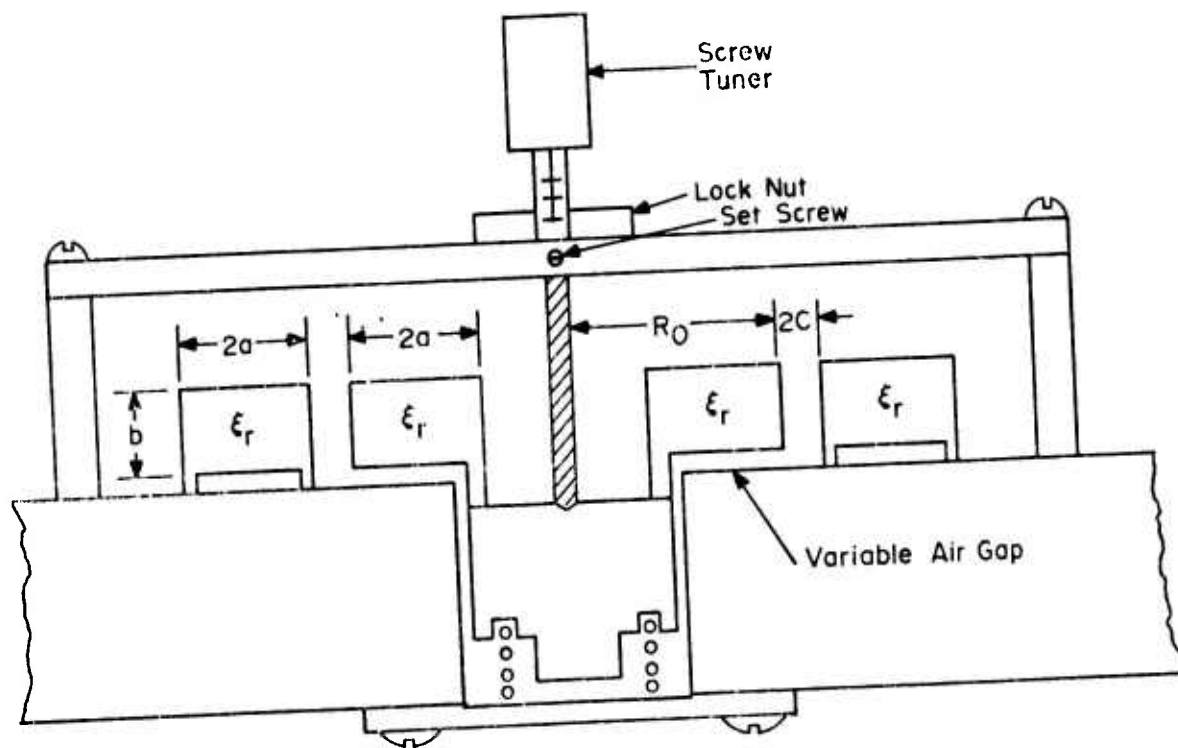
c. An Experimental Tunable Bandpass Filter

An experimental tunable bandpass filter was constructed for K-band operations. The tunable filter consists of a dielectric ring mounted in a bandpass configuration between two sections of dielectric waveguide which form the input and output feed lines. The ring structure rides on a piston which is spring-loaded and mounted in the metal baseplate. A tuning screw is mounted above the ring, and used to control the piston movement and, in turn, the gap between the ring and baseplate. A cross section sketch of the device is shown in Figure 12.

Figure 13 is a photograph of the experimental K-band filter mounted on a test plate. The dielectric ring is seen in the center of the test plate with the micrometer tuning screw mounted above it. Three of the output ports of the device are fed into standard metal waveguide-to-dielectric image guide launchers for the connection of test equipment. The fourth port is terminated with a ferrite load.

The material used for the dielectric guides and ring structure was Custom Materials High-K 707L plastic with a dielectric constant of $\epsilon_r = 9.8$. This material has a higher loss tangent than alumina ceramic, but is much easier to machine and work with for laboratory prototypes.

The tunable filter shown in Figure 13 was continuously tunable over a 3 GHz range as the air gap was increased from 0.0 to 0.022 in. The 0.0 in. gap is only approximate, since the tuning mechanism did not enable the complete elimination of all the air gap beneath the ring. Although the response could be easily tuned over the 3 GHz range, the useful tuning range due to increased insertion loss at larger gaps was about 2 GHz. This increase in insertion loss is attributed to the fact that as the gap is increased there is a decoupling of the ring from the fringe fields of the feed line. The tuning characteristics of a single resonant response for the experimental filter are presented in Figure 14.



$2a = .106''$
 $b = .096''$
 $R_0 = .3395''$
 $2c = .053$
 $\epsilon_r = 9.8''$

Fig. 12 CROSS SECTION OF TUNABLE MILIC BAND PASS FILTER

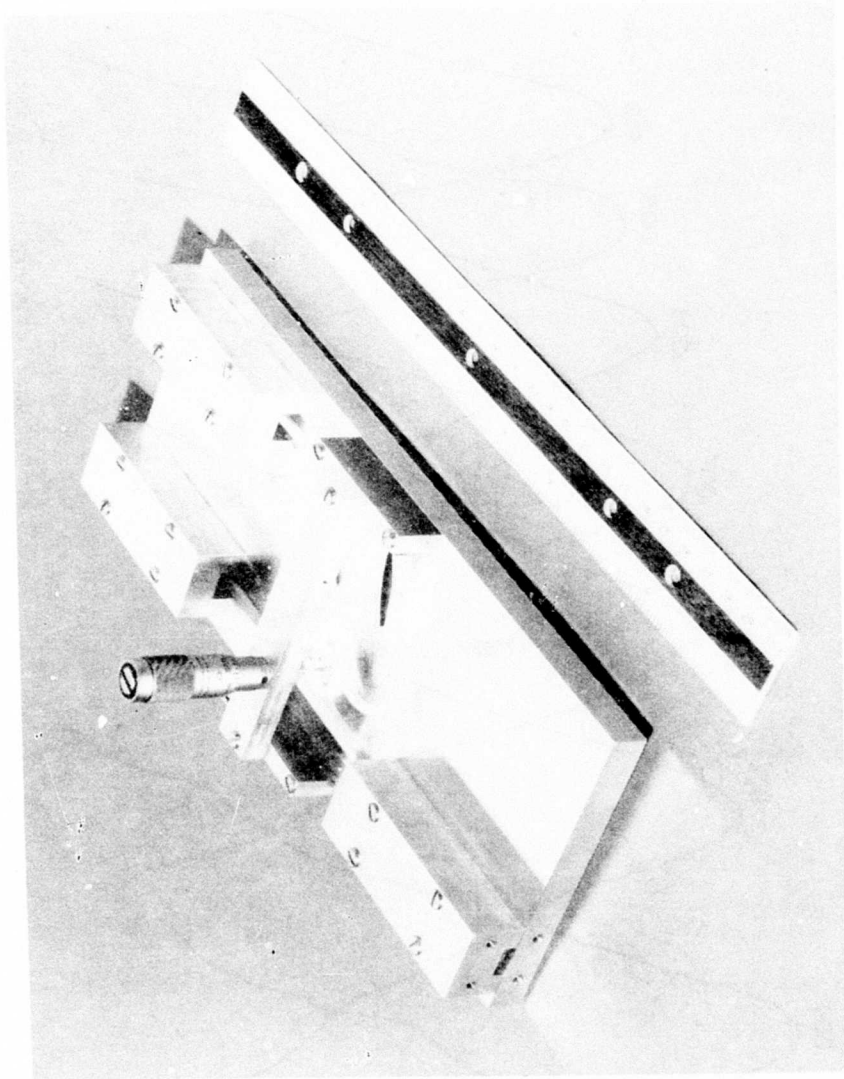


Fig. 13 K-BAND TUNABLE MILIC BANDPASS FILTER

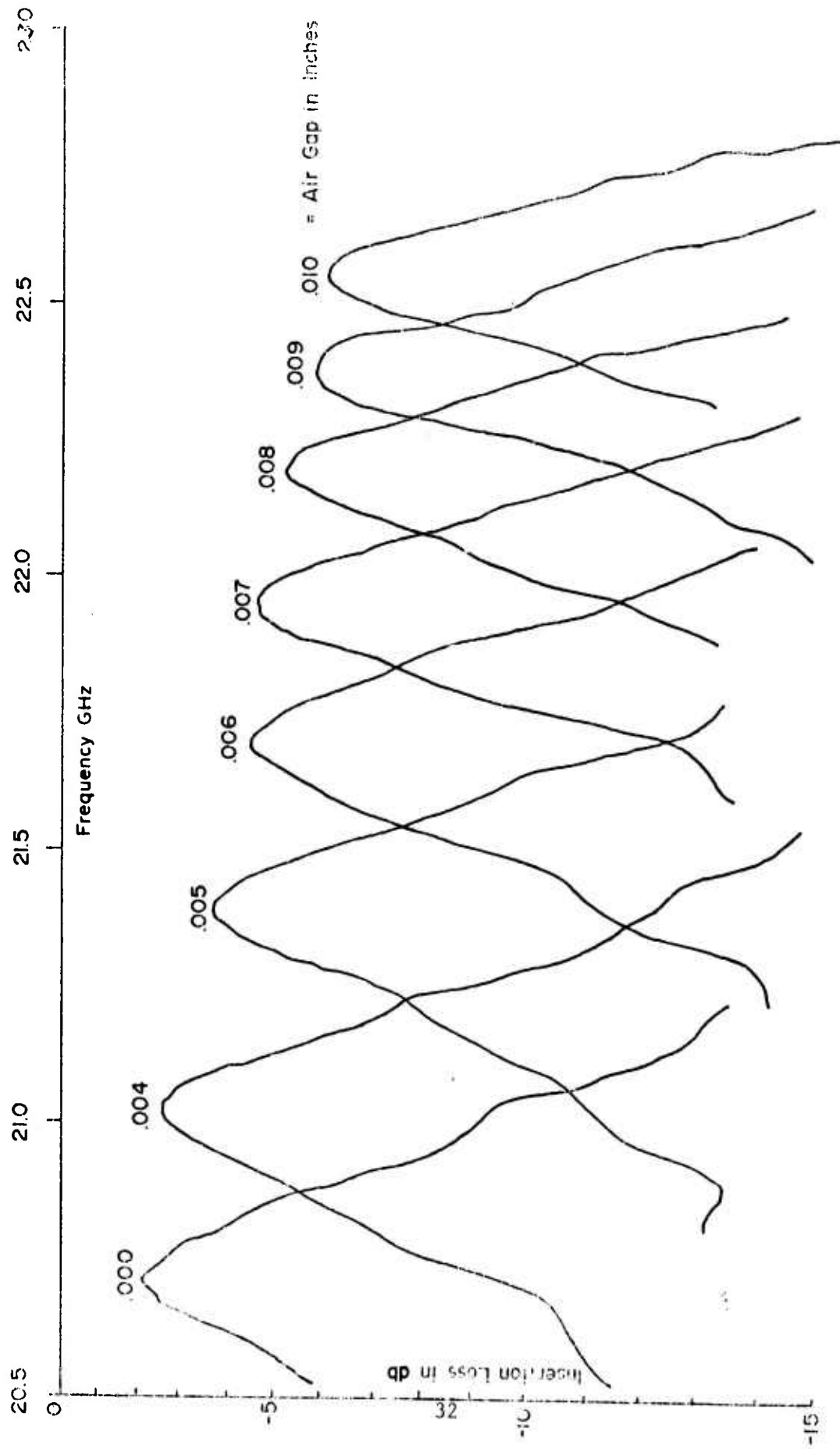


Fig. 14 INSERTION LOSS AND TUNING CHARACTERISTICS OF EXPERIMENTAL MILIC FILTER

In Figure 14 the continuous tuning of the filter can be seen as the gap is varied from 0.0 to 0.010 in. As the air gap is increased, the resonant response is seen to tune upward in frequency as would be expected from the theoretical results of Figure 11.

The center frequencies of the bandpass responses are plotted in Figure 15 for the complete tuning range of the filter from 0.0 to 0.022 in. gap. Also presented in Figure 15 are the theoretical center frequencies for the filter using the computer simulation mentioned earlier. It can be seen that there is reasonable correlation between the theoretical and experimental data. The discrepancy above the 0.005 in. gap is attributed to the approximations in the simulation. The discontinuity in the tuning of the experimental filter below a gap of 0.005 in. is attributed to the tuning mechanism.

4. Conclusions and Extensions

The effort under this program has resulted in the development of a mechanically tunable bandpass ring coupler. The tunable feature increases the usefulness of such a device, not only in the data bus system, but also in other communication and radar systems. The application of this device has been demonstrated by incorporating it into the Model 400 Data Bus System as described in Part II of this report. Without the tunable feature, it is very difficult to obtain similar responses from two couplers. This difficulty arises because the responses of individual rings are found to have slightly different physical dimensions arising from machine tolerances. With the help of the tunable feature, one coupler is designed to have a fixed frequency response and the other is made tunable. Slight differences in center frequency are then easily aligned with the tunable coupler.

The couplers developed under this program have a typical rejection of 10 to 15 db. This rejection may not be adequate in a number of cases. Furthermore, the couplers have a peak at multiple frequencies. It is highly desirable to reduce these multiple peaks in order to increase the number of channels. To further improve the coupler design in these two respects, the multiple ring configuration of Figure 16 is suggested. The coupler consists of two rings, one having a fixed frequency response and the other a tunable feature. In addition, the ring dimensions are chosen to be different. With the proper choice of dimensions, it is possible to design two rings tuned to the same center frequency but having different multiple peak responses. Consequently, the composite response for the two rings will have sharper skirts at the

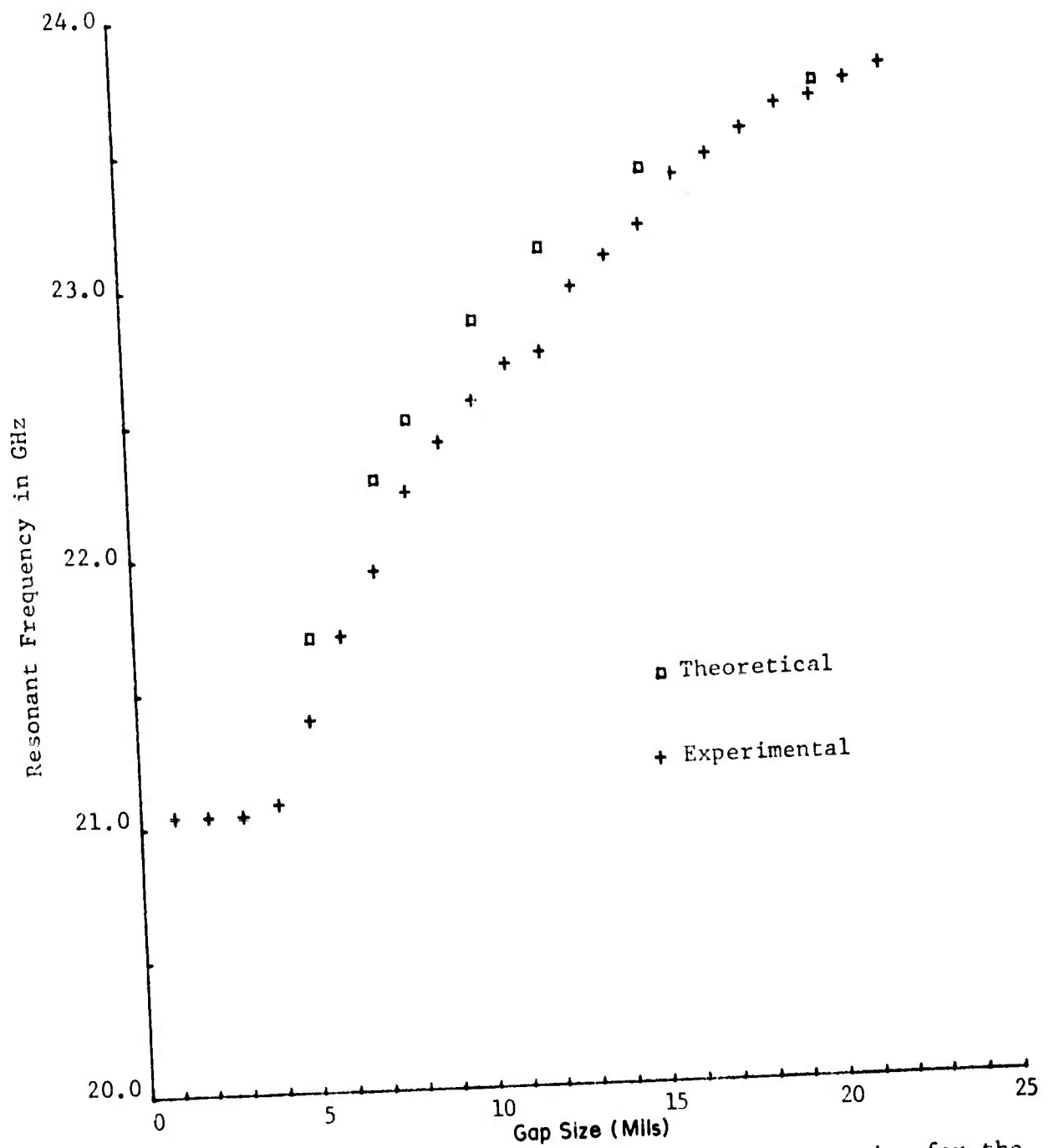


Figure 15 - Theoretical and Experimental Center Frequencies for the Laboratory Prototype Filter

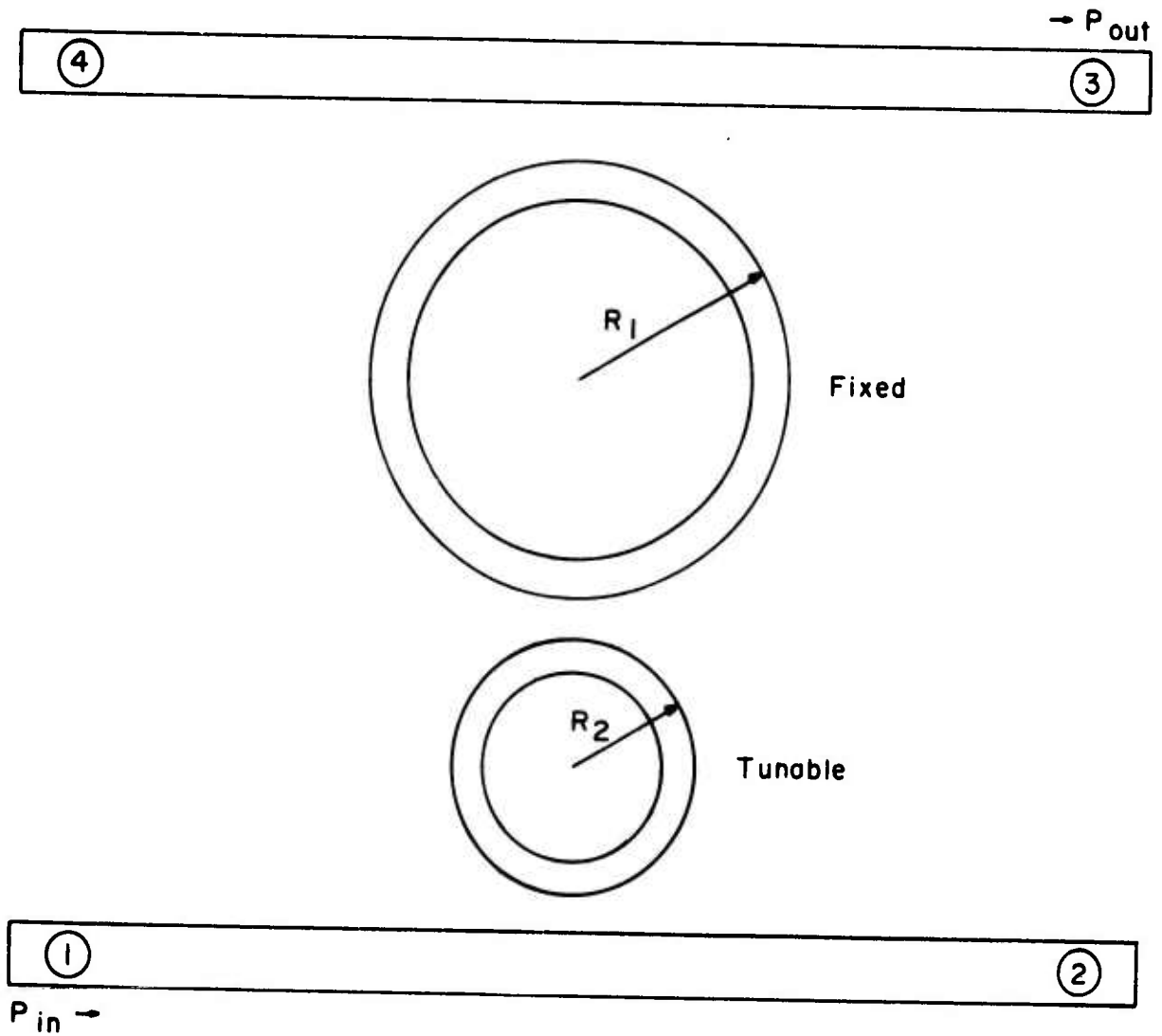


Fig. 16 DOUBLE RING BANDPASS COUPLER

center frequency and the response at other frequencies will be greatly decreased. Slight variations in the center frequency responses of the two rings can easily be aligned by the tunable ring. Development of such an improved device will further increase its usefulness.

SECTION III

PART II

MODEL 400 DATA BUS SYSTEM

1. General System Description

The Model 400 system is a part of the overall data bus system shown in Figure 17. It consists of three MODEM terminals connected in series with the nonmetallic dielectric cable as shown in Figure 17. The Multiplex Terminal Units (MTUs), where the A/D conversion and time division multiplexing are achieved, are not part of the Model 400 system and must be provided externally. As shown in Figure 17, terminals Nos. 1 and 2 are connected by a short cable, whereas a 100 ft cable is used to connect terminals Nos. 2 and 3. Dielectric cable is the main data bus external to the terminals but due to use of MILIC technology inside the terminals, MILIC main bus is used inside. The interfacing between the MILIC main bus and dielectric cable is carried out by appropriate launchers also shown in Figure 17.

A photograph of the three MODEM terminals mounted on a standard rack is shown in Figure 18. Visible in the photograph is a 4 ft section of the dielectric waveguide bus which connects terminals Nos. 1 and 2. The 100 ft section of the cable connecting terminals Nos. 2 and 3 is not shown in the figure except for cable launchers. A view of one terminal MODEM is shown in Figure 19. The dielectric cable is connected at the "Bus Connectors" which are standard K-band waveguide flanges (UG-595U). The launchers on the dielectric waveguide bus are also made to attach to a standard K-band flange.

Each MODEM terminal unit has a provision for a maximum of four modules, each of which may be either a transmitter or a receiver. The transmitters and receivers are modularized and are interchangeable to facilitate reconfiguration of the functional operation of the terminal. Associated with each module are connectors marked A, B, C, and D on the front panel, as shown in Figure 19. Each of these connectors could act as either an input or an output port depending on whether the module is a transmitter or receiver. Each of these modules operates at a predetermined microwave carrier frequency in the Ku-band (22 to 30 GHz). The Model 400 system in its present form has two Frequency Division Multiplex (FDM) data channels with their carrier frequencies being nominally at 23 GHz and 23.5 GHz respectively. Both channels can be operated simultaneously with independent data channels.

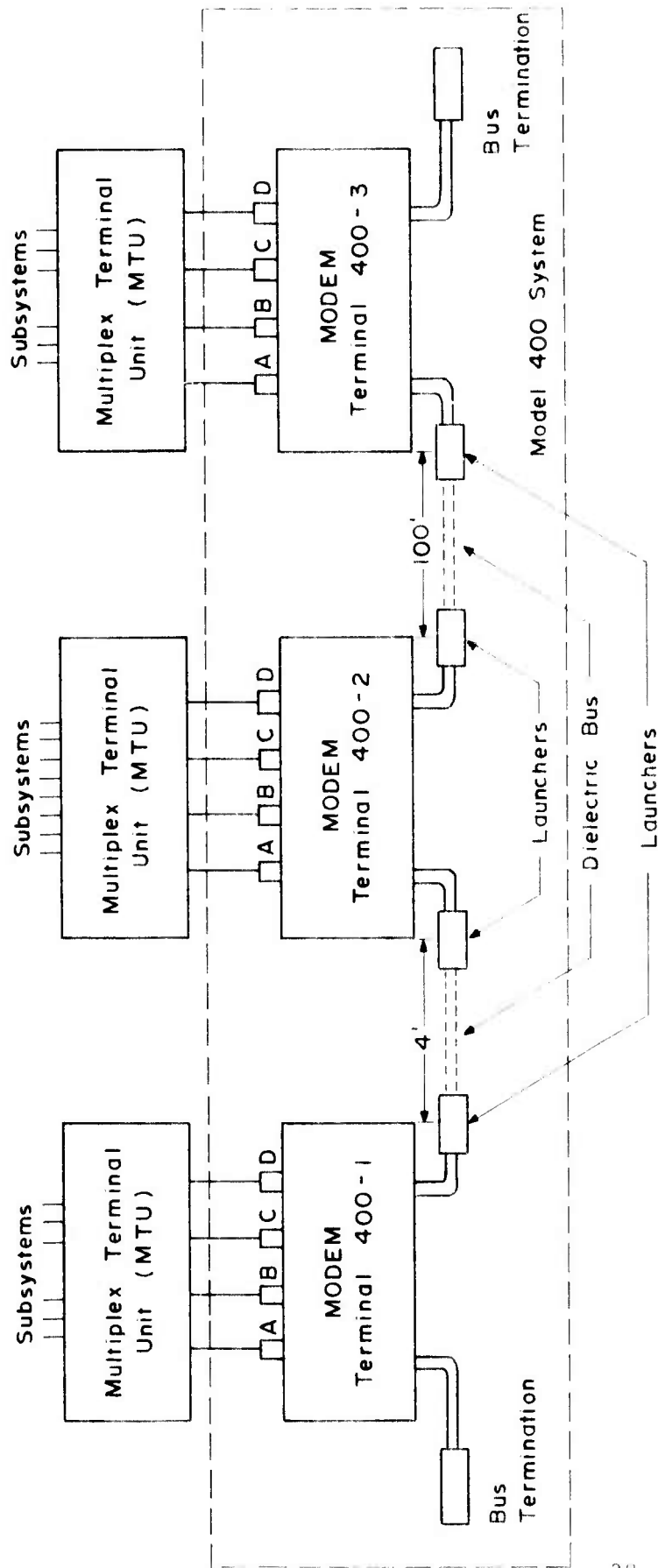


Fig. 17 BLOCK DIAGRAM OF A THREE TERMINAL DIELECTRIC WAVEGUIDE MICROWAVE DATA BUS SYSTEM

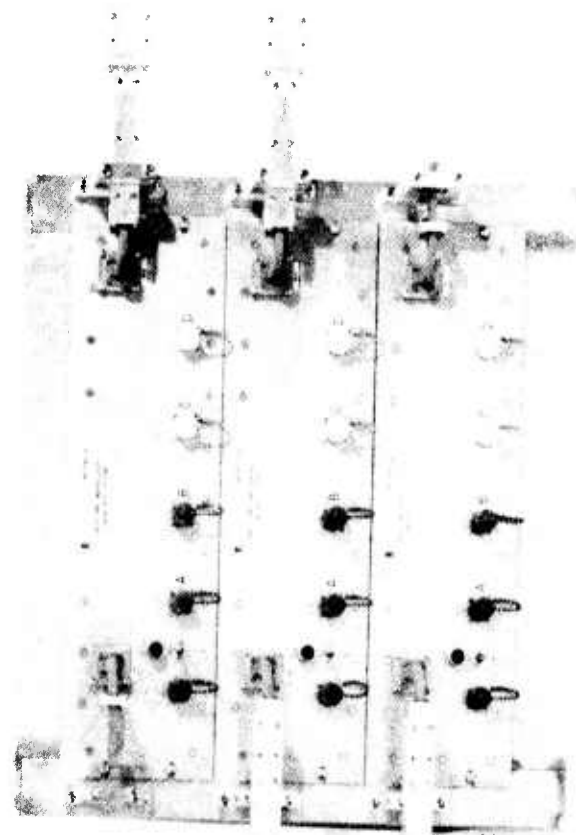


Fig. 18 RACK MOUNTED MODEM UNITS

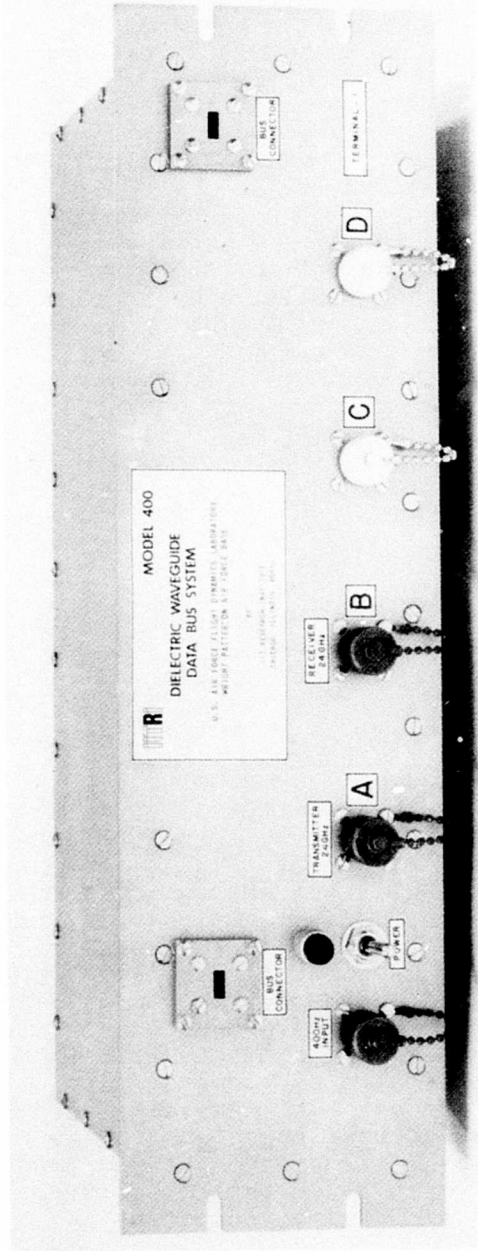


Fig.19 A TERMINAL OF THE MODEL 400 DATA SYSTEM

The layout of the modules for each terminal of the Model 400 system is shown in Figure 20. Each terminal houses the MILIC main bus, as shown, together with the modules. Terminal No. 1 houses one 23 GHz transmitter and receiver. The other two positions are blank and could be used for future expansion. In terminal No. 2, one 23 GHz transmitter and receiver module each are installed together with a receiver module operating at 23.5 GHz. Terminal No. 3 contains one transmitter and one receiver at 23 GHz together with one transmitter at 23.5 GHz. The fourth blank position in terminals Nos. 2 and 3 is available for future expansion.

Each of the modules is placed close to the MILIC main bus. Couplers mounted on these modules are used to couple microwave signals to or extract them from the main bus. The 23 GHz channel in the system uses broad-band couplers, whereas the 23.5 GHz channel uses frequency selective ring couplers. The input/output connectors for each module are also shown in Figure 20. Photographs of top and bottom views of the three terminals are shown in Figures 21 through 23 and Figures 24 through 26 respectively.

A generalized block diagram of the transmitter and receiver modules is shown in Figure 27. The transmitter module consists of a Gunn oscillator, a driver circuit and a coupler. The oscillator output is coupled to the MILIC main bus through the coupler. In the 23 GHz channel, wide-band couplers are used, whereas narrow-band frequency selective couplers are incorporated in the 23.5 GHz channel. The oscillator is pulse-modulated (interrupted CW) by a digital signal from a MTU through a driver circuit. The interrupted CW modulation is achieved by direct pulsing of the B^+ supply of the Gunn device.

In the receiver module, the microwave signal is extracted from the MILIC main bus through a coupler. The signal is then mixed with a local oscillator giving an output at an IF of 160 MHz, which is then amplified. A Gunn oscillator provides the local oscillator signal which couples into the mixer through a 10 db MILIC coupler. The 23 GHz channel consists of a separate preamplifier and a main amplifier at 160 MHz. Both of these amplifiers use hybrid thin film technology. The 23.5 GHz channel uses only one main amplifier also employing hybrid thin film technology. The IF amplifier drives an envelope detector which utilizes a Schottky barrier diode. This is followed by a threshold circuit employing a voltage comparator. The threshold level is set to be on the linear portion of the detector transfer function. This circuit converts the received on/off RF pulses to the standard digital output.

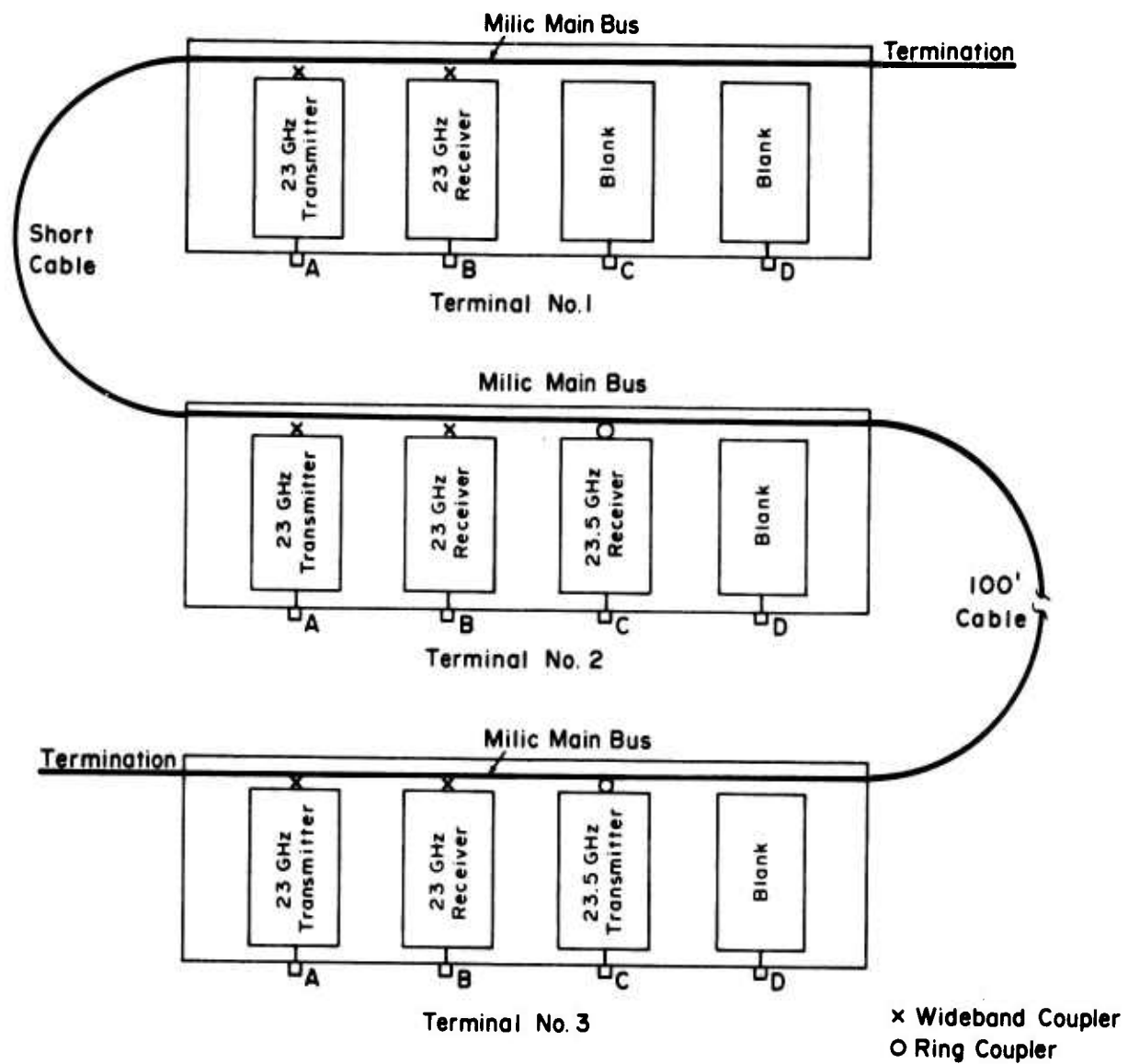


Fig. 20 MODEL 400 DATA BUS SYSTEM LAYOUT

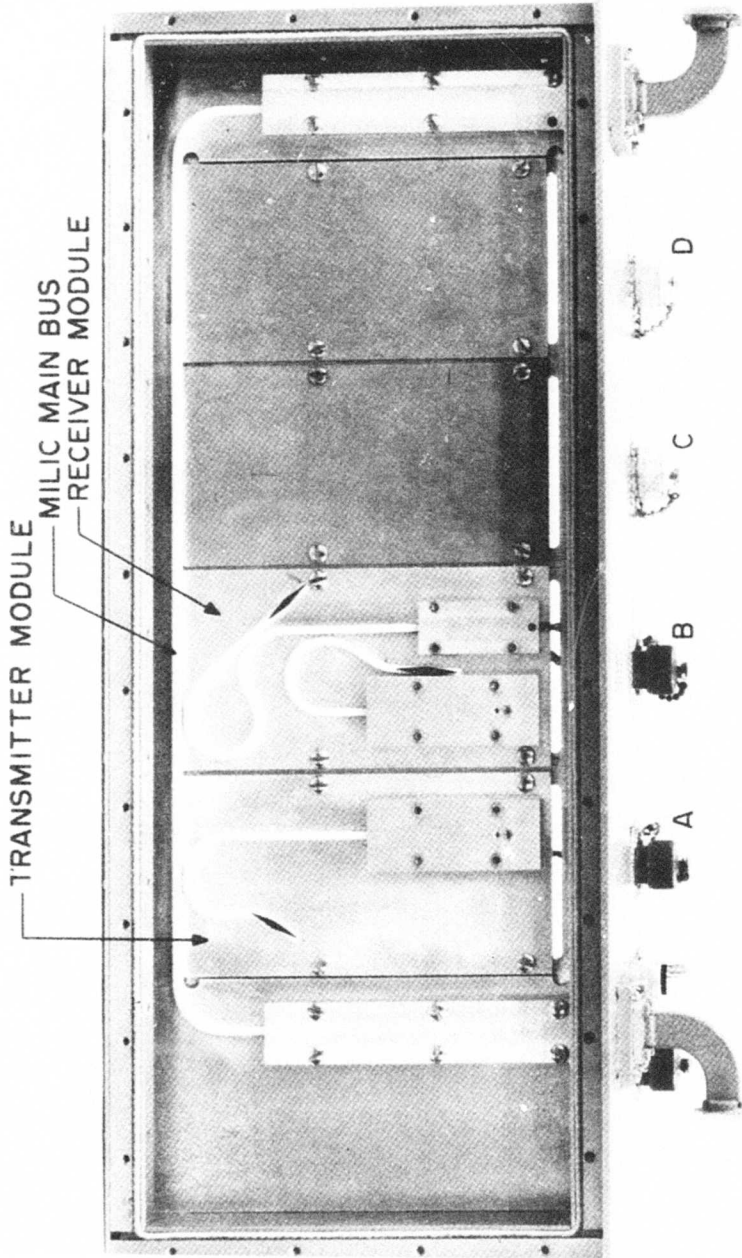


Fig. 21 TERMINAL NO. 1 TOP VIEW

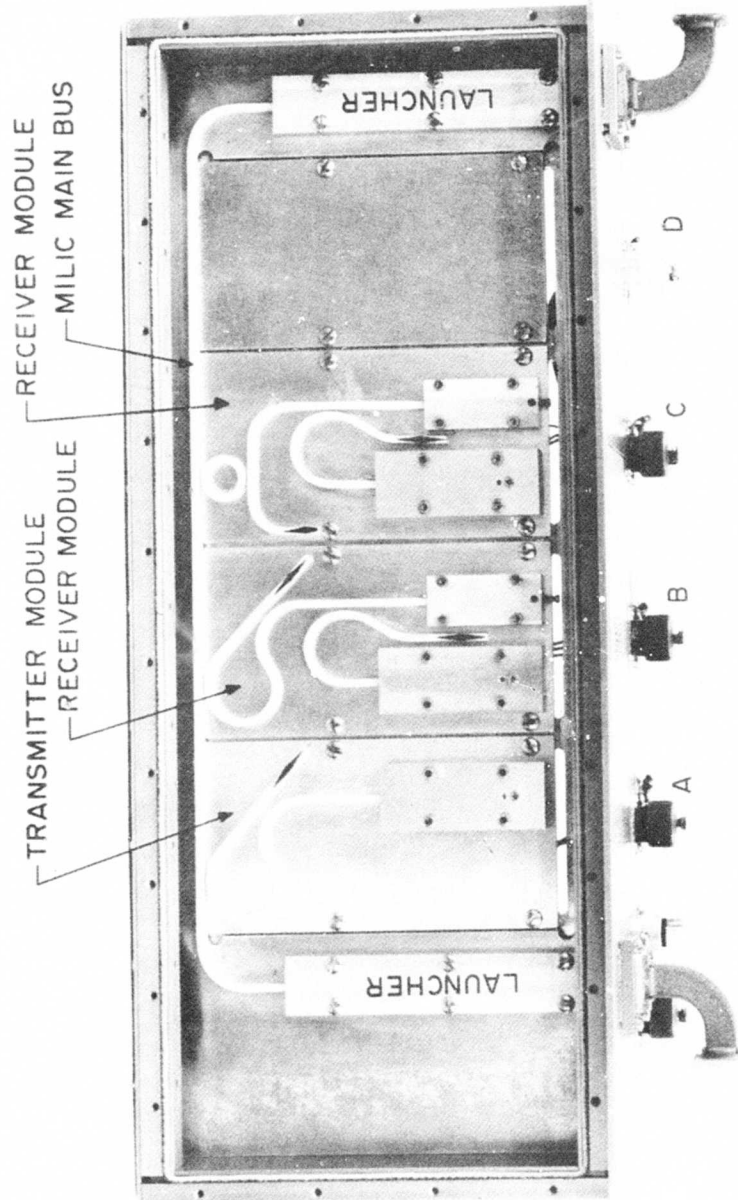


Fig. 22 TERMINAL NO. 2 TOP VIEW

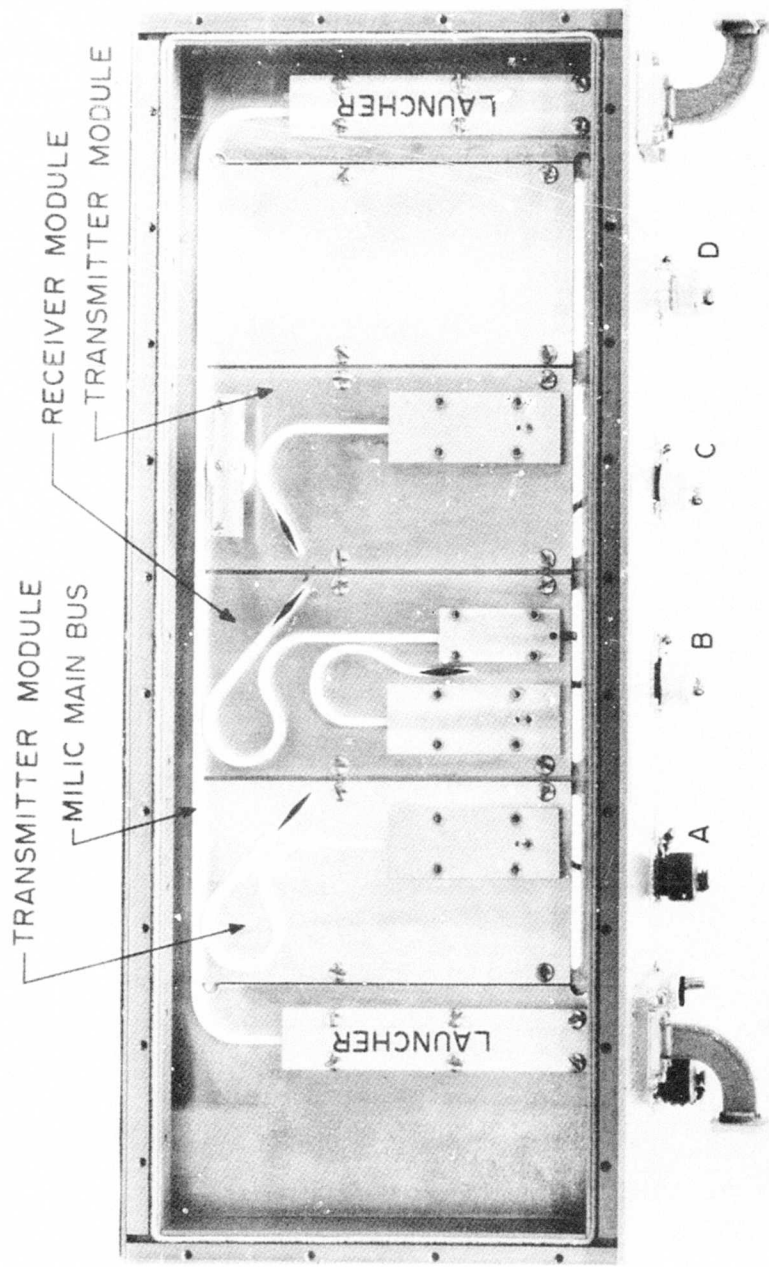


Fig. 23 TERMINAL NO.3 TOP VIEW

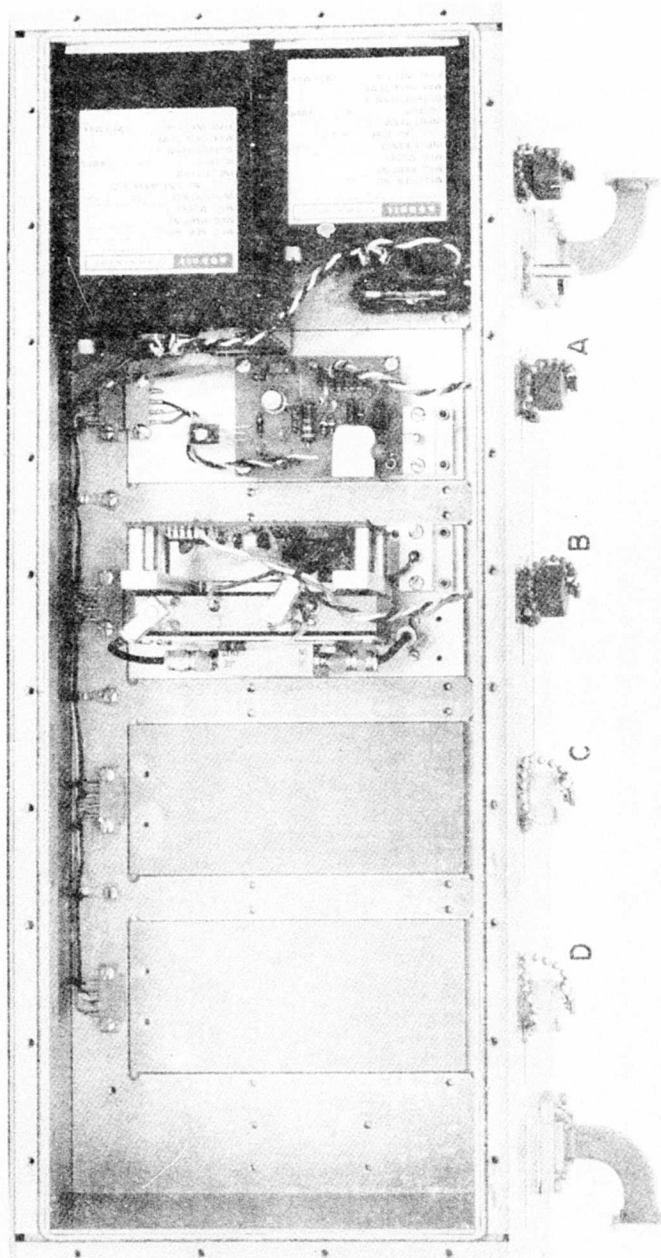


Fig. 24 TERMINAL NO. 1 BOTTOM VIEW

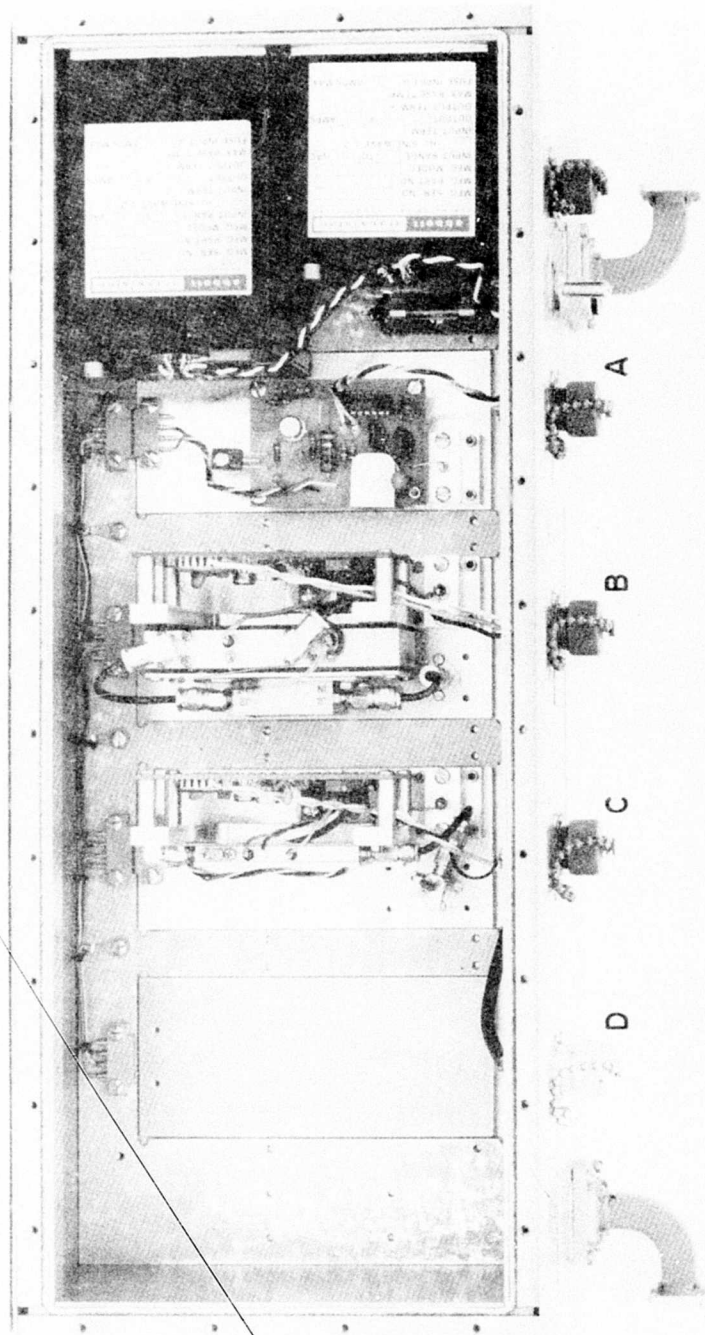


Fig. 25 TERMINAL NO. 2 BOTTOM VIEW

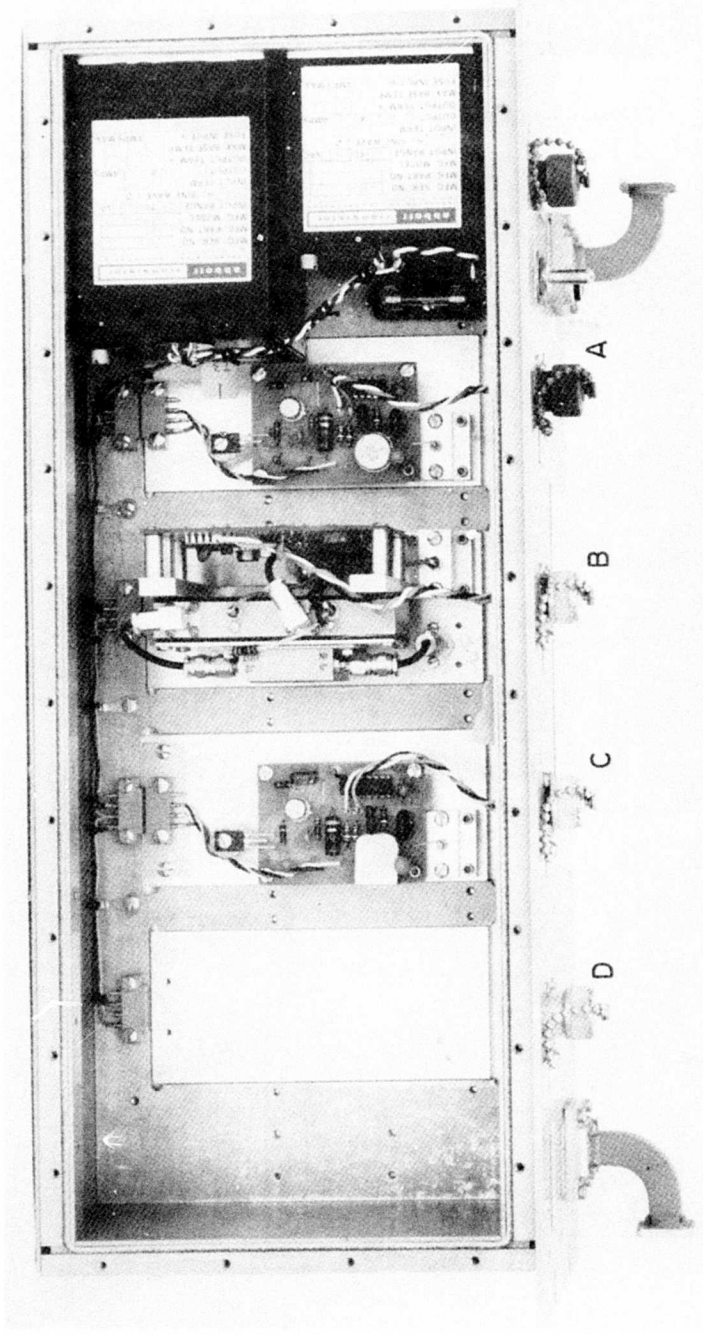


Fig. 26 TERMINAL NO.3 BOTTOM VIEW

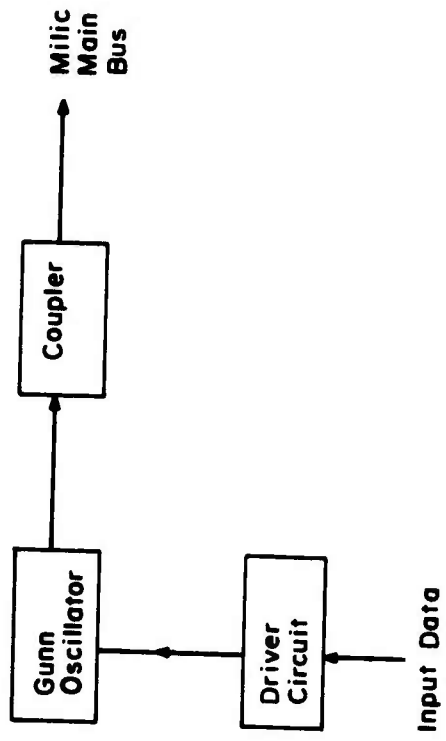


Fig. 27a TRANSMITTER MODULE BLOCK DIAGRAM

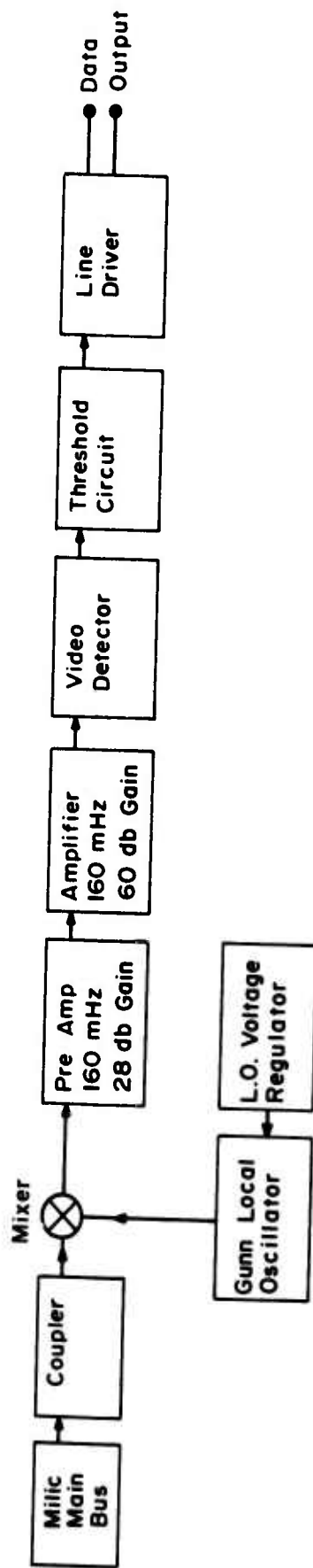


Fig. 27b RECEIVER MODULE BLOCK DIAGRAM

2. Description of 23.5 GHz Channel

A single ring bandpass coupler has been implemented in the 23.5 GHz channel for the Model 400 data bus system. This demonstrates the actual application of the ring coupler described earlier in Part I. In this channel both the transmitter and the receiver modules use a ring coupler for coupling energy into the main bus line. Because of their frequency selective nature, it is important that couplers in both the transmitter and receiver modules be tuned to the same frequency. As mentioned earlier, it is difficult to fabricate two rings of identical dimensions. Consequently, the concept described earlier for tuning these couplers was very useful in this application. A transmitter module was designed employing a mechanically tunable ring coupler. The transmitter oscillator can also be mechanically tuned in order to adjust to the bandpass response of the ring. The receiver module, on the other hand, uses a fixed response bandpass ring filter at 23.461 GHz. The transmitter ring coupler is tuned to this frequency using the tuning mechanism described below.

Photographs of the transmitter and receiver modules are shown in Figures 28 and 29 respectively. The transmitter module contains the Gunn oscillator, ring coupler on the top side and the driver circuitry underneath the baseplate. The oscillator frequency can be adjusted by the dielectric screw. The ring coupler can be re-tuned by loosening the set screw and tuner lock nut, and adjusting the tuning screw. A clockwise rotation of the tuning screw will cause a reduction in the air gap beneath the ring, and thus a downward frequency tuning. Care should be taken not to force the tuning mechanism. The coupler has been set up to have a minimum air gap of approximately 0.001 in. beneath the ring. This was done to avoid an accidental detachment of the dielectric ring from the piston under undue pressure on it. After proper adjustment of frequency, the tuning screw position can be locked by the set screw and lock nut.

The receiver module contains a Gunn oscillator used as a local oscillator (LO), mixer, and ring coupler mounted on the top side and IF/video circuitry mounted underneath the plate. As shown in Figure 29 the ring coupler is of the fixed response type. The LO and mixer adjustments can be carried out by the tuning screws as shown.

The transmitter and receiver modules are housed in terminals Nos. 2 and 3 respectively. This channel can be used for transferring digital data at the rate of up to about 10 Mb/s.

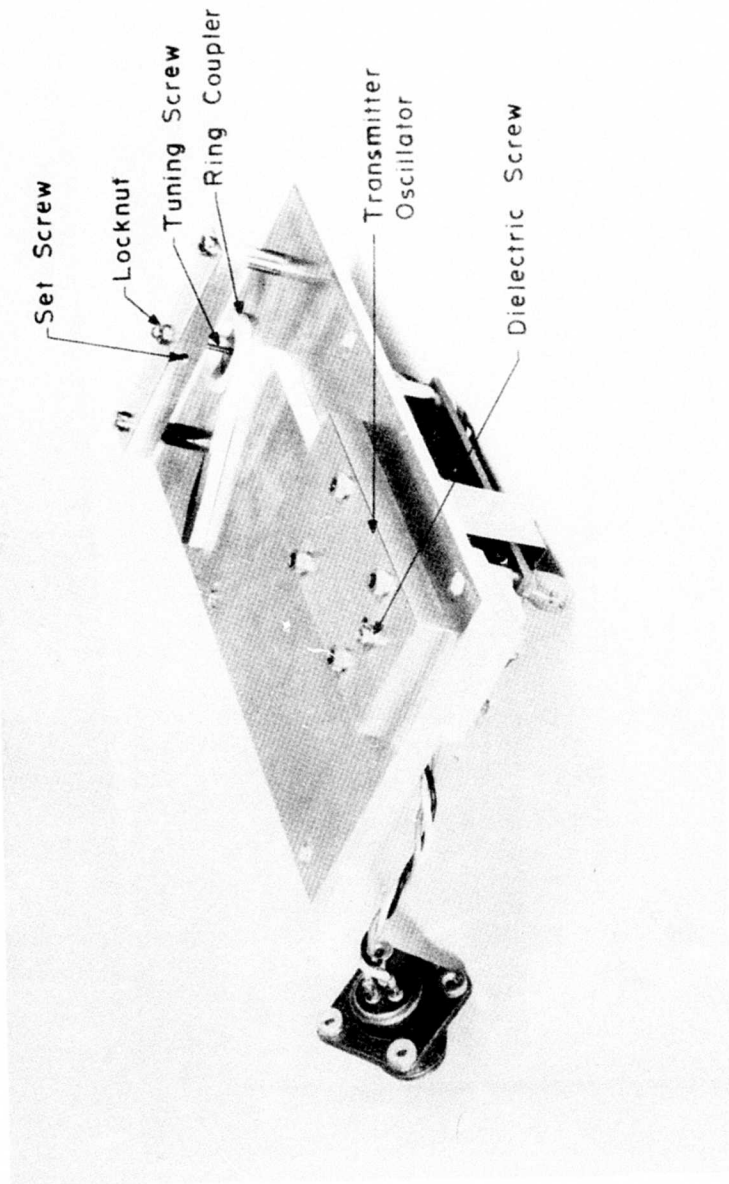


Fig. 28 TRANSMITTER MODULE (23.5 GHz CHANNEL)

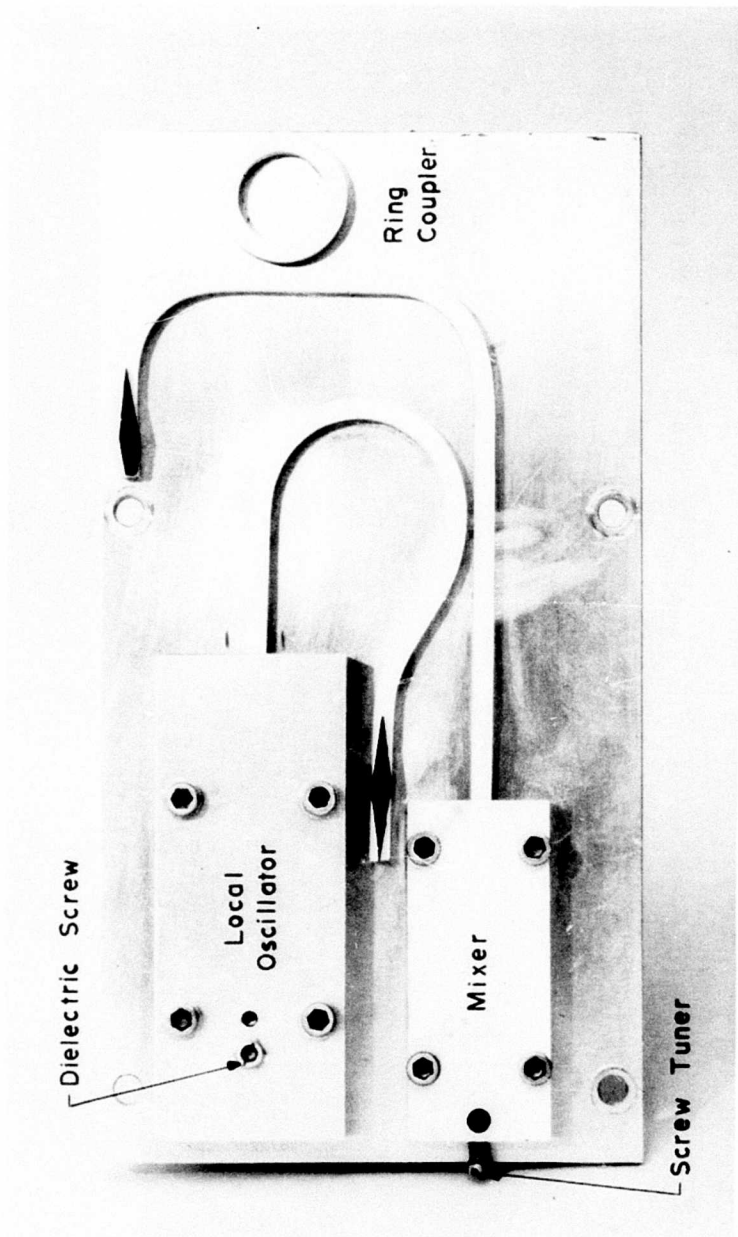


Fig. 29 RECEIVER MODULE (23.5 GHz CHANNEL)

3. Description of 23 GHz Channel

The 23 GHz channel is similar to the 23.5 GHz channel except that it uses wide-band couplers instead of frequency selective ring couplers. Furthermore, in-between the wide-band couplers and the oscillator (or mixer), an additional 3 db coupler is used. This configuration provides bidirectional signal flow capability as discussed further in Section 2b of Part III. For this channel, data can be inputted at any one of the three transmitter modules located one each on the three MODEM terminals. The data can be outputted from any of the three receiver modules located on the three terminals. Data rates of up to about 10 Mb/s can be achieved on this channel.

4. Component Description

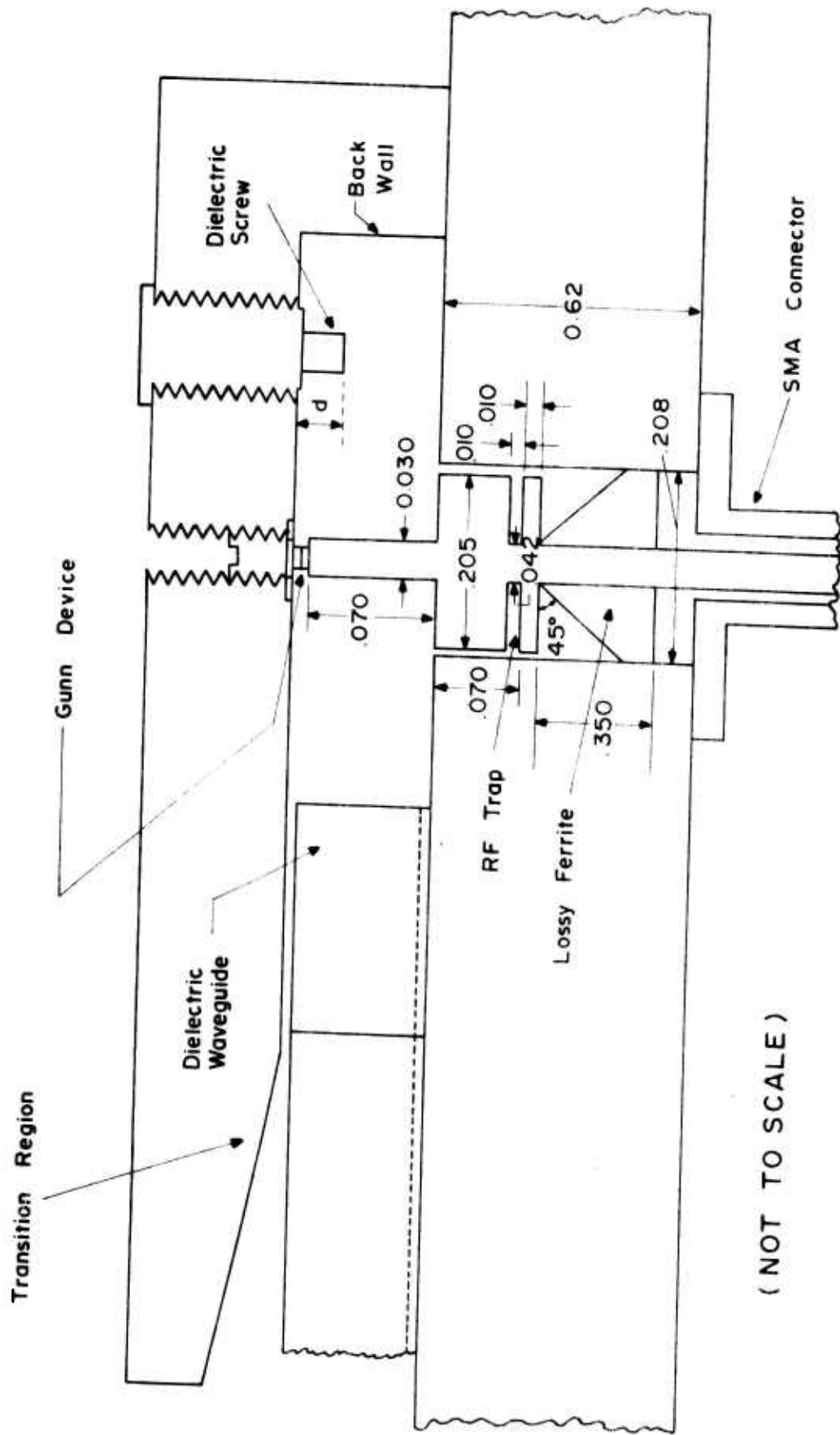
a. Oscillator Design

The data bus system required the development of eight Gunn diode oscillators. Six of these oscillators were used in the three rebuilt 23 GHz channels. The remaining two oscillators were used in the 23.5 GHz channel. An identical design was used for both transmitter and local oscillators. The bias circuit was slightly modified for the local oscillators which did not require any modulation capability.

The oscillators finally used in the Model 400 system represent a significant improvement over those developed previously under Contract F33615-73-C-0263. The new oscillator design incorporates a new cavity design which has resulted in better stability and more power output.

The oscillator cavity design chosen is shown in Figure 30. This oscillator consists of a post-mounted Gunn device* in a direct coupled waveguide cavity. The frequency of operation is determined by the distance from the post to the back wall, which should be approximately a half guide wavelength at the operating frequency. Mechanical tuning is provided by a dielectric screw which is placed between the post and back wall in a position of high electric field. The dielectric screw tunes the oscillator down in frequency as tuner depth, d , increases. Therefore, the oscillator is initially designed to operate at a slightly higher frequency, and is tuned down by use of the dielectric screw.

*Type No. MA-49179-118, 49180-118, Microwave Associates, Burlington, Massachusetts.



(NOT TO SCALE)

Fig. 30 DIRECT COUPLED OSCILLATOR CAVITY WITH POST MOUNTED GUNN DEVICE

The direct coupled cavity oscillator with the post-mounted diode has proven to be a successful design for use with MILIC technology. It provides for the integration of a rectangular metal waveguide to MILIC transition in the front portion of the mount (shown in Figure 30). The Q of this oscillator mount was measured and found to be on the order of 210.

Each of the eight oscillator mounts was individually tested in order to insure proper operation. The mounts to be used as local oscillators were required to operate in a CW mode, and to be continuously tunable over a frequency range of both high and low IF frequencies. The four transmitter oscillators were evaluated under both CW and pulsed modulation operating conditions before being included in the system. A typical set of tuning curves for a 23 GHz transmitter oscillator mount is presented in Figures 31 and 32. The power output versus bias voltage data are given in Figure 31. A typical mechanical tuning response is shown in Figure 32 for the dielectric screw tuner.

The performance data for the four transmitter oscillators are presented in Table 1. The output power of the oscillators was measured by placing the mount on a test plate which fed a 5 in. section of dielectric line and a transition to rectangular metal waveguide. Therefore, standard waveguide test equipment could be used.

TABLE 1. Transmitter Oscillator Data

Data Bus Terminal	Frequency	Output Power CW dbm	Bias Voltage
1	23.0	+13.0	5.00
2	23.0	+12.0	5.25
3	23.0	+14.0	5.75
3	23.461	+12.0	5.00

The procedure for tuning these oscillators consists of first adjusting the center frequency with the dielectric screw. Subsequent to frequency tuning, the power output should be maximized by adjustment of the bias voltage.

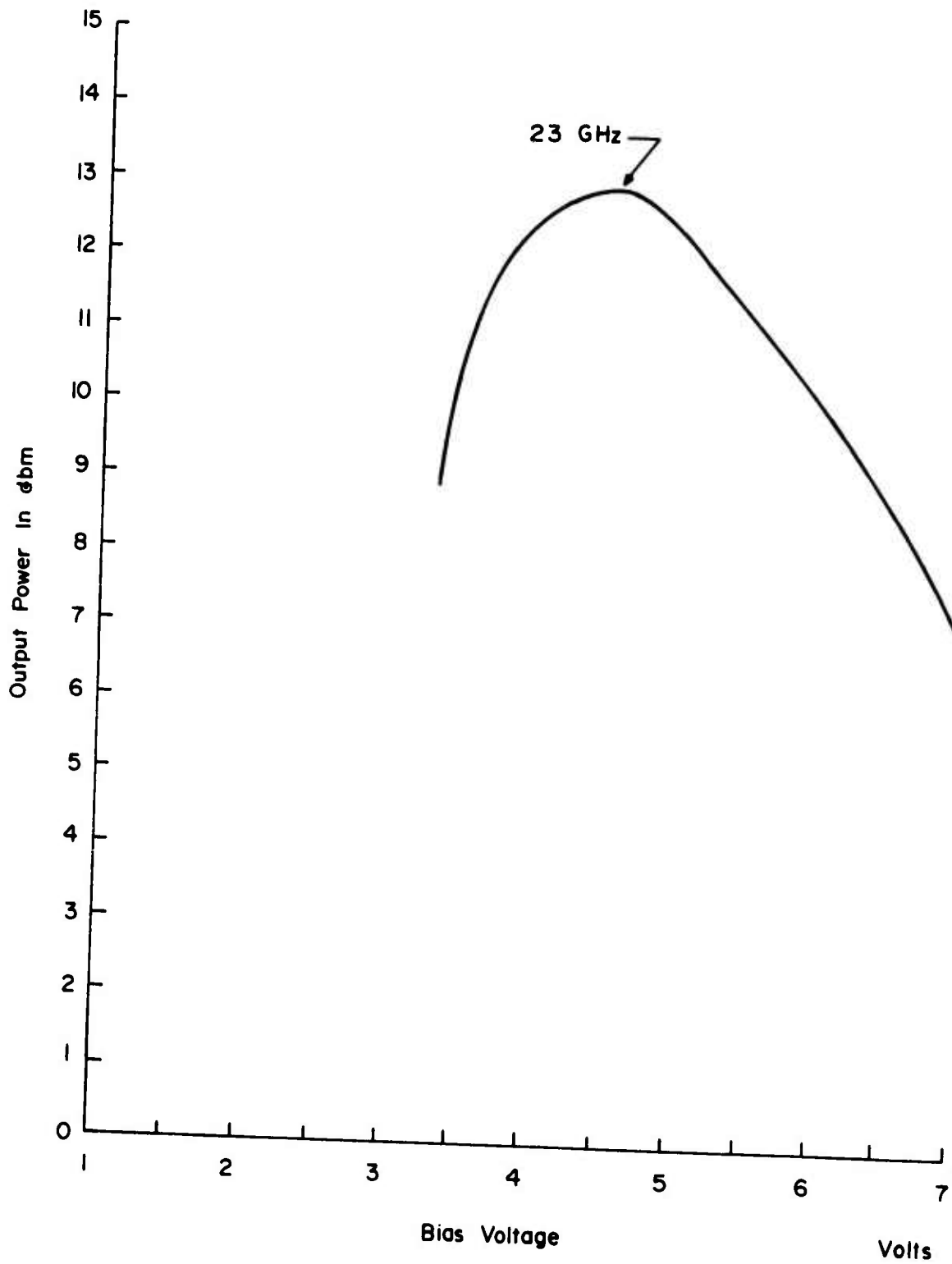


Fig. 31 TUNING CURVE FOR TYPICAL 23 GHz TRANSMITTER OSCILLATOR (Measured)

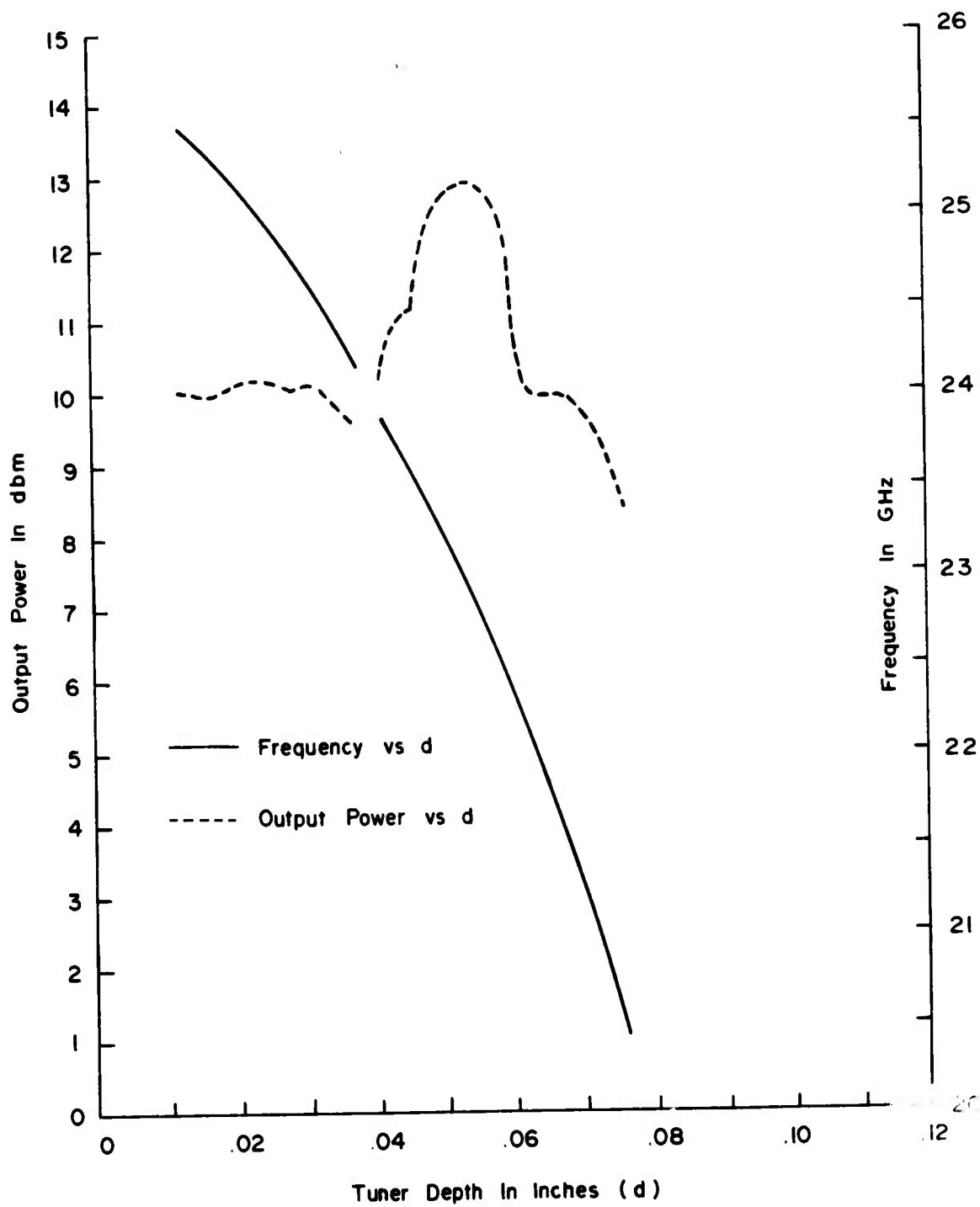


Fig. 32 MECHANICAL TUNING CURVE FOR TYPICAL 23 GHz TRANSMITTER OSCILLATOR (Measured)

Interrupted CW modulation of the transmitter is accomplished by direct pulsing of the B⁺ supply to the Gunn diode oscillator. The driver schematic is given in Figure 33. A μ A 9615 IC line receiver accepts standard digital signals from a twisted-pair or single-ended line. When no input line is connected, the input is biased internally to turn off the oscillator. The line receiver output in the form of TTL logic levels is applied to an MH 0026 clock driver IC which drives the Gunn device. The output pulse level is determined by the B⁺ to the MH 0026 which is supplied by an adjustable regulator circuit consisting of an LM 723 IC and an M5E370 current boost transistor.

b. Mixer Design

The four mixer diode mounts used on the receiver modules were of the same type developed under the previous Contract F33615-73-C-0263. Three of the receivers were designed to operate at an RF frequency of 23 GHz, while the new unit was developed at 23.461 GHz.

The data bus system employs a Schottky-barrier mixer diode to provide an intermediate frequency difference between the transmitter signal and the local oscillator drive. The semiconductor device is a Microwave Associates MA40015 Schottky-barrier mixer diode with a 6.5 db noise figure. It is mounted in a reduced height waveguide structure for impedance matching purposes. The IF output is taken through an OSM connector located on the underside of the receiver module. A choke is provided to prevent leakage of the K-band frequencies through the IF output. A cross section of the mixer mount is shown in Figure 34.

c. IF/Video System

The IF section of the 23 GHz receivers operates at a 160 MHz center frequency with a 50 MHz bandwidth. It consists of separate preamplifiers and main amplifiers, both of which are hybrid thin-film units. The preamplifiers are RHG Electronics Laboratory Model ICFT16050, with a nominal gain of 25 db, noise figure of 30 db, and a 200 ohm input impedance to match the mixer.

The main amplifiers are RHG Model ICE16040. The nominal maximum gain is 60 db and can be reduced to approximately 40 db by means of a gain control. The gain is adjusted to keep the noise level below the video threshold level so no noise is introduced into the system in the absence of signals.

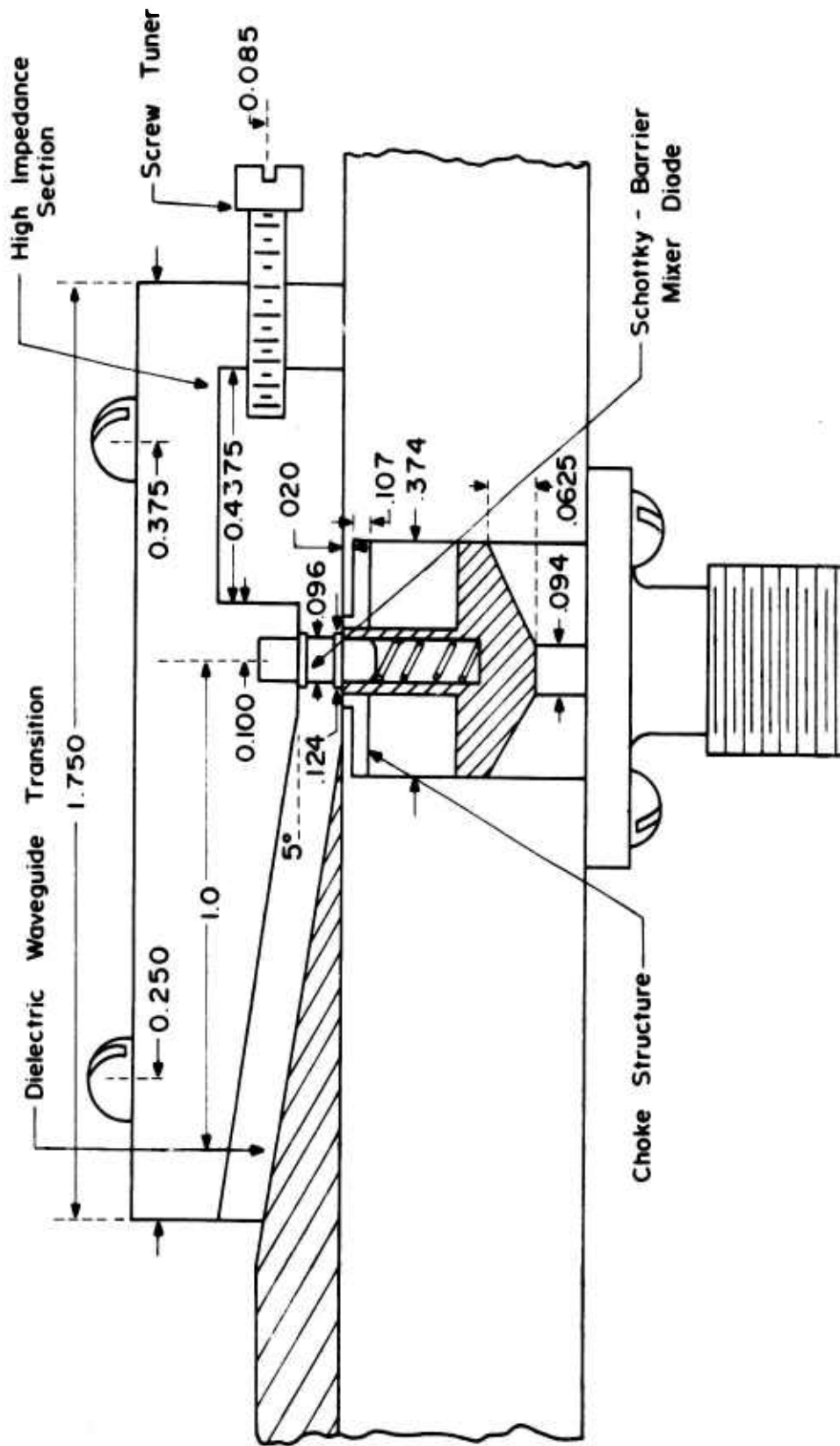


Fig. 34 CROSS SECTION OF K - BAND MIXER MOUNT

The 23.5 GHz receiver uses a single IF amplifier having a low-noise input stage and input impedance to match the mixer. The center-frequency is 120 MHz and the bandwidth is 100 MHz. Other characteristics are similar to the amplifiers described above. This unit is manufactured by LEL/Varian and is Model ICA-1-120-100-50-S-200-12.

The video circuitry and LO voltage regulator are contained on a printed circuit board and are shown schematically in Figure 35. This board is the same in the 23 and 23.5 GHz receivers.

The IF amplifier drives an envelope detector which utilizes an HP 5082-2301 Schottky-barrier diode. The detector has a threshold effect in that its reduced sensitivity at very low signal levels prevents much of the system noise from being detected. Conversely, limiting in the IF amplifier reduces the detector output on high-level signals.

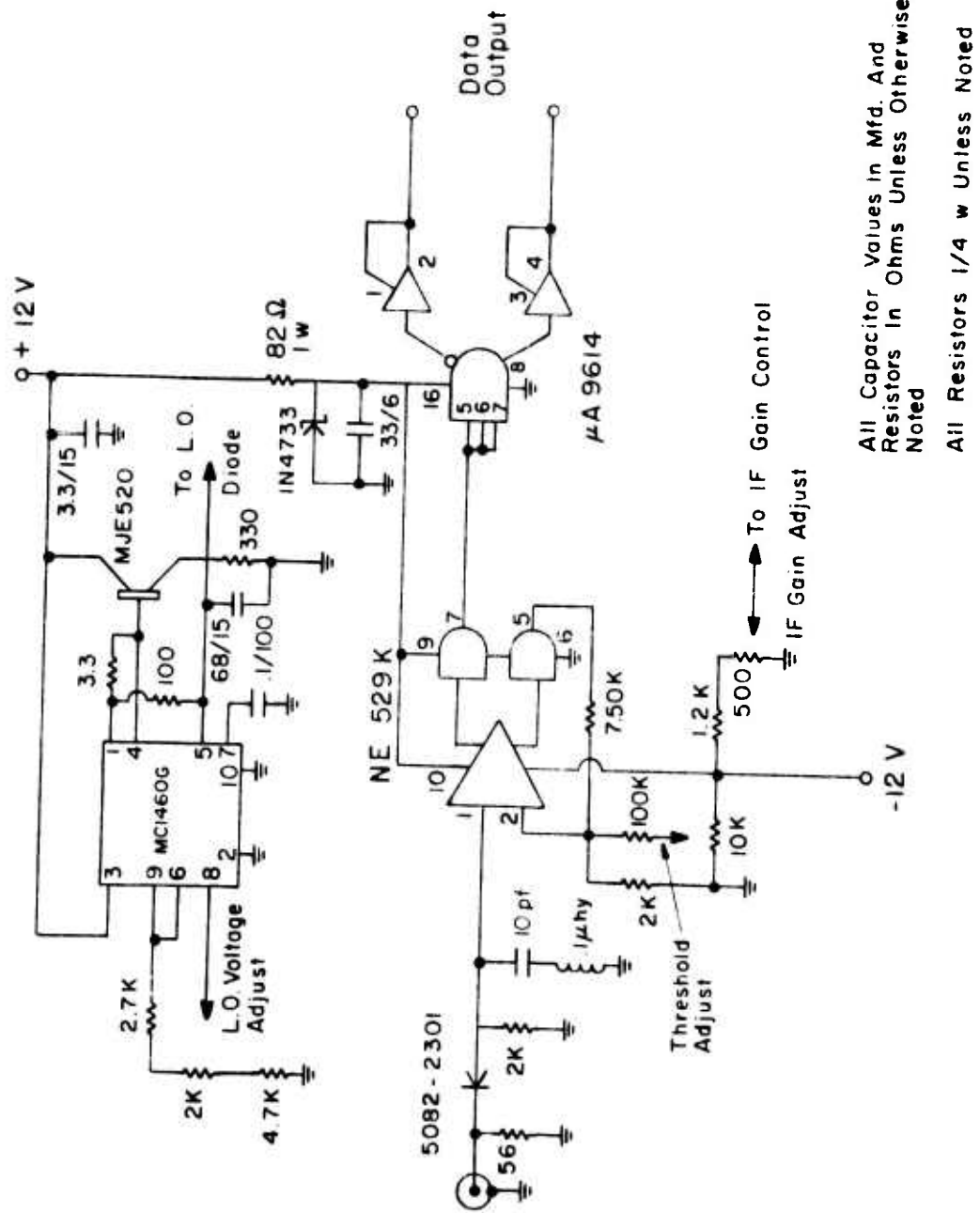
The video detector drives a threshold circuit employing an NE529 IC voltage comparator. This circuit converts the received pulses to a standard TTL digital signal. The threshold circuit is followed by a μ A 9614 IC line driver which is capable of driving a single-ended or twisted-pair line with standard logic signal levels.

The video board includes an MC1460 IC voltage regulator with an M5E520 current boost transistor to supply the Gunn LO diode. It has an output range of 5 to 7 volts.

d. Data Bus Cable

Three different lengths of dielectric data bus cable were delivered with the previous system. The cable lengths consisted of 4, 20, and 100 ft sections including launchers at each end for terminal interface. This section describes the relevant performance characteristics of the cables.

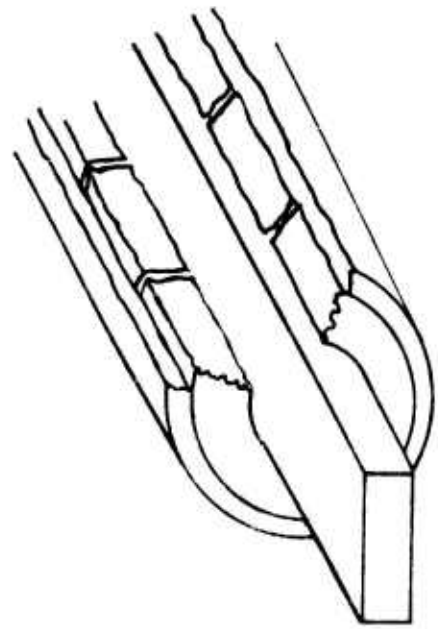
Each consists of a rectangular waveguide core of polyethylene surrounded by a low density polystyrene foam and encased in a heat-shrink jacket. This rectangular core has the advantage that the electric field polarization is controllable, and always maintained normal to the broad wall of the dielectric waveguide core. The rectangular cross section prevents the electric field from rotating even if the cable is curved or twisted. The isolating medium is a polystyrene foam formed by toroidal doughnut sections 0.75 in. long. The outer jacket is a heat-shrinkable tubing used to keep the form cylinders in place on the core. The construction of the dielectric waveguide bus is shown in Figure 36.



All Capacitor Values in Mfd. And Resistors in Ohms Unless Otherwise Noted

All Resistors 1/4 w Unless Noted

Fig 35 RECEIVER SCHEMATIC



(NOT TO SCALE)

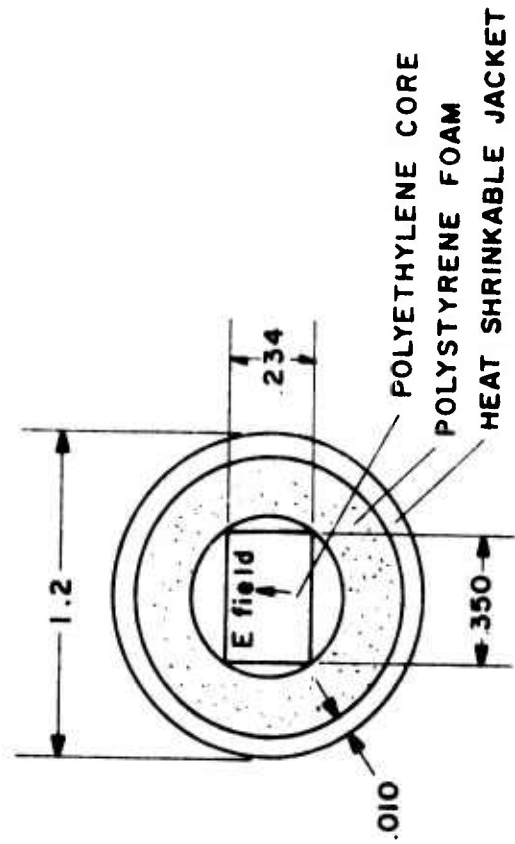


Fig. 36 CONSTRUCTION OF THE DIELECTRIC WAVEGUIDE BUS

The launchers provide a gradual transition from the TE₁₀ mode of rectangular metal waveguide (K-band WR-42) to the rectangular E₁₁ mode of the dielectric waveguide. The two halves of the launcher clamp together, capturing the center core which is tapered to a point within the launcher.

The attenuation characteristics of the different length cables are shown in Figure 37. At the main system operating frequency of 23 GHz the cables have 2.00, 6.75, and 27.2 db attenuation for the 4, 20 and 100 ft cables respectively. Included in these figures are the losses of the mode transitions at both ends of the cable. Therefore, using the 27.2 db figure for the 100 ft cable, a cable loss for the dielectric bus can be estimated at 0.272 db/ft.

e. MILIC Main Bus

The loss of the MILIC main bus in each of the three MODEM terminals was also determined under no-load conditions. The insertion loss is shown in Figure 38. The losses shown include two rectangular metal waveguide-to-image waveguide transitions and the MILIC main bus line. Blank modules were used in the MODEM; therefore the results are for an unloaded main bus. Typically, the main bus causes an insertion loss of 5 to 7 db over a very wide frequency band. A return loss measurement on the three MODEMs gave a VSWR of 1.1 to 1.2 over the frequency range of 19 to 26 GHz.

5. Test Results

The Model 400 Data Bus System was tested by simultaneously applying digital data of different bit rates to both channels. For the 23 GHz channel, all possible combinations of inputs and outputs were tested. Typical inputs and outputs from the system for the two channels are shown in Figures 39 and 40 respectively. The data rates used in this example were 100 db/s and 1 Mb/s respectively for the 23 GHz and 23.6 GHz channels.

In addition, tests were also conducted to determine the signal margin at each receiver input. The signal margin has been defined as the degree to which the signal at a receiver input exceeds the minimum level required to operate the receiver. This has proven to be a useful measure of system performance and a means of diagnosing malfunctions such as increased loss or reduced gain in some portion of the system or detuning of the oscillators. This measurement was made by inserting a variable attenuator in series with the dielectric

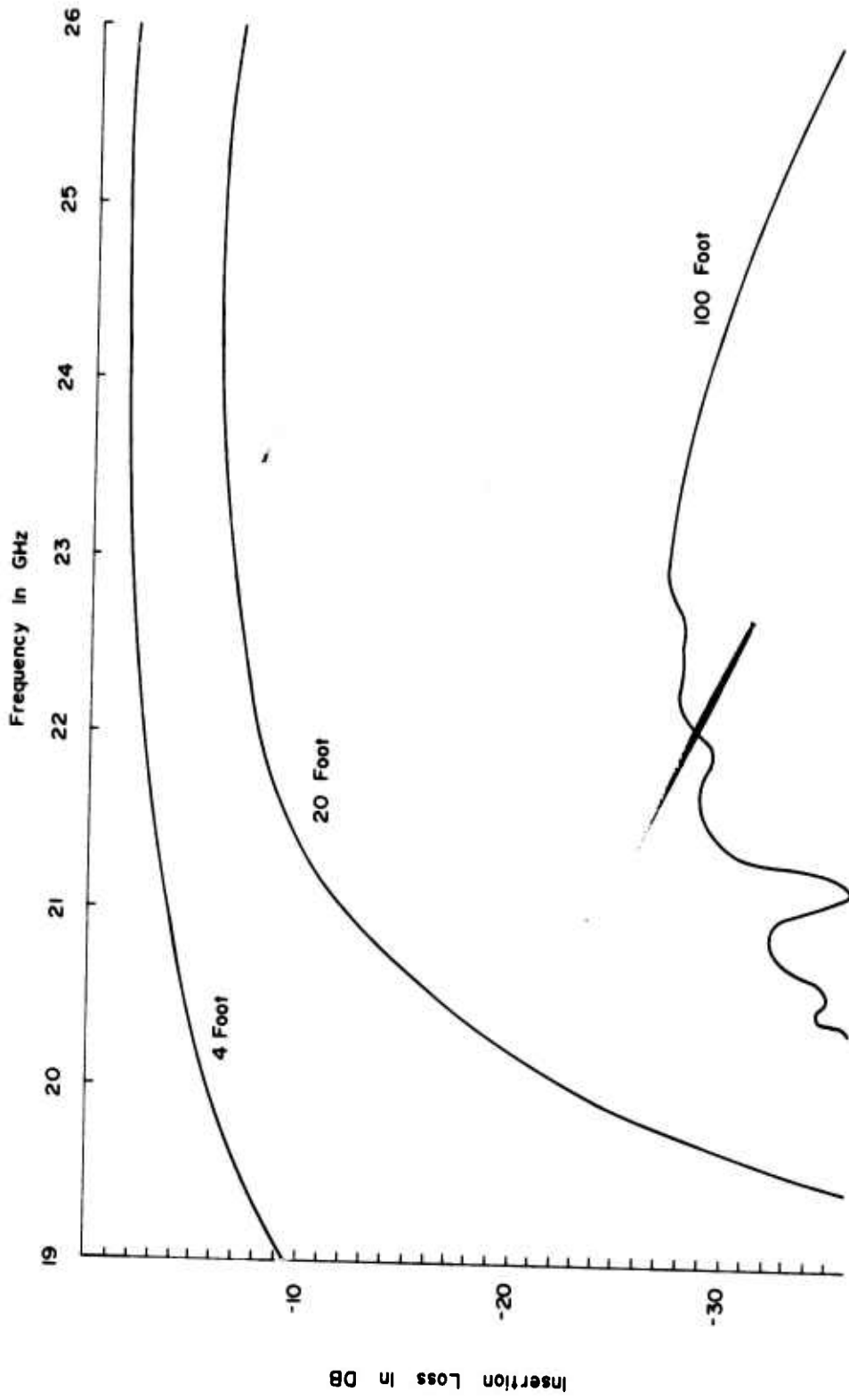


Fig. 37 ATTENUATION CHARACTERISTICS OF THE THREE DATA BUS CABLES

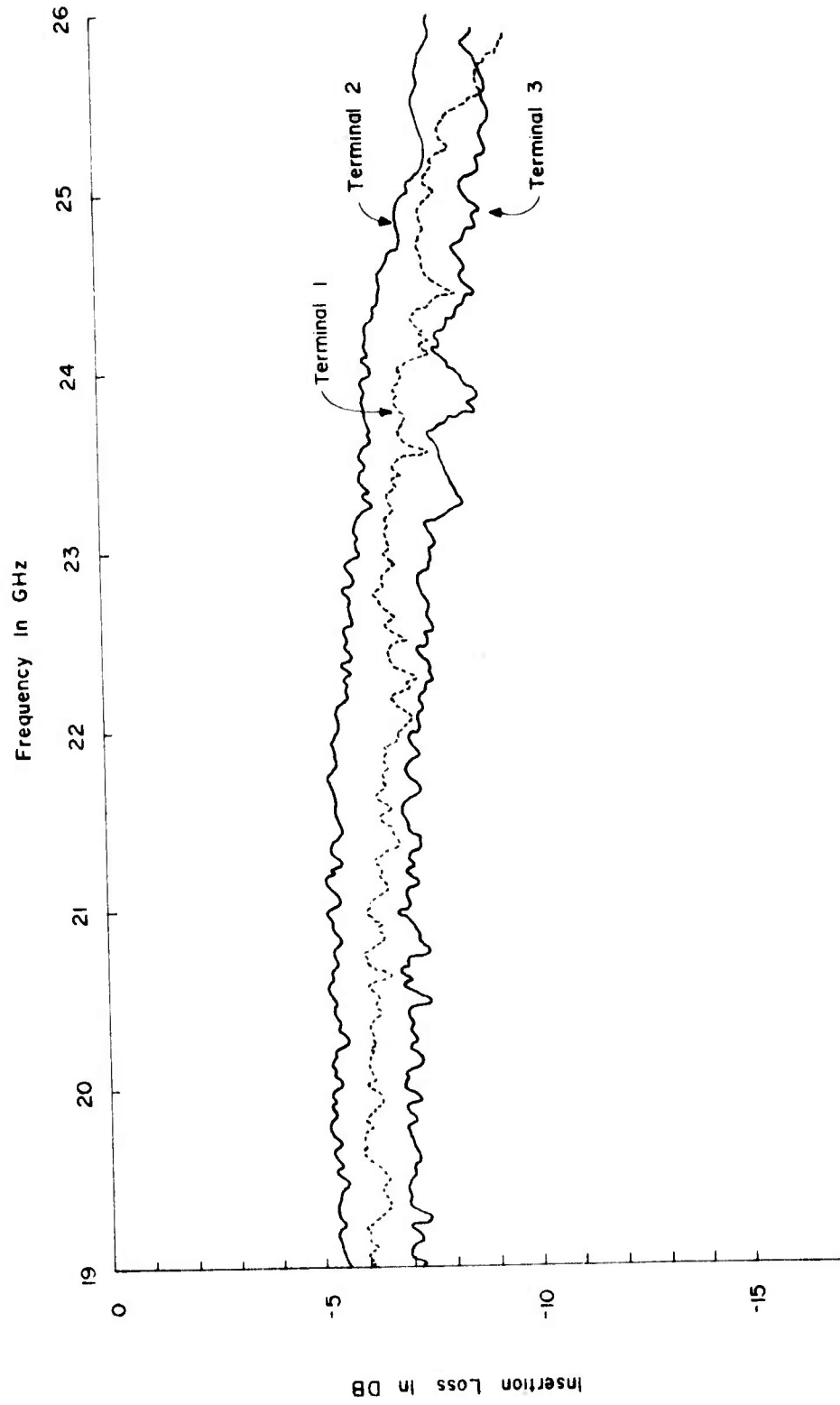


Fig 38 INSERTION LOSS OF THE MILIC MAIN BUS INSIDE THE MODEMS

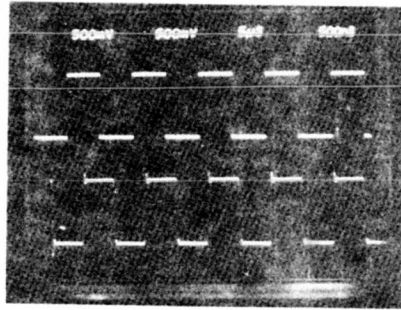


Fig. 39 INPUT DATA WAVEFORMS

Top - 23.0 GHz Channel
 Bottom - 23.5 GHz Channel

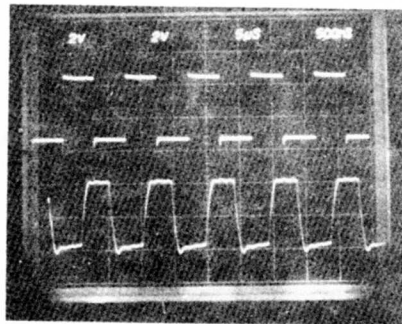


Fig. 40 OUTPUT DATA WAVEFORMS

Top - 23.0 GHz Channel
 Bottom - 23.5 GHz Channel

cables and noting the attenuation that can be added without degrading the receiver output. Some form of standard digital waveform was transmitted for this test, usually a square wave. The test was repeated for all combinations of transmission paths between the three terminal MODEMs. Typical results are given in Table 2.

TABLE 2. Signal Margin Test Results

Channel	Terminal Number of Transmitter	Terminal Number of Receiver	Margin (db)
23.0 GHz	1	2	37
	1	3	15
23.0 GHz	2	1	28
	2	3	20
23.0 GHz	3	1	13
	3	2	13
23.5 GHz	3	2	29

The above results show that for any given combination the signal margin is better than at least 10 db. Such a margin is sufficient for all practical purposes.

6. Conclusions and Extensions

The Model 400 Data Bus System in its present configuration operates with two Frequency Division Multiplexed (FDM) data channels. Transmission of data on both channels can be simultaneously carried out. Data rates of up to about 10 Mb/s on each channel can be achieved. In addition to demonstrating multi-channel operation, the system also has the capability of bi-directional signal flow. For the 23 GHz data may be inputted at any one of the three MODEMs and outputted at any of them. For the 23.5 GHz channel, signal flow is possible only from MODEM 2 to MODEM 3, although this channel capability can be enhanced at a later date.

The Model 400 system also demonstrates the application of tunable narrow-band frequency selective couplers. As discussed in Parts II and IV, such filters result in small insertion loss and are ideal for data bus applications.

During the present program, considerable effort was spent on redesigning the data bus components, such as oscillator, mixer and RF circuitry. This has resulted in a system which is considerably stable and more reliable. This system can be easily extended to include additional channels. In summary, the system demonstrates the capability of dielectric cable and MILIC technology for transferring multi-channel bi-directional data signals on an airborne platform.

SECTION IV

PART III

DATA BUS SYSTEM DESIGN APPLICABLE TO YF-16 FLIGHT CONTROL SIGNALS

1. Introduction

The purpose of this part of the report is to present the results of the study conducted on the dielectric data bus concepts and their application to the YF-16 flight control signals. In the following sections, generalized concepts applicable to the dielectric waveguide data bus system are presented. This is followed by a description of the signal flow requirements of the YF-16 flight control signals. The model of these requirements is presented both in schematic and tabular forms. Finally, a conceptual data bus configuration meeting the signal flow requirements has been presented. It should be emphasized that this configuration shows only one possible means of accommodating the signal flow requirements. Finally, considerations relating to redundancy and data format are presented.

2. Dielectric Waveguide Data Bus Concepts

a. Generalized Block Diagram

A representative dielectric waveguide data bus system is shown in Figure 41 in block diagram form. The important components of the system consist of the dielectric waveguide as the transmission medium, frequency selective ring couplers, MODEMs and the Multiplex Terminal Units (MTU). In the figure, the transmission line is shown to have five stations at which multi-channel signals are either coupled to or extracted from the main bus. At each station, one or more ring couplers can be simultaneously used. A modulated microwave carrier signal centered at a given frequency is coupled to, and/or extracted from, the transmission medium at each ring coupler. In the Frequency Division Multiplex (FDM) concept, one predetermined channel frequency is assigned to only one carrier signal entering the bus from any station. Another signal entering the bus from the same or another station must do so at a different channel frequency. However, any carrier signal at a given channel frequency can be extracted at one or more stations simultaneously.

The flexibility of the system can be shown by an example. Consider the case of a carrier signal at frequency f_5 in Figure 41. This signal enters the bus at station No. 5

SECTION IV

PART III

DATA BUS SYSTEM DESIGN APPLICABLE TO YF-16 FLIGHT CONTROL SIGNALS

1. Introduction

The purpose of this part of the report is to present the results of the study conducted on the dielectric data bus concepts and their application to the YF-16 flight control signals. In the following sections, generalized concepts applicable to the dielectric waveguide data bus system are presented. This is followed by a description of the signal flow requirements of the YF-16 flight control signals. The model of these requirements is presented both in schematic and tabular forms. Finally, a conceptual data bus configuration meeting the signal flow requirements has been presented. It should be emphasized that this configuration shows only one possible means of accommodating the signal flow requirements. Finally, considerations relating to redundancy and data format are presented.

2. Dielectric Waveguide Data Bus Concepts

a. Generalized Block Diagram

A representative dielectric waveguide data bus system is shown in Figure 41 in block diagram form. The important components of the system consist of the dielectric waveguide as the transmission medium, frequency selective ring couplers, MODEMs and the Multiplex Terminal Units (MTU). In the figure, the transmission line is shown to have five stations at which multi-channel signals are either coupled to or extracted from the main bus. At each station, one or more ring couplers can be simultaneously used. A modulated microwave carrier signal centered at a given frequency is coupled to, and/or extracted from, the transmission medium at each ring coupler. In the Frequency Division Multiplex (FDM) concept, one predetermined channel frequency is assigned to only one carrier signal entering the bus from any station. Another signal entering the bus from the same or another station must do so at a different channel frequency. However, any carrier signal at a given channel frequency can be extracted at one or more stations simultaneously.

The flexibility of the system can be shown by an example. Consider the case of a carrier signal at frequency f_5 in Figure 41. This signal enters the bus at station No. 5

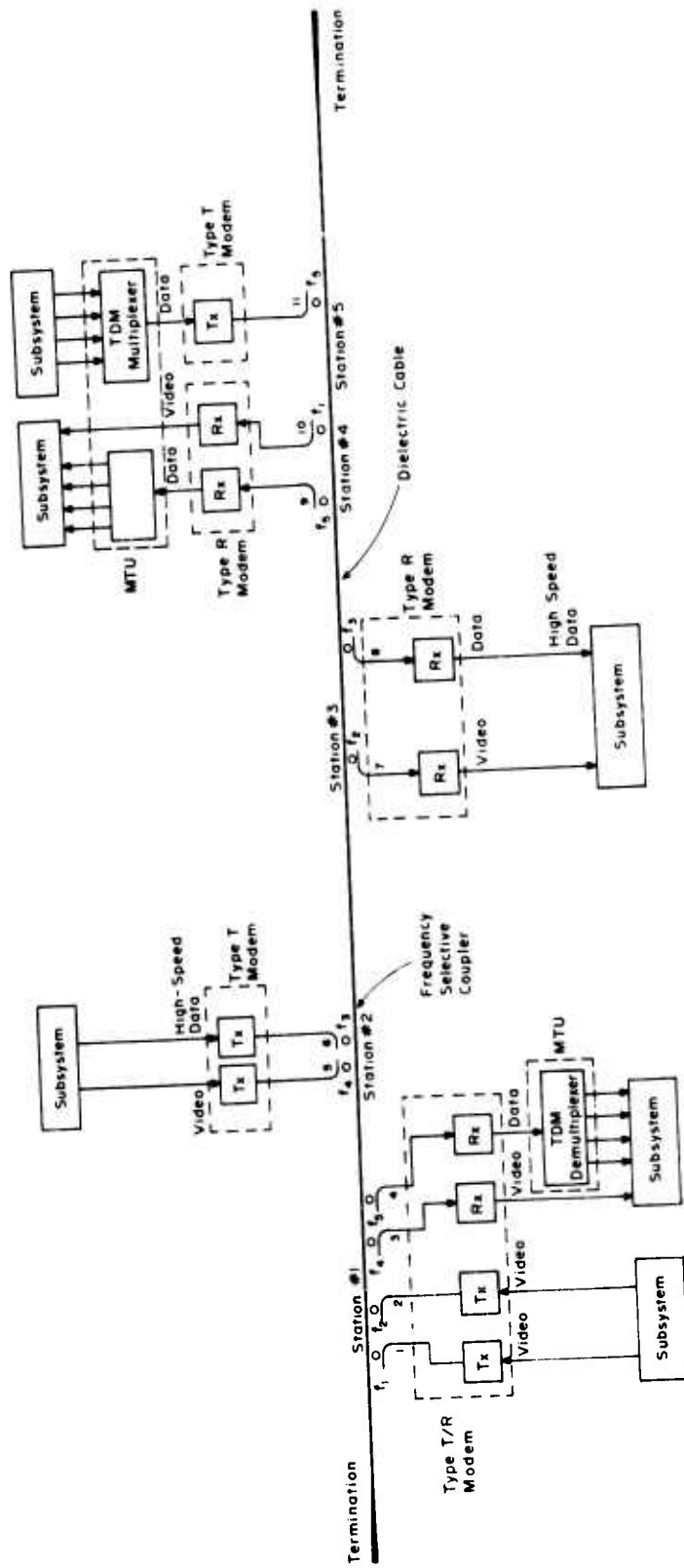


Fig. 41 FDM DATA BUS SYSTEM BLOCK DIAGRAM

(coupler No. 11), and is simultaneously extracted at stations Nos. 1 (coupler No. 4), and 4 (coupler No. 9) respectively. In general, the flexibility of the system allows simultaneous coupling and/or extraction of a total of m signals at any station, each signal being centered at a different frequency. The m signals may all enter or all be extracted from the bus, or some of these signals may enter the bus with the remaining signals being extracted from it in any combination. Furthermore, the value of m may change from station to station. In the figure, $m = 4$ at station No. 1 and consists of two signals entering the bus and the other two signals extracted from the bus. At station No. 2, $m = 2$ with both signals entering the bus and so on. The system configuration of Figure 41 thus offers great flexibility and a modular design feature. It should be noted from the figure that there is simultaneous bi-directional flow of signals along the bus.

The MODEMs serve the purpose of processing the inputs from and outputs to the MTU so as to make them compatible with the carrier frequency signals required for the data bus. For the dielectric waveguide data bus system, the MODEM can perform both functions of transmitter and receiver. Such a MODEM is referred to as a Type T/R MODEM in the figure. Obviously, it can be modularly designed to have just the transmit (Type T) or receive (Type R) features as shown in the figure. Further, it is possible for either type to have a modular capability for the addition of more channels for future expansion. The three terminals of the Model 400 System described earlier in Part II are examples of MODEMs.

The inputs to the MODEM can be either a baseband analog signal or digital data or both. The FDM dielectric data bus system has the flexibility of handling both analog and digital signals simultaneously. Furthermore, these inputs need not all be of the same bandwidth or bit rate. The MODEMs can be individually tailored to accommodate signals of different bandwidths without too much difficulty. The modularity and flexibility of the dielectric data bus system presents a tremendous advantage for any practical system design.

The MTUs serve the purpose of converting the input signals from the subsystems into signal inputs compatible with the input to the MODEMs. Such functions as A/D or D/A conversion, multiplexing, demultiplexing, etc., are performed in this unit. Design of such units is well within the state-of-the-art. In some instances, the signals from the subsystems may be compatible with the requirements of the MODEM inputs. In these cases, the MTU may not be required at all, as shown in the generalized configuration of Figure 41.

b. Duplex Operation

The representative diagram of Figure 41 uses a simple ring coupler arrangement. This technique limits the coupling of the signal in one direction only depending on the orientation of the coupler post with respect to the main line. This is further illustrated in Figure 42a. However, if in a system application it becomes necessary to transmit the signal in both directions, two arrangements for bi-directional coupling are shown in Figure 42b. In the first arrangement, an additional "3 db" coupler is used. The flow of signals in the two directions is shown by solid and dotted arrows. This configuration suffers a 3 db loss due to the additional coupler. In the second arrangement, the same signal is coupled to the main bus by using two separate ring couplers, each operating at a different frequency. Thus, the two-directional signal flow is achieved at two separate channel frequencies. The signal flow directions for the receive and transmit modes are shown in the figure.

c. Coupling Considerations

In a data bus system design, the insertion loss and coupling ratio of the ring couplers must be taken into account. These terms are defined in Figure 43. The insertion loss of the couplers arises due to power split alone and due to mismatch losses, etc. For bandpass ring couplers, the insertion loss due to power split alone is a function of frequency, whereas that due to mismatch, etc., is fairly constant over a wide bandwidth. At frequencies other than the resonant frequency of the ring coupler, the losses due to power split alone are negligible and the total insertion loss is primarily governed by the mismatch losses only. This lies typically in the 0.1 to 0.3 db range. At resonant frequency, on the other hand, losses due to power split alone constitute a major component of the total insertion loss, which lies typically in the 1 to 2 db range, depending on the coupling ratio.

The differences in the insertion loss of the coupler at resonance and at off-resonance are exploited in the data bus applications. This feature may be viewed by considering the coupler as a channel dropping filter in that only those signals tuned to the resonant frequency of the ring are extracted from the main bus. Other microwave signals flowing on the bus are transmitted through the coupler without significant losses. If, instead of the frequency selective ring couplers, wide-band couplers were used, the insertion loss at resonance and at off-resonance would have been approximately the same. Thus, the use of ring couplers offers a tremendous advantage in data bus applications since it reduces the power requirements of transmitters or increases the length of the dielectric cable over which communication can be achieved.



Fig. 42a UNIDIRECTIONAL COUPLING ARRANGEMENT

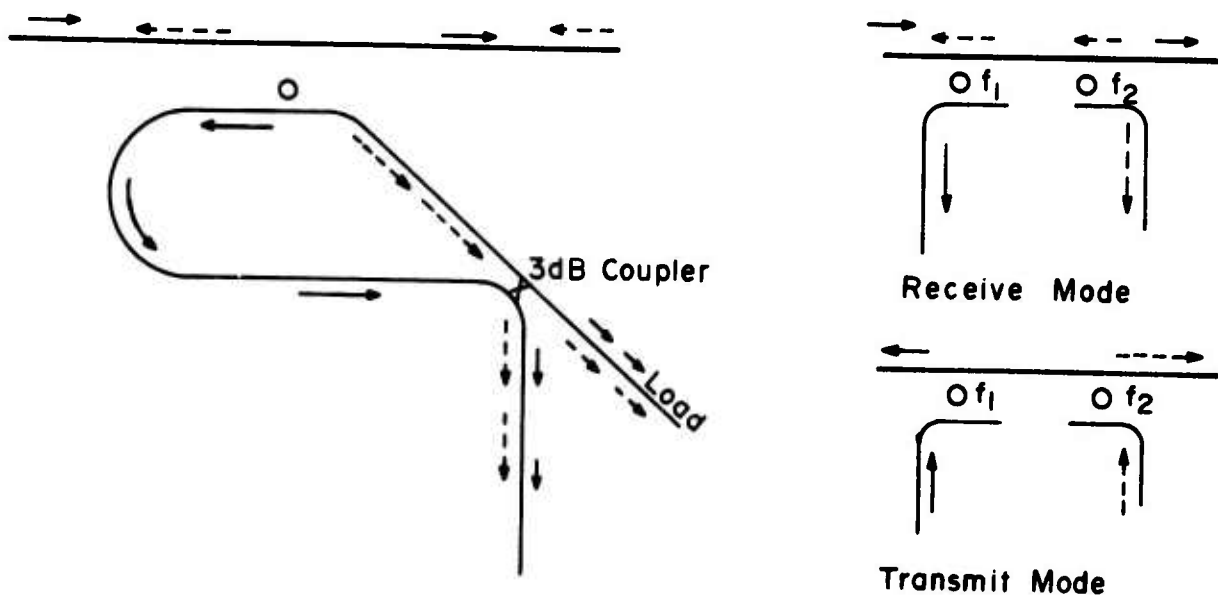
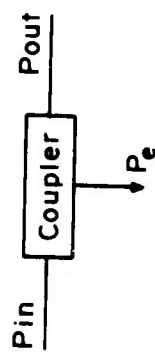


Fig. 42b BIDIRECTIONAL COUPLING ARRANGEMENT



$$\text{Insertion Loss} = \frac{P_{out}}{P_{in}}$$

$$\text{Coupling Ratio } x = \frac{P_e}{P_{in}}$$

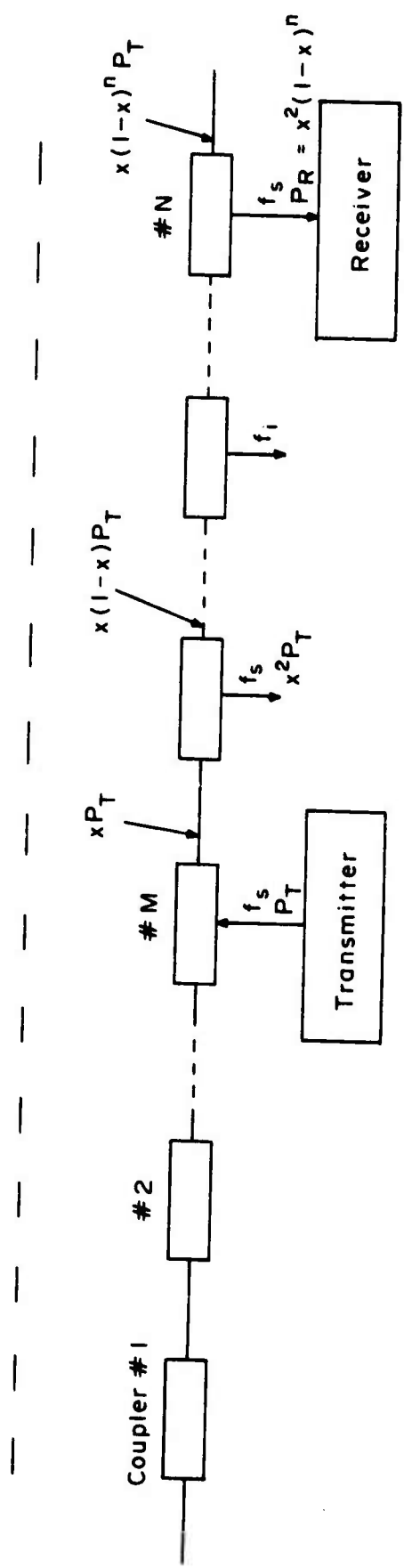


Fig. 43 POWER DISTRIBUTION ALONG A BUS

As mentioned above, the insertion loss at resonance depends on the coupling ratio. An important consideration in system design is to determine the optimum coupling ratio. To do so, consider the generalized model of Figure 43. In the figure, a number of couplers are shown connected to the transmission line. At coupler No. M, a transmitter with power output of P_T is connected and this microwave signal is extracted at coupler No. N into a receiver. Both couplers Nos. M and N are tuned to the same frequency, f_s . Thus, there are $(N-M-1)$ intermediate couplers. From among these $(N-M-1)$ couplers, let us further assume that m number of them are tuned to a frequency other than f_s and the remaining n number are tuned to f_s . Signals at other carrier frequencies are not shown in the figure. We can relate these numbers with the example of Figure 41 for better understanding. Consider the signal at frequency f_s of Figure 41 entering the lens at coupler No. 11 (thus, $M = 11$), and being extracted at coupler No. 4 (thus, $N = 4$). During its passage from coupler No. 11 to coupler No. 4, it passes through a total of 6 (i.e., $N-M-1$) intermediate couplers. From among these couplers, $m = 5$ (Nos. 5, 6, 7, 8, 10) are tuned to a frequency other than f_s , and the remaining $n = 1$ (No. 9) is tuned to f_s . This example illustrates the terminology.

The total insertion loss between the transmitter and the receiver is then given from Figure 43 as follows:

$$\frac{P_R}{P_T} = L = X^2(1 - X)^n + m\ell + \text{cable loss} \quad (27)$$

where

- L = total insertion loss
- X = coupling factor of those couplers tuned to the signal frequency
- ℓ = insertion loss of a coupler tuned to a frequency other than the signal frequency
- m = number of intermediate couplers between signal source and sink, and tuned to a frequency other than signal frequency
- n = number of intermediate couplers between signal source and sink and tuned to the signal frequency.

The optimum coupling ratio is obtained when maximum signal power is transferred between the transmitter and the receiver. This is obtained by solving for

$$\frac{d}{dx} \left(\frac{P_{on}}{P_i} \right) = 0$$

This yields

$$x = \frac{2}{n + 2} \tag{28}$$

Table 3 shows the value of the optimum coupling ratio X for various values of n. These results are plotted in Figure 44a. For n > 20, the optimum coupling ratio lies in the 10 to 15 db range, and does not change significantly. If the number of intermediate couplers n is less than 20, a smaller coupling ratio in the 6 to 10 db range is optimum. It should be emphasized that the coupling ratio varies with n and does not depend on m. Further, the value of n will, in general, vary with different signals because of the relative locations of the transmitters and receivers for these signals. Thus, an optimum value of the coupling ratio for a carrier signal may not be optimum for another carrier signal passing through a different number of intermediate couplers, although in such a case, both signals may flow through some common couplers. In such a situation, it seems reasonable to select 6 db as a coupling ratio for all coupling, assuming that taps are less than 20. Such a value is not too far from an optimum and provides some standardization of components of the data bus.

The insertion loss of a 6 db coupler tuned to the center frequency can now be determined. The loss due to power split alone for various coupling ratios is given in Table 4. For a 6 db coupler, a loss of 1.2 db will be encountered. In addition, a mismatch loss of 0.3 db is assumed, giving a total insertion loss for each a coupler of 1.5 db. This compares with a loss of 0.3 db only for couplers tuned to frequencies other than the signal frequency. If a wide-band coupler was to be used instead of a ring coupler, its loss would also have been approximately 1.5 db at all frequencies. The above conclusion is of significant importance in the data bus context. It shows the advantages of the ring couplers for coupling signals to and from the data bus.

TABLE 3. Optimum Coupling Ratio

No. of Intermediate Couplers n	Optimum Coupling Ratio X in db
2	-3.00
3	-3.98
4	-4.77
5	-5.44
10	-7.78
15	-9.29
20	-10.41
25	-11.30
30	-12.04
35	-12.67
40	-13.22
50	-14.15
60	-14.91
100	-17.08

TABLE 4. Insertion Loss for Couplers

Coupling Ratio	Theoretical Loss Due to Power Split
3 db	30.0 db
6 db	1.2 db
10 db	0.5 db
15 db	0.1 db
20 db	<0.1 db
30 db	<0.1 db

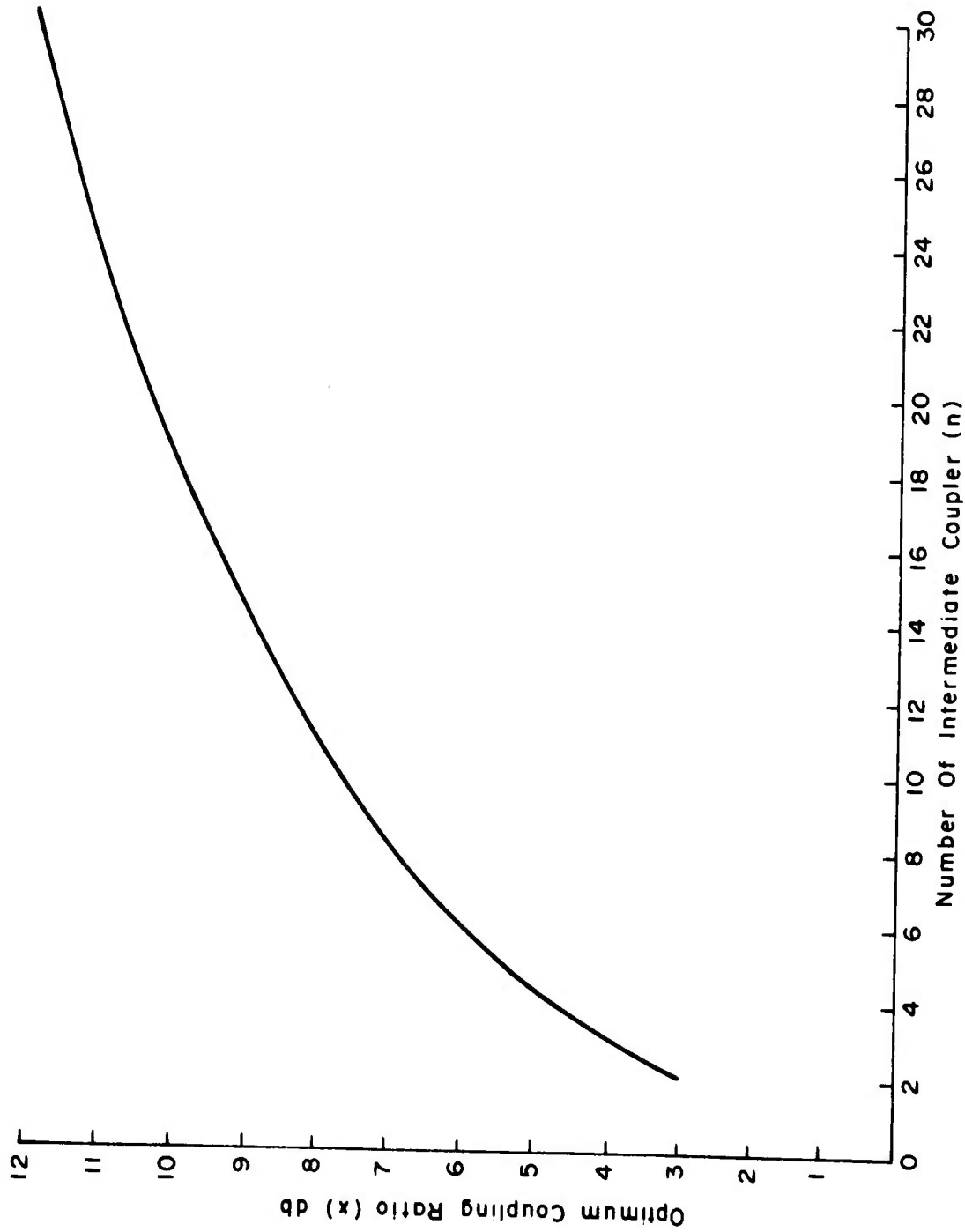


Fig. 44 OPTIMUM COUPLING RATIO

d. Interchannel Interference Considerations

An FDM data bus system can suffer from the problem of interference in the desired channel caused by normal signals in other adjacent channels. Fortunately, for the dielectric waveguide data bus system using frequency selective couplers, this is not a serious problem, as shown below.

In a dielectric data bus system, the rejection of undesired signals from adjacent channels is primarily done at the IF stage of the receiver. The frequency selective couplers provide some additional rejection. If all the signals on the bus at a particular coupler are at equal levels, the selectivities of the IF filter and ring coupler determine the signal-to-interference (S/I) ratio for the desired signal. Typical values of the selectivities of the IF and ring couplers are assumed to be 70 db and 20 db respectively. However, in the data bus, with signals entering and leaving the bus at different points and varying amounts of attenuation along the bus and intermediate couplers, the signal levels may not all be equal at any particular tap. Thus, the actual S/I ratio may not be as large as that established by the IF filter. This is illustrated with the following example.

Consider the situation of Figure 45 in which the data bus is shown to have 20 couplers of 6 db coupling ratio each at desired signal frequencies. Signals at different channel frequencies are shown to enter the bus at couplers Nos. 2, 7, 10, 12, and 20. Any one or all of these signals may be extracted from any desired coupler. In particular, let us consider the case in which signals extracted at coupler No. 1 consist of the desired signal at frequency f_s entering the bus at coupler No. 20 and all other undesired signals at different frequencies entering the bus at other couplers, as shown. Let us further assume that among the 18 intermediate couplers, five couplers are tuned to frequency f_s and the remaining 13 couplers are tuned to other frequencies. It is also assumed that all signals enter the bus at equal levels assumed to be 0 dbm. The level of undesired signal at frequency f_1 at the output port of coupler No. 1 (or alternately at the input of the IF amplifier) is -26 dbm and is due to a coupling loss of 6 db at coupler No. 2 and a 20 db rejection due to the selectivity of coupler No. 1 tuned to frequency f_s . The cable losses have been neglected in this example. The level of desired signal at frequency f_s is -26 dbm and consists of two coupling losses of 6 db each at couplers Nos. 1 and 20, insertion loss of 7.5 db due to five intermediate couplers tuned to f_s at 1.5 db each, and 6.5 db due to the remaining 13 couplers at 0.5 db each. Thus, in this example, the levels of the desired and undesired signals are the same.

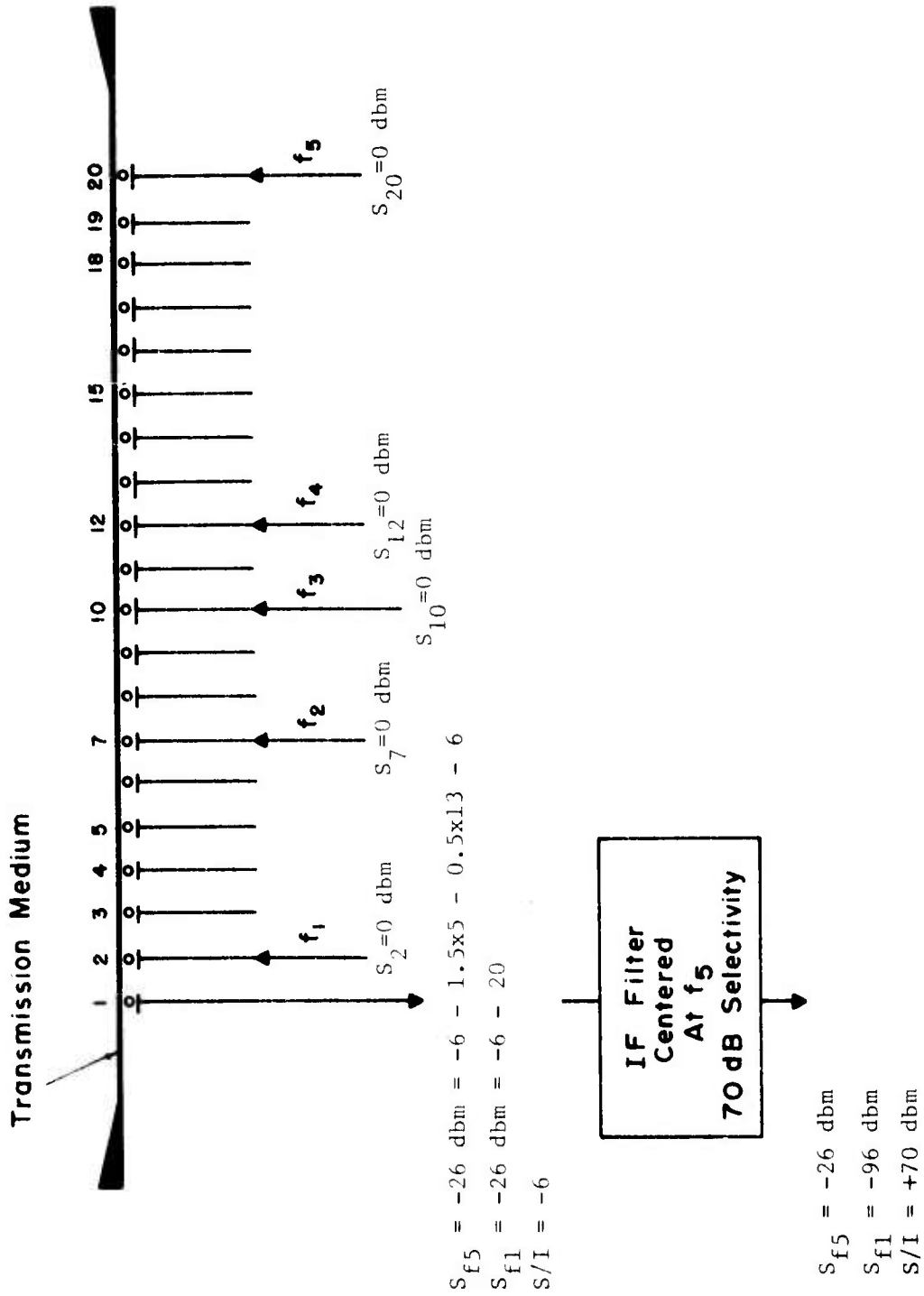


Fig. 45 ADJACENT CHANNEL INTERFERENCE EXAMPLE

Consequently, the IF filter selectivity determines the S/I ratio. If instead of frequency selective couplers, wide-band couplers were used, the undesired signal would not have undergone a 20 db rejection and the S/I ratio at the output of the IF amplifier would have been +50 db. This is still more than adequate. In the above example, if the number of intermediate couplers tuned to f_s was increased from 5 to 18, the signal level at frequency f_s at the output port of coupler No. 1 is reduced to -39 dbm. This is obtained by a 6 db loss due to couplers Nos. 1 and 20, and a 27 db loss due to 18 couplers at 1.5 db each. The signal to S/I in such a case at the output of the IF amplifier will be +57 db. However, it is still quite high and acceptable. This example illustrates that interchannel interference is not a serious problem in the data bus configuration using frequency selective couplers.

3. YF-16 Data Bus System Configuration

a. Introduction

The objective of this study program was to develop a data bus configuration tailored to accommodate the signal flow requirements of a specific platform and to demonstrate the applicability of the dielectric waveguide for such a situation. Flight control signals of the YF-16 aircraft were chosen as an illustrative example. A model of the flight control signal flow requirements for this aircraft was established from a study of information provided by the Air Force. Based on these requirements, a dielectric data bus configuration was developed in block diagram form. It shows the multiplexing and coupling of various signals along the length of the data bus. All the flight control signals are digitized in appropriate number of bits so as to meet the resolution requirements. The system uses both frequency and time division multiplexing and provides for multi-channel bi-directional flow of information along the bus. Finally, additional features for the system such as redundancy and data format are identified.

b. YF-16 Flight Control Signal Flow Requirements

The major components of the flight control system are the sensors, electronic subassemblies and actuators. The relative locations of these components on-board the YF-16 are shown in Figure 46. As shown, most of the sensors and electronic subassemblies related to flight control signals are located in the front of the aircraft. The Leading Edge flap drive unit, the actuators for flaperon, horizontal tail and rudder controls are distributed over the remainder of the aircraft as shown.

The signal flow between various components was examined in some detail. A model of the signal flow is shown in Figure 47 in a schematic form. This information is also provided in Tables 5 and 6. In Table 5, most of the sensor-oriented signals are given, whereas the actuator-related signals are included in Table 6. Figure 47 shows at a glance all the point-to-point wiring that is necessary. The relative locations of the sensors, subassemblies, actuators, etc., are maintained in Figure 47, although this figure is not drawn to scale. In the dielectric data bus configuration discussed in the next section, all of the signal flow is carried on a single cable.

From Figure 47, the Air Data Converter (ADC) accepts inputs from the two Angle of Attack (AOA) transmitters, Flight Control Computer (FCC) and air flow data from the probes. After appropriate processing in the ADC, signals are sent to the Leading Edge (LE) Driver Unit and cockpit instrumentation assembly. The ADC also accepts the feedback signals from the LE driver unit. The Flight Control Computer (FCC) accepts information from the three rate gyros, accelerator assemblies, rudder pedal, sidestick controller and manual trim panel. Signals from these sources are processed in the FCC, which in turn generates five different signals for the five actuators. The FCC also sends several signals to the cockpit instrumentation assembly which also accepts monitoring signals from the five actuators as shown.

The detailed characteristics of the various flight control signals are presented in Table 7. It can be observed that signals are primarily analog and consist of both dc and ac voltages. The bandwidth of each of these signals is on the order of a few tens of Hertz. Consequently, for digitization purposes, a sampling rate of 100 Hz or more will be adequate. The voltage range for these signals varies considerably. For example, the range is ± 0.5 VAC for stick force and 10 VDC for angle of attack. In Table 7, the required resolution of signals, for which information was available, is also given. This signal resolution is then converted into the voltage resolution requirement. Examination of the ratio of the maximum voltage range of a signal to the required voltage resolution shows that it lies typically in the 1000 to 2000 range. However, for certain cases, such as angle of attack, this ratio is 4000. Thus, in order to digitize each of these signals, a minimum of 10 bits to a maximum of 12 bits will be necessary to meet the resolution requirements.

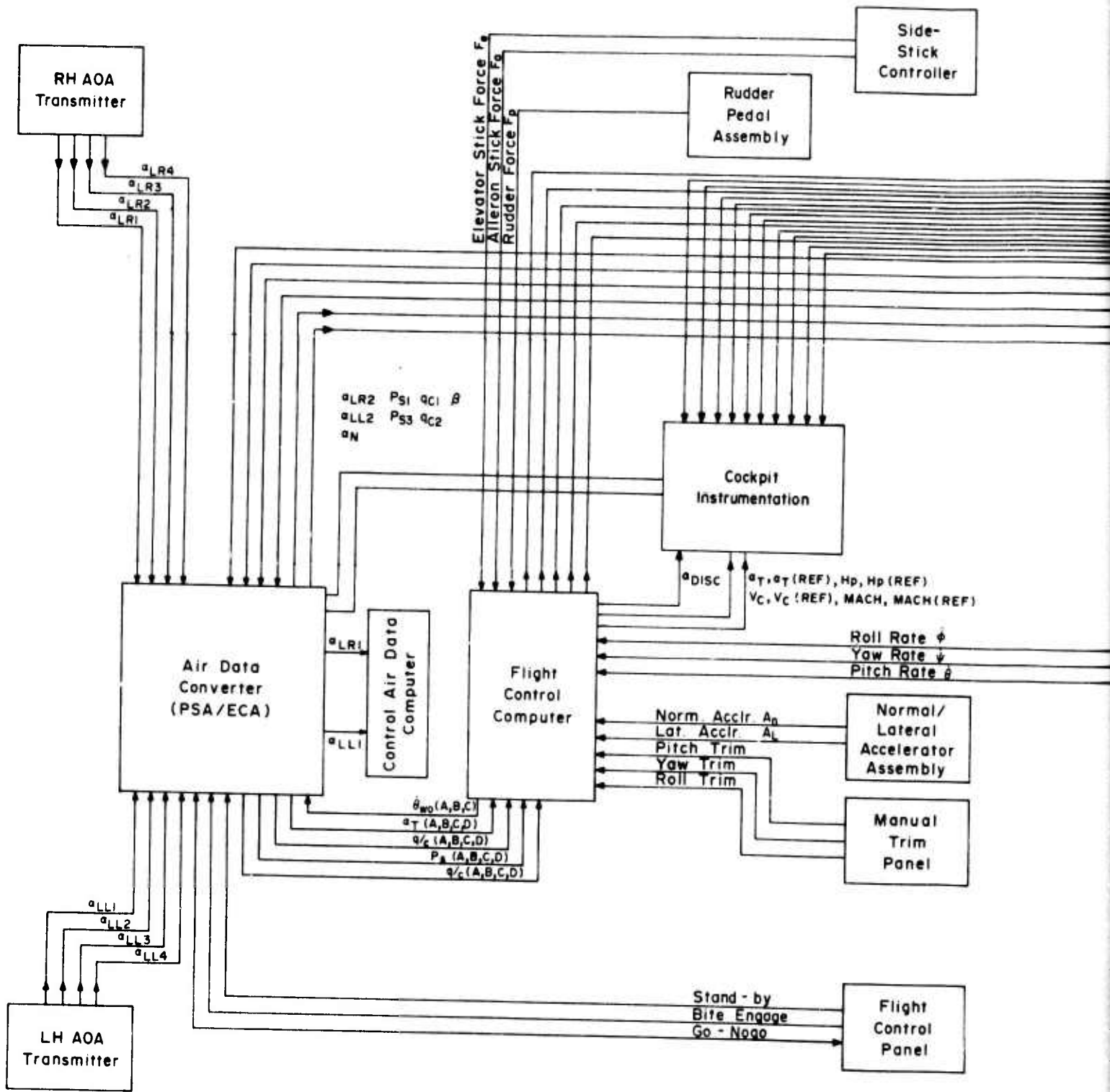
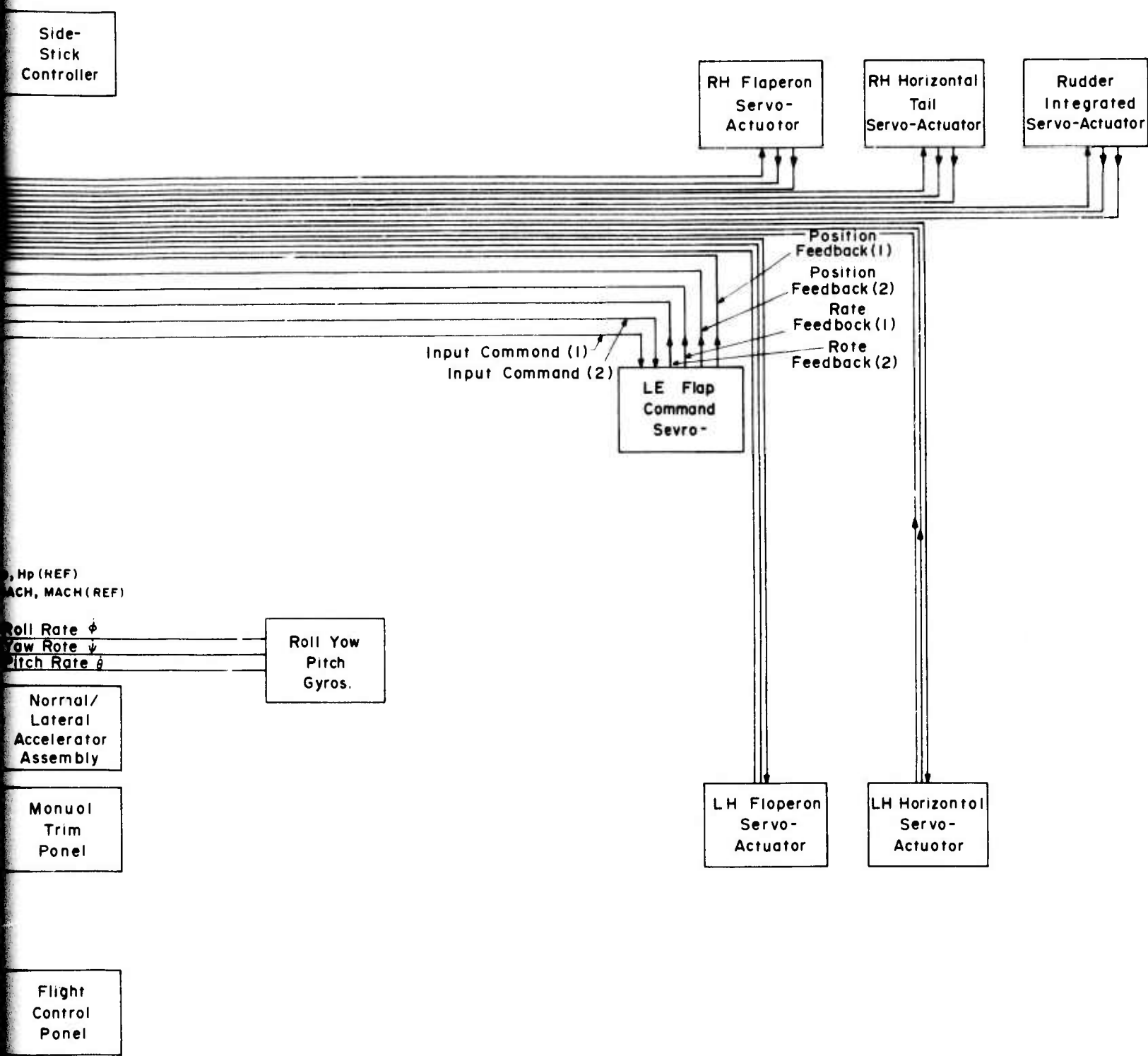


Fig. 47 YF-16 FLIGHT CONTROL SIGNALS



FLIGHT CONTROL SIGNALS FLOW DIAGRAM

2

TABLE 5. Signal Flow Requirements

From \ To	Air Data Converter (PSA/ECA)	CADC	FCC	Cockpit Instrumentation	Flight Control Panel
Right Hand Angle of Attack Transmitter	α_{LR1} α_{LR2} α_{LR3} α_{LR4}				
Left Hand Angle of Attack Transmitter	α_{LL1} α_{LL2} α_{LL3} α_{LL4}				
Air Data Converter (PSA/ECA)		α_{LR1} α_{LL1}	q_c (A, B, C, D) P_s (A, B, C, D) q_c/p_s (A, B, C, D) α_T (A, B, C, D)	α_{LR2} , α_{LL2} , α_N P_{s1} , P_{s3} q_{c1} , q_{c2} , β	Go/No-Go
Flight Control Computer (FCC)	$\dot{\theta}_{wo}$ (A, B, C)			α_T , α_T Ref. H_D , H_P Ref. V_c , V_c Ref. MACH, MACH Ref. α_{DISC}	
Rudder Pedal Assembly			Pedal Force (0 - 6.6 VAC)		
Side Stick Controller			Roll Stick Force (0 - ± 0.6 VDC) Elevator Stick Force (0 - ± 0.6 VDC)		
Normal Accelerometer			Normal Acceleration (+5.88 VAC) (-2.94 VAC)		
Lateral Accelerometer			Lateral Acceleration (4.8 VAC)		
Flight Control Panel	Standby BITE Engage				
Manual Trim Panel			Yaw Trim (0 - ± 7.9 VDC) Roll Trim (0 - ± 14.7 VDC) Pitch Trim (± 15 VDC?)		
Pitch Gyro Assembly			Pitch Rate (5 VAC)		
Roll Gyro Assembly			Roll Rate (16.8 VAC)		
Yaw Gyro Assembly			Yaw Rate (3.75 VAC)		

TABLE 6. Signal Flow Requirements

To From	Air Data Converter (PSA/ECA)	FCC	Cockpit Instrumentation	Leading Edge Command Servo	Right Hand Flaperon Actuator	Left Hand Flaperon Actuator	Right Hand Horizontal Tail Servo	Left Hand Horizontal Tail Servo	Rudder Servo Actuator
Air Data Converter (PSA/ECA)		q_c (A,B,C,D) P_S (A,B,C,D) q_c/P_S (A,B,C,D) α_T (A,B,C,D)	α_{LR2} , α_{LL2} , α_N P_{s1} , P_{s3} q_{c1} , q_{c2} , β	Input Command (1) Input Command (2)					
Flight Control Computer FCC	θ_{wo} (A,B,C)				Servo- Actuator Signal Signal (2.4 VDC)				
Leading Edge Command Servo	Position Feedback (1) Position Feedback (2) Rate Feedback (1) Rate Feedback (2)		P_{s1}						
Right Hand Flaperon Actuator			Monitor (1) Monitor (2)						
Left Hand Flaperon Actuator			Monitor (1) Monitor (2)						
Right Hand Horizontal Tail Servo			Monitor (1) Monitor (2)						
Left Hand Horizontal Tail Servo			Monitor (1) Monitor (2)						
Rudder Servo			Monitor (1) Monitor (2)						

TABLE 7. Signal Characteristics

Signal	Input Gradient	Range	Resolution		Frequency
			Signal	Voltage	
<u>PITCH</u>					
Elevator Stick Force (F_e)	20 mV/#	0.5 VAC			
Pitch Rate ($\dot{\theta}$)	56 mV/deg/sec	± 3 VAC	0.01 deg/sec	0.56 mV	40-60 Hz
Norm. Accl. (A_n)	0.625 VDC/g	± 7.5 VDC	0.01 g	6.25 mV	40-60 Hz
Angle of Attack (α)	0.25 V/deg	10 VDC	0.1 deg	25 mV	
Trim	± 14.3 VDC max	± 14.3 VDC			
<u>ROLL</u>					
Stick Force (F_a)	40 mV/#	± 0.5 VAC			
Roll Rate	56 mV/deg/sec	± 20 VAC	0.01 deg/sec	0.56 mV	40-60 Hz
Trim	± 14.3 VDC max	± 14.3 VDC			
<u>YAW</u>					
Pedal Force	74.3 mV/#	± 5.56 VAC			
Yaw Rate	56 mV/deg/sec	± 5.92 VAC	0.01 deg/sec	0.56 mV	40-60 Hz
Lateral Accl.	0.625 VDC/g	± 1 VDC	0.005 g	0.31 mV	40-60 Hz
Trim	± 7.9 VDC max				
<u>AIR DATA</u>					
Angle of Attack (α_T)	10 VDC/40°	$\pm 40^\circ$	± 0.1 deg	25 mV	
Static Pressure (P_S)	10 VDC/31 in. Hg	0-31 in. Hg	0.0031 in. Hg	1 mV	
Differential Pressure (q_C)	10 VDC/50 in. Hg	0-50 in. Hg	0.005 in. Hg	1 mV	

c. YF-16 Data Bus Configuration

Based on the signal flow requirement of the YF-16 flight control signals, a dielectric data bus configuration has been developed. In this configuration, three physically separate data buses (A,B,C) are proposed, as shown in Figure 48. Data Bus A interconnects signals between LH AOA transmitter, ADC, CADC, FCC, Accelerometer and Rate Gyros. Data Bus B interconnects signals between RH AOA transmitter, ADC, CADC, FCC, and Rudder/Side Stick assembly. Finally, Data Bus C is used to interconnect the LE Driver Unit and all the five actuators with the ADC and FCC. It also transfers signals from the ADC and FCC to the cockpit instrumentation subassembly. Data Buses A and B run to the left hand (LH) and right hand (RH) sides of the front of the aircraft. These lengths are on the order of 20 to 30 ft, depending on actual layout. These two buses carry most of the sensor information to and from the electronic subassemblies. The third data bus, C, carries primarily the actuator information. Its length will typically be less than 100 ft. Each data bus carries signals on a number of FDM channels. Data Bus A is shown to have four channels with their center frequencies being f_{A1} , f_{A2} , f_{A3} , and f_{A4} respectively. Data Buses B and C have respectively three and four channels as shown. The direction of signal flow at each of the channel frequencies is marked on Figure 48. It should be emphasized that the configuration of Figure 48 represents only one possible approach for accommodating all the signal flow requirements. In this approach, the number of FDM channels has been kept small. Some variations in this configuration can be easily accommodated. Further details for each data bus are presented below.

Data Bus A carries the following signals:

- | | | | | |
|--|---|-----------|-----------|-----------|
| • LH Angle of Attack Information | } | Channel 1 | | |
| • p_s (A,B,C,D) | | } | Channel 2 | |
| • q_c (A,B,C,D) | } | | Channel 3 | |
| • q_c/p_s (A,B,C,D) | | | } | Channel 4 |
| • α_T (A,B,C,D) | | | | Channel 5 |
| • Acceleration (normal, lateral) | } | Channel 6 | | |
| • Trim Information (roll, yaw, pitch) | | Channel 7 | | |
| • Rate Gyro Information (roll, yaw, pitch) | | Channel 8 | | |

The above information transfer is achieved by using four FDM channels each centered at f_{A1} , f_{A2} , f_{A3} , and f_{A4} respectively. Bandpass ring couplers are used to couple signals in and out of the bus at each frequency as shown in Figure 49.

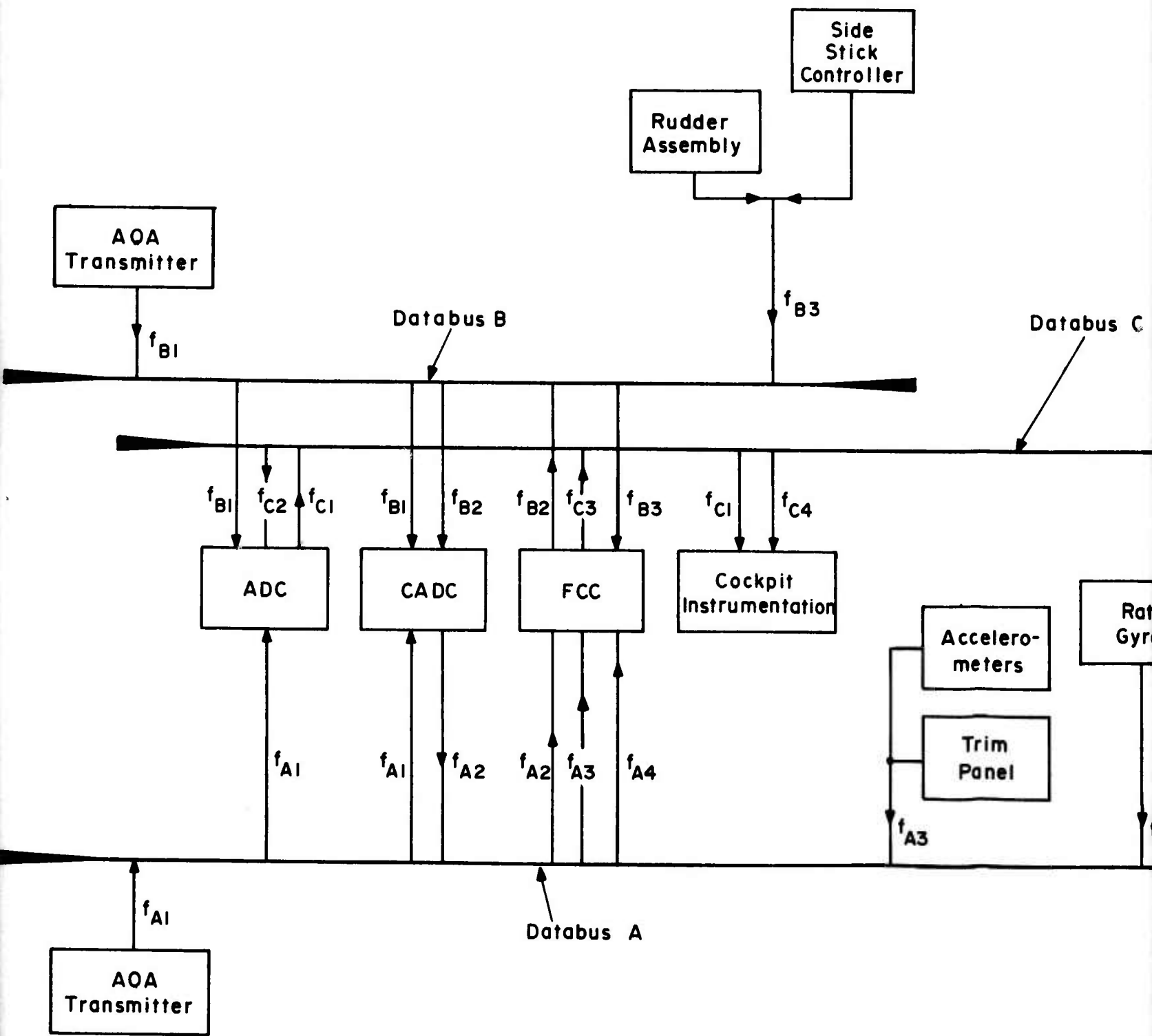
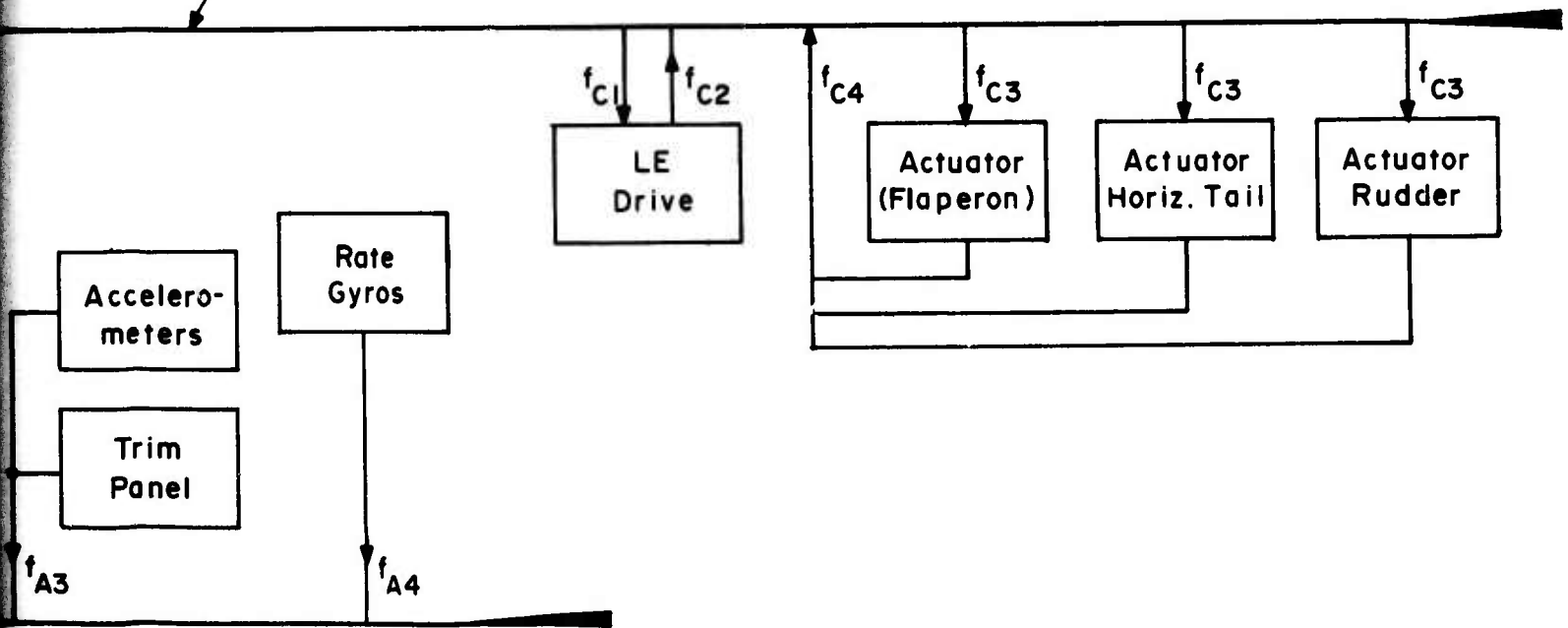


Fig. 48 DATA BUS LAYOUT

or

Databus C



DATA BUS LAYOUT

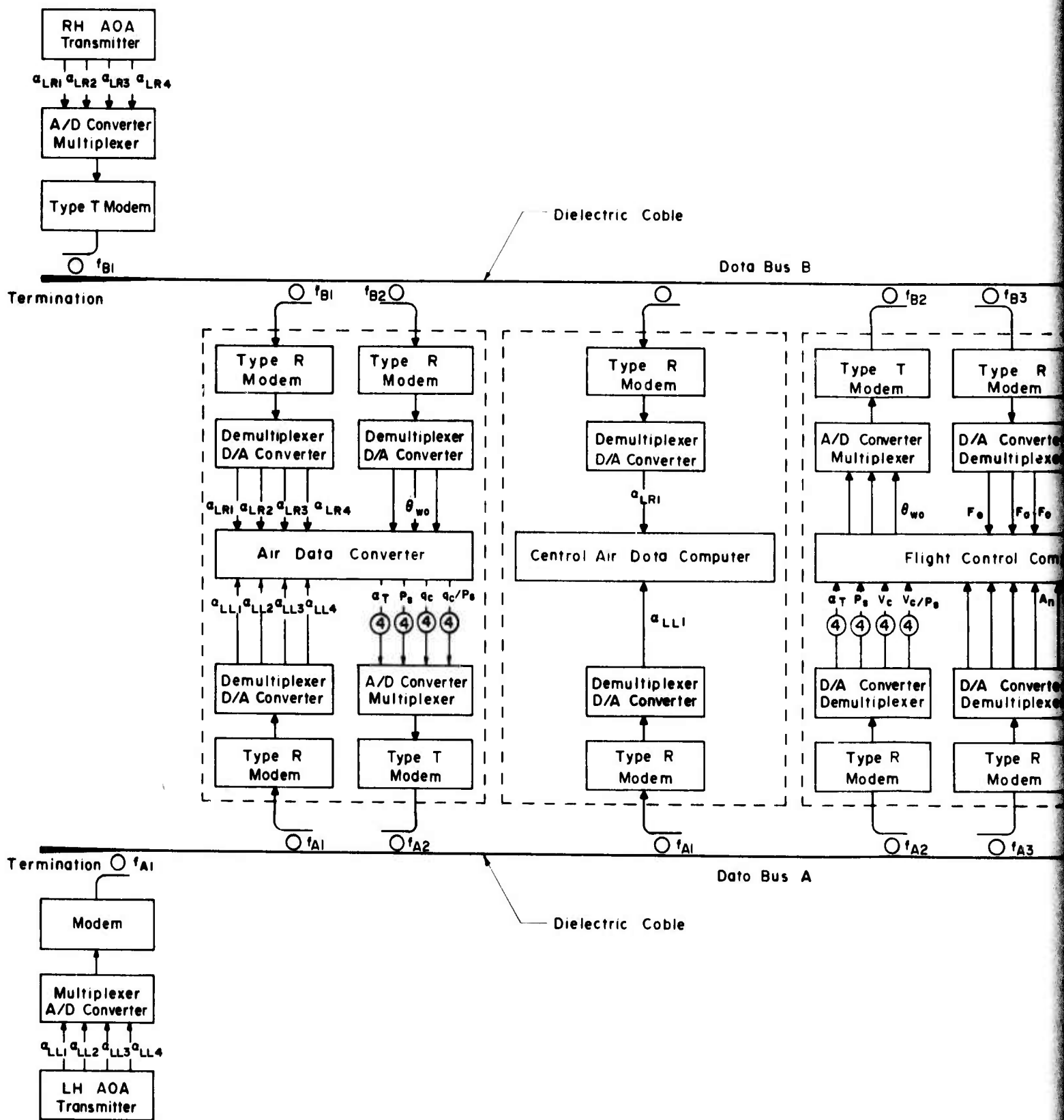
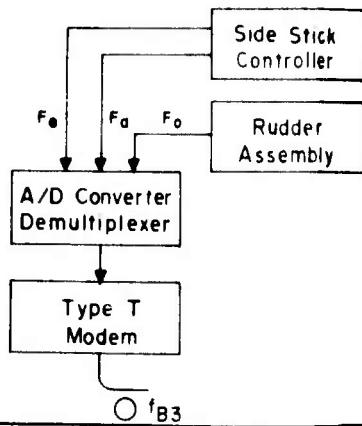
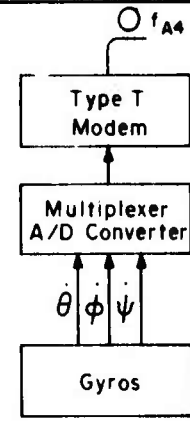
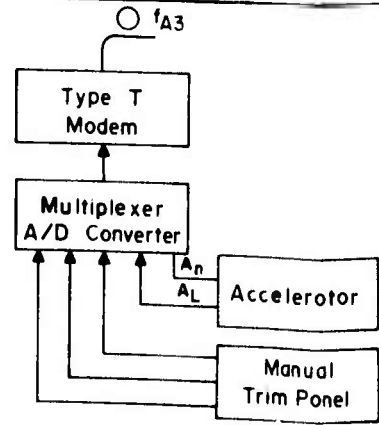
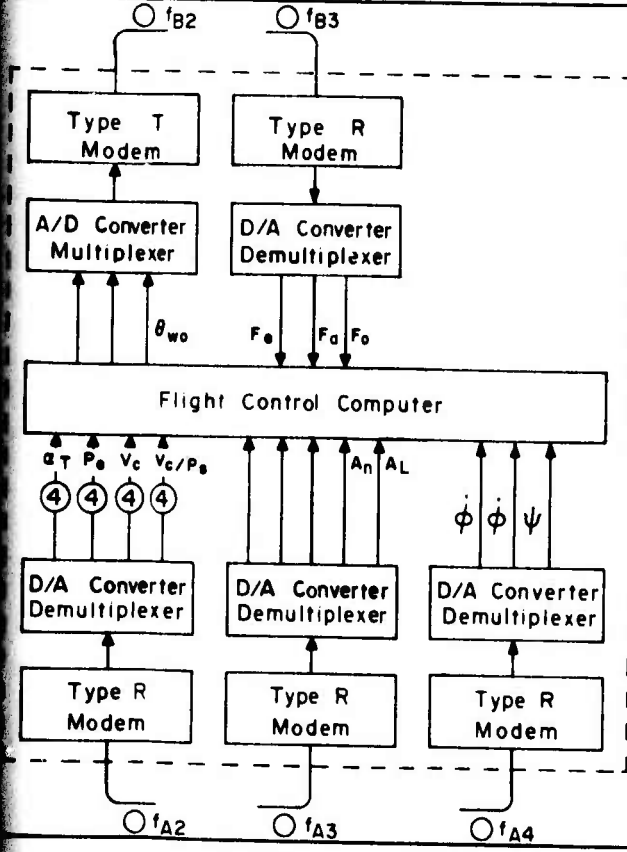


Fig. 49 YF-16 DATA BUS SYSTEM DESIGN



B



Termination

DESIGN

2

The LH AOA information consists of four different signals (α_{LL1} , α_{LL2} , α_{LL3} , and α_{LL4}). Each of these signals is A/D converted and then time division multiplexed to give a composite digital signal. The digital signal is then used in the MODEM to modulate a microwave carrier and coupled to the bus. Assuming a 12 bit binary encoding at a sampling rate of 100 Hz, the data rate for each of the four AOA signals ($\alpha_{LL1} \dots \alpha_{LL4}$) is 1200 b/s. After time division multiplexing, the data rate for the composite signal will be approximately 5 kb/s. Information carried on Channel 1 is extracted at both the ADC and CADC.

All the four AOA signals are extracted by going through demodulation, demultiplexing and D/A conversion. Channel No. 2 of Data Bus A carries information from ADC to FCC. The information consists of 16 different signals. In this case also, assuming a sampling rate of 100 Hz and 12 bit binary encoding, the data rate for the composite signal is given approximately by 20 kb/s (obtained by $100 \times 12 \times 16 = 19,200$). Channel No. 3 on this bus carries the acceleration and manual trim information consisting of five different signals. The data rate for the composite signal is approximately 6 kb/s ($\approx 100 \times 12 \times 5 = 6000$). Finally, Channel No. 4 carries the information from the rate gyros to the FCC. In this case, three different signals are multiplexed, giving a data rate of approximately 4 kb/s for the composite signal.

Data Bus B carries the following signals:

- RH AOA Information Channel 1
- $\dot{\theta}_{wo}$ (A,B,C) Channel 2
- Sidestick and Rudder Forces Channel 3
(F_e, F_a, F_o)

The above information transfer is achieved over three FDM channels centered at f_{B1} , f_{B2} , and f_{B3} respectively. The RH AOA information on Channel No. 1 is processed in the same way as LH AOA signal on Data Bus A. Channel No. 2 of Data Bus B carries the $\dot{\theta}_{wo}$ information from the FCC to the ADC. The bit rate for the composite signal is approximately 4 kb/s. Finally, on Channel No. 3, the side stick and rudder force information is transmitted. The data rate for these composite signals is also approximately 4 kb/s.

Data Bus C carries all the actuator information and signals to the cockpit instrumentation as follows:

- Input Commands (2)
 - α_{LL2} , α_{LR2} , α_N , β
 - P_{s1} , P_{s3} , q_{c1} , q_{c2}
 - Feedback (rate and position)
 - Five Actuator Signals
 - Monitor Signals from Actuators
- } Channel 1
 Channel 2
 Channel 3
 Channel 4

Four FDM channels are used in Data Bus C. In Channel No. 1, the input commands to the LE Driver Units and eight other signals going to the cockpit instrumentation are multiplexed together. This information is then extracted at two locations as shown in Figure 50. The data rate for the composite signal in this case is approximately 22 kb/s. Channel No. 2 carries the four feedback signals from the LE Driver to the ADC. The data rate is approximately 5 kb/s. The five actuator signals from the FCC are multiplexed on one channel. This information is then extracted at three stations and distributed to the actuators. Finally, the fourth channel carries the monitor information from the five actuators to the cockpit instrumentation subassembly.

The information transfer between various sensors/sub-assemblies/actuators is carried out continuously in real time. This simplifies the data format considerably. In this case, a data word needs to consist of only a frame pulse, TDM data stream and parity bit. Destination and other bus command information are not required for this application.

The Model 400 System can operate with either binary, return-to-zero (RZ), non-return-to-zero (NRZ), or Manchester coded signals. However, Manchester coding is recommended in order to be compatible with MIL-STD-1553.

In summary, the configurations of Figures 49 and 50 show that all the signal flow requirements can be easily accommodated using the dielectric data bus concepts. In fact, the Model 400 System described in Part II can be further expanded to four FDM channels and used to test the flow of information by using actual or simulated signals.

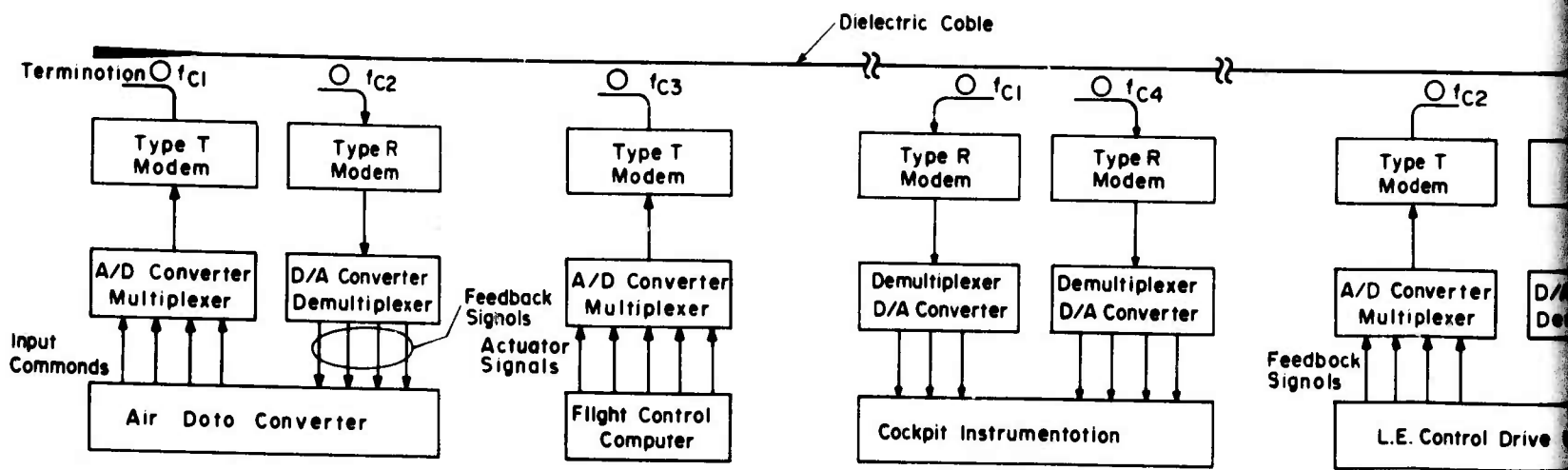
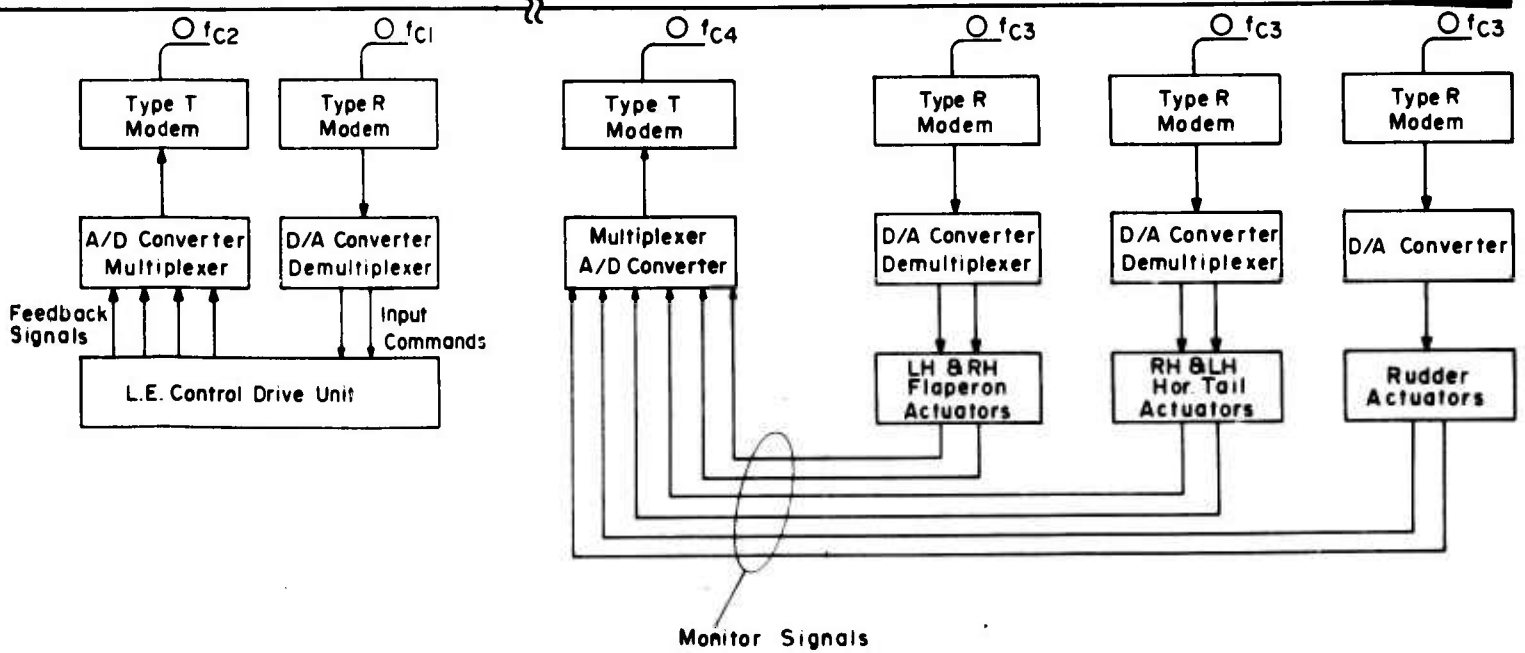


Fig. 50 YF-16 DATA BUS SYSTEM



YF-16 DATA BUS SYSTEM DESIGN

2

d. Redundancy Considerations

In order to ensure the safety of the aircraft, redundancy must be provided for the flight control signals. For the dielectric data bus system configuration discussed in the last section, two types of redundancy can be simultaneously provided. First, redundancy is achieved by transmitting simultaneously the same information on any given channel over two or three other FDM channels on the same cable. This will ensure against failure of the MODEM for any given channel. In addition, physical redundancy can be achieved by using three dielectric cables carrying all the information in parallel. These cables can be routed differently so as to reduce the probability of all three cables damaged simultaneously.

4. Conclusions

The study of the YF-16 data bus system described in this section demonstrates the applicability of dielectric waveguide for use as the transmission medium. The data bus configuration accommodates all the flight control signal flow requirements. The signal flow is achieved by using a number of FDM channels carrying independent data. Three physically separate data buses are proposed. Two of these buses are of relatively short lengths on the order of 20 to 30 ft, while the third bus extends from approximately the cockpit area to the rear of the aircraft. The data rate of signals on each FDM channel is in the 5 to 25 kb/s range. This presents no problems with the dielectric data bus. In fact, a considerable amount of additional data capacity is available on the bus and can be used to transfer other information such as TV or other avionics signals. To ensure safety of flight, redundancy provisions are also provided. Redundancy can be achieved not only by providing additional dielectric cables, but also by adding more channels on the same bus. While additional dielectric cables provide protection against damage to the cable, more channels on the same bus provide protection against equipment failure in any channel.

SECTION V

CONCLUSIONS AND RECOMMENDATIONS

The overall program has resulted in the following:

- Improvement and expansion of the Model 400 Dielectric Waveguide Data Bus System
- Development of a new tunable bandpass ring coupler
- Development of a dielectric data bus configuration applicable to YF-16 flight control signals.

The Model 400 Data Bus System was expanded to include an additional FDM channel. Furthermore, the MILIC and other components of the terminal MODEMs were redesigned so that the present system is more reliable and stable. The two FDM channels of the present system can carry digital data at rates of up to about 10 Mb/s over about 100 ft of dielectric cable. In order to facilitate addition of the second FDM channel into the Model 400 System, frequency selective tunable ring couplers were developed in MILIC technology. Such couplers offer considerable advantages over wide-band couplers as explained in this report. In this context, a new coupler design providing a tunable feature was invented. The availability of this tunable feature simplifies the alignment procedures considerably. Finally, during a study program, a dielectric waveguide data bus configuration applicable to YF-16 flight control signals was developed. The system accommodates all the signal flow requirements. The system has considerable excess capacity so that TV or other avionics signals can also be carried over the same data bus. This program has thus not only resulted in the demonstration of multi-channel bi-directional flow of signals on dielectric waveguide, but also has shown the applicability of dielectric data bus concepts to a specific aircraft (YF-16).

It is highly recommended that the present Model 400 System be integrated with some actual flight control sensors/actuators, etc. By interfacing the sensors/actuators with the Model 400 MODEMs through appropriate multiplexing units, performance of the actual signal transfer can be evaluated. During this evaluation phase, more channels can be added to the Model 400 System in order to configure the complete YF-16 data bus system presented in this report.

While the Model 400 Data Bus System meets almost all the requirements for such systems, it suffers from a drawback as far as its size and weight are concerned. It is therefore proposed that future efforts in dielectric waveguide systems

should be aimed at reducing size and weight. This can be achieved by operating at a higher millimeter-wave frequency (such as 60 GHz) and designing the MODEMs keeping size and weight considerations in mind.

APPENDIX

MILLIMETER IMAGE LINE INTEGRATED CIRCUITS (MILIC)
TECHNOLOGY

APPENDIX

MILLIMETER IMAGE LINE INTEGRATED CIRCUITS (MILIC) TECHNOLOGY

1. Introduction

To be useful, an integrated circuit technique must employ a waveguide that is surface-oriented and capable of fabrication by some kind of planar technique. The Millimeter Image Line Integrated Circuit (MILIC) technology described below is a true planar integrated circuit technology and has very desirable attenuation properties within the wavelength of interest (1.5 to 30 mm). Over the last few years, considerable progress has been made in the development of a family of passive and active signal processing components so as to make use of this technology possible for building integrated systems. Within this Appendix, various aspects of this technology will be discussed. Topics include: the insular and image waveguide and circuit components, transmission line properties, passive and active components, integrated assemblies, etc.

2. The Insular Guide

The insular waveguide and its special case, the image waveguide, are both dielectric waveguides in which both horizontal-plane and vertical-plane guiding take place because of refractive effects between the dielectric and surrounding media. This is an approach different from conventional waveguide structures (such as metal tubular guide, microstrip, slot line and others) in which metal structures determine the guide path of the transmission line. The primary advantage of the insular/image waveguide approach for microwave integrated circuits (MICs) is lower waveguide attenuation and high component Q. In receivers, this means improved noise figure; in transmitters, it means better oscillator stability; in highly selective circuits, it means narrower filter bandwidth.

The insular waveguide configuration is shown in Figure A-1. It consists of a high permittivity rectangular dielectric waveguide resting on a low-permittivity substrate which, in turn, rests on a high-conductivity ground or image plane. Generally speaking, the waveguide dielectric constant should be about six or greater and can extend upwards toward 100. The dielectric substrate should have a dielectric constant of 2.6 or less. Low-loss dielectric and ceramic materials are available to meet both dielectric requirements.

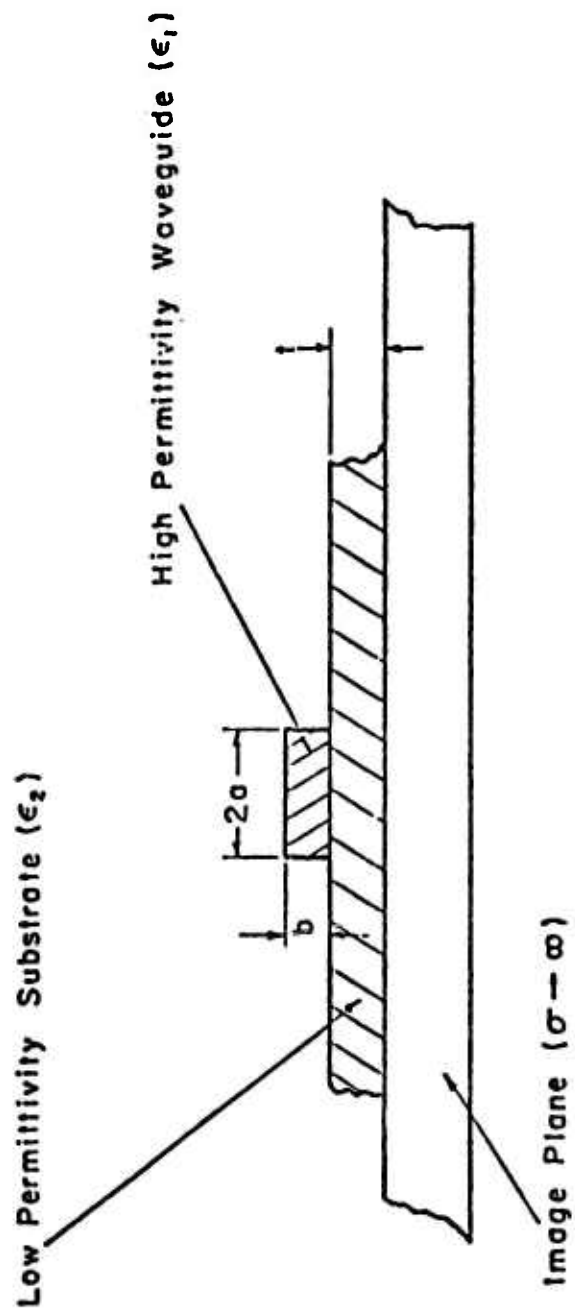


Fig. A-1 THE HIGH PERMITTIVITY INSULAR WAVEGUIDE

3. The Image Waveguide

The special case of the insular waveguide where $t = 0$ is known as the high-permittivity rectangular image waveguide. This configuration is shown in Figure A-2. It is also a low-attenuation waveguide, but the attenuation factor will exceed that of the insular guide due to losses in the ground plane. Depending on the thickness t of the isolating substrate, the ground plane losses in the insular waveguide can be reduced or virtually eliminated.

The image line was considered as a form of waveguide in the 1940's and 1950's. The early investigations were limited to the semicircular dielectric image line in which low permittivity ($\epsilon_r \approx 2.5$) materials were used. Because only low permittivity materials were used, the early investigators found that the image line showed rather poor guidability. That is, unless a rather large radius of curvature was used, the line had a tendency to radiate significant amounts of the energy it was guiding.

Early work also included investigations of passive devices. Launchers from waveguide, horns, wires and slots, and coaxial cables were designed. The image line as an antenna was evaluated. Various forms of dielectric resonators were also considered as well as directional couplers. Very little practical value was derived from the early work, primarily because of the low-permittivity materials used and the resulting tendency towards radiation at curves and discontinuities.

The dielectric image waveguide (or the insular waveguide), even though it is an open form of waveguide, has been shown to be a useful and practical waveguide by using high-permittivity dielectric material. The image line is a refractive waveguide in which guiding takes place because of velocity slowing in the guide medium. The confinement of the energy to the guide depends primarily on the index of refraction and, to a lesser extent, on frequency and guide dimensions. It has been shown in experiments at IITRI that a significant improvement in guidability is realized by increasing the relative permittivity to six or greater. Guides with permittivity as high as 90 have been fabricated.

The demonstration of useful guiding, the availability of theory for the high-permittivity rectangular image line, and the development of several passive and active devices in X-, Ku- and V-bands now make it a very attractive technology for use at the millimeter wavelengths.

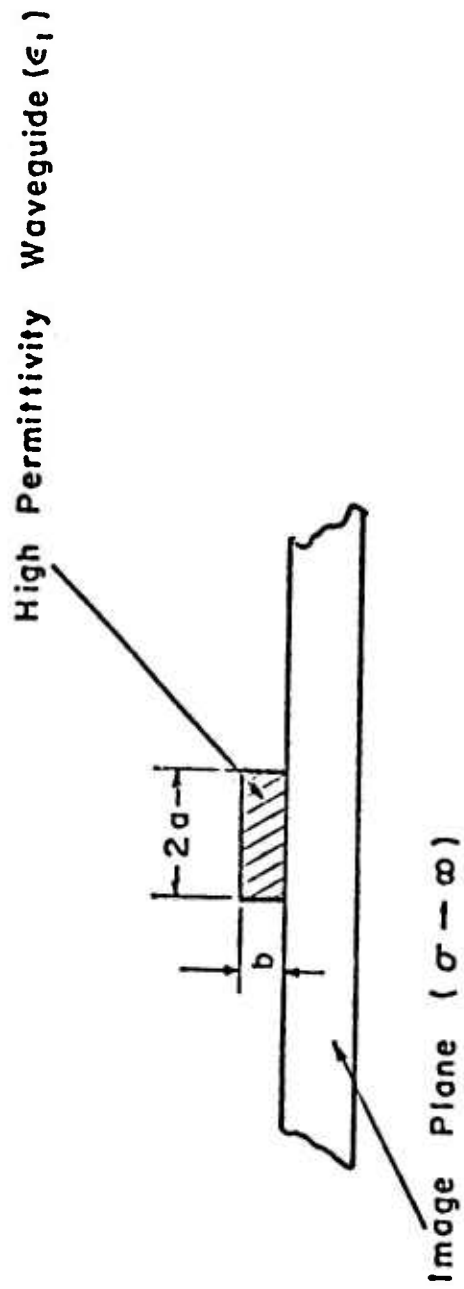


FIG. A-2 THE HIGH PERMITTIVITY IMAGE WAVEGUIDE

4. Properties of Insular and Image Waveguide

The various transmission line properties of the two waveguide forms shown earlier in Figures A-1 and A-2 are reviewed below. Basically, the analysis of the image waveguide, its modes, losses and coupling properties, is largely completed. Beyond these basic properties, consideration has also been given to radius of curvature, power handling capability, isolation, temperature effects, and bandwidth as discussed in sections below.

Throughout much of the discussion which follows, the terms image and insular waveguides will be used virtually interchangeably except when the properties of one or the other configuration become of particular importance to the particular topic under consideration.

a. Modes and Guide Wavelength

The image guide of rectangular cross section $2a$ by b supports, through total internal reflection, a family of hybrid modes designated as E_{mn}^y . The subindices state the number of extrema (m in the x direction and n in the y direction) of the electric or magnetic field components. These modes are essentially TEM modes with their electric field virtually along y (vertically) and magnetic field along x (horizontally). The fundamental mode is E_{11}^y , whose field amplitudes have one maximum in each direction of the guide's transverse plane. It is of interest here to note that the E_{11}^y has a cutoff frequency of zero,* whereas all higher-order modes have a nonzero cutoff frequency.

Dispersion curves (guide wavelength versus frequency) for various guide dimensions and dielectric constants are quite similar to those of a rectangular metallic waveguide, except that the fundamental mode E_{11}^y has zero cutoff frequency. For single mode operation, the choice of the guide cross sectional dimensions must be based on the cutoff frequency of the next higher-order mode, which, for an aspect ratio of $a/b > 1$, turns out to be the E_{21}^y mode. On the basis of the dispersion curves, it has been established that an aspect ratio of $a/b = 1$ provides the maximum separation between the E_{11}^y and E_{21}^y modes, and therefore the maximum single-mode operating bandwidth for a given dielectric constant. Consider, for example, the interesting case where the waveguide core is alumina ($\epsilon_r = 9.0$,

*In practice, the dielectric image guide has a "cutoff" defined by the inability of the guide to suitably control the direction of the propagating waves along a curved section of waveguide.

$a/b = 1$). It is found that the normalized height of the guide defined as

$$B = \frac{4b}{\lambda_0} \sqrt{\epsilon_r - 1} \quad (\text{A.1})$$

must lie in the range

$$1 \leq B \leq 1.34 \quad (\text{A.2})$$

where the lower bound is dictated by the practical requirement of good guidability, i.e., low radiation loss in curved guides, at low frequencies. Thus, at 9.3 GHz and for $B = 1$, the cross sectional dimensions for the image guide are $2a = 0.250$ in. by $b = 0.125$ in. For 60 GHz operation, the alumina image waveguide dimensions would be approximately 0.025×0.050 in. At 94 GHz, the alumina image waveguide dimensions would be approximately 0.025×0.030 in.

b. Losses in Insular and Image Waveguide

Theoretical as well as experimental results of conductor and dielectric losses in the image waveguide reveal that conductor losses predominate despite the fact that the image guide has a single conducting wall (ground plane). One possible way of completely eliminating conductor losses is to replace the ground plane by a low ϵ_r dielectric substrate. In practice, however, the unavailability of a conducting ground plane is undesirable from the viewpoint of device mounting and the absence of a good heat sink for various devices. The best compromise appears to be the insular waveguide shown in Figure A-1. This proposed waveguide configuration is a slight variation of the image waveguide, and as such its propagation characteristics should be similar to those of the corresponding image guide, provided the insulation layer has a low dielectric constant with respect to that of the waveguide core. If that is the case, the fields would decay exponentially from the lower interface of the waveguide core into the insulation. Considering the fact that the fields decay very rapidly outside the guide, one would also expect that the induced current distribution in the ground plane would decrease accordingly as the thickness of the insulation is increased.

Recent experimental results in J-band indicate that only a very thin insulating layer is required to dramatically reduce conductor loss. Measurements of alumina ring resonators in the image line configuration gave unloaded Q_s of about 4500. The waveguide cross section was 0.100×0.200 in. Inserting a

0.010 in. thick teflon insulating layer increased the Q to 9000. This Q is 1.6 times higher than expected in silver-plated air-filled waveguide at the same frequency.

c. Isolation Between Waveguides

Considering the nature of the image guide structure, it is essential that the problem of isolation between waveguides be thoroughly examined. As mentioned previously, there are actually two distinct mechanisms that affect the isolation between two image guides or an image guide and a metallic plate that might be part of the waveguide package. These are: (a) proximity effects due to field extent, and (b) radiation effects due to either abrupt discontinuities or curved waveguide sections.

It has been determined that the fields decay exponentially outside the waveguide in both x- and y-directions. Theoretical calculations show that fields outside the image guide decay very rapidly indeed. For example, placing a metallic wall or obstacle about an inch away at 10 GHz from the air/dielectric interface of the image guide would scatter fields that are at least 58 db down from those at the guide interface. This level of isolation between the scattered back fields or field coupled from one waveguide to another nearly will be sufficient in most cases to isolate circuit functions which use the image guide as a transmission medium.

However, it is well known that, when two open waveguides are placed in proximity to each other, a certain percentage of power per unit length is transferred from the primary (source) to the secondary guide, and that eventually, if sufficient coupling length is provided, most of the power will end up in the secondary guide. Theoretical calculations show that for typical cases, at an operating frequency of 10 GHz, the coupled field into the output port of the secondary guide would be -67 db with respect to the field at the input port of the primary guide for a length of $l = 0.151$ in. which decreases to -47 db for $l = 1.51$ in. Further, theory shows that the isolation between guides increases substantially as frequency of operation increases. To further increase isolation, the separation between guides must be increased.

d. Effects of Temperature

The effect that temperature variations have on circuit performance is manifested in two ways. First is the effect of temperature on transmission line properties, and second is the effect of variations of transmission line properties on specific circuit components. In this section, consideration will be given to the effect on transmission line properties of temperature change.

By far the most important parameter which describes the transmission line in relationship to distributed circuit components is the waveguide wavelength λ_g . This parameter is, of course, related to the propagation velocity of the wave in the waveguide. If the guide wavelength changes with respect to the physical length of a device, or vice-versa, then the behavior of the device is usually affected. The frequency of a resonator or the coupling of a directional coupler will usually change as a result. Such properties as operating bandwidth, circuit isolation, and impedance are generally affected in only a second-order way by temperature variations and will not be considered in this discussion. Temperature dependence of the loss tangent may be severe in some materials and should not be ignored in material selection.

The present consideration then reduces to changes of guide wavelength or physical dimensions due to temperature variations. To a first approximation, the guide wavelength depends on $\sqrt{\epsilon}$. Therefore, the dependence of λ_g on temperature change in the dielectric of the waveguide is:

$$\lambda_g \approx \frac{TC}{2}$$

where TC is the temperature coefficient of ϵ . The TC is unitless and generally is expressed in parts per million per degree centigrade.

The coefficient of linear expansion (CLE) of the dielectric waveguide affects circuit components directly and, therefore, affects the relationship of guide wavelength to the physical length of the waveguide. Thus, a change in physical length will directly affect the length of a coupler or resonator. Changes in cross sectional dimensions will affect guide wavelength (velocity), but this is a second-order effect which will be small in the usual circuit. Thus, in discussions of temperature effects on circuit components, the magnitude of the CLE and the polarity and magnitude of TC/2 should be of primary importance.

e. Bandwidth of the Waveguide

The operating bandwidth of the dielectric image or insular waveguide is determinable from the dispersion curves. The upper frequency limit is determined by the ability of the waveguide to support the first higher order mode (the same limitation that exists in metal waveguides). The lower frequency limit is less easily defined. It approximates a type of cutoff condition but is characterized by poor "guidability" rather

than very high attenuation as in metal waveguide. Also, it is impossible to specify exactly the lower frequency (and thus the bandwidth) without knowledge of the minimum radius of curvature (and the maximum allowable attenuation due to radiation) to be used in the waveguide circuitry.

Therefore, a number of parameters are required before the operating bandwidth can be specified. The parameters of primary importance are:

Dielectric constant	ϵ
Aspect ratio	a/b
Minimum radius of curvature	R_{\min}
Maximum allowable attenuation due to radiation from curved waveguide	α_{\max}

Allowing for some variation in the lowest possible operating frequency, the bandwidth of the waveguide will be in the range 35 to 50 percent for an alumina waveguide with $a/b = 1:1$.

5. Image Waveguide Passive Components

Over the last few years, several passive waveguide components have been successfully built and demonstrated at IITRI and other organizations. The state-of-the-art in some of these components is very well documented and, therefore, we shall not present a detailed description here. It is sufficient to say that the following components have been built and tested at IITRI and their typical performance is as follows.

a. Directional Couplers

Directional couplers using two parallel coupled lines of dielectric image or insular waveguide have been developed for use in MILIC systems from Ku- to V-band (12 to 75 GHz). The coupling obtainable in these MILIC couplers can be varied from almost a total transfer of energy to very loose coupling. The directivity of these devices has been measured and found to be on the order of 20 db or greater.

b. Ring Bandpass Filters

A resonant dielectric ring structure positioned between two parallel feed lines acts as a narrow bandpass filter. These devices have been designed and fabricated in the 12 to 75 GHz range over the past few years. A ring bandpass filter has been

incorporated into a V-band receiver unit previously delivered to ECOM by IITRI. A tunable bandpass filter is also incorporated into a data bus system delivered by IITRI to the Air Force Flight Dynamics Laboratory.

c. Ring Band Rejection Filters

A resonant dielectric ring placed next to a section of dielectric image line can be used as a band reject filter. Instead of passing energy from one line to the other as described previously for the bandpass filter, the ring is used to suck out and absorb a given frequency band.

d. Isolators

Ferrite isolators have been developed which integrate into the MILIC dielectric waveguide. The device developed has been called a fringe field isolator because it uses the transverse fields extending out of the dielectric region for its operation. An experimental Ku-band device was constructed with the following characteristics:

Center Frequency	14.5 GHz
Isolation	11 to 18 db
Insertion Loss	1.1 to 1.9 db
Bandwidth	5% between 10 db points isolation

A V-band isolator was also developed with the following performance:

Center Frequency	61.25 GHz
Isolation	10 db
Insertion Loss	1 db
Bandwidth	250 MHz between 8 db points

e. Dielectric Antennas

Dielectric rod antennas are ideally suited for use with the MILIC technology as either a primary antenna or a feed antenna. This is because the dielectric waveguide used as the transmission medium in the receiver or transmitter circuitry can be formed directly into an antenna structure.

IITRI has performed an extensive analysis and experimental evaluation of dielectric antenna structures compatible with the MILIC technology. Antenna gains have been obtained on the order of 15 db. This work was done both at Ku- and V-bands.

f. Launchers into Image Waveguide from Metal Waveguide

In order that compatibility be established between the image waveguide technology and current waveguide, it is necessary that highly efficient transitions of launchers be developed to couple field energy from one type of waveguide to the other. Several launchers over the frequency band 15 to 60 GHz have been built and tested at IITRI.

6. Active Devices

An important aspect of any MIC technology is incorporation of active devices. The requirements for mounting active devices in MILIC are virtually the same as for microstrip integrated circuits. Therefore, much of the commercial development of devices and packages for current MICs will carry over to MILIC. Recent years have witnessed dramatic progress in the state-of-the-art of such devices through K-band and above. Point contact diodes and, more recently, Schottky-barrier diodes are available commercially for use in excess of 60 GHz in mixer and detector applications. Varactors have been produced for use in multipliers to 60 GHz. Avalanche oscillators have been built with useful power levels up to 110 GHz. Gunn and IMPATT oscillators offer the possibility of high power millimeter operation.

The two considerations which predominate in consideration of active devices are physical compatibility and electrical impedance matching over some desired operating bandwidth. The sections below will consider various types of active devices for MILIC system applications beginning with a discussion of packages.

a. Device Packages

The semiconductor devices required for the lower millimeter frequencies (60 GHz and below) are commercially available in pill-type packages. Above this frequency range, packageless chip-type devices are available and would be more suitable. Avalanche diodes and others requiring rapid heat dissipation are typically the threaded stud type. The Gunn diode package can be used at 60 GHz because package parasitics are less detrimental to device operation.

b. Oscillator/Mixers

Oscillator mounts which integrate with the dielectric waveguide circuitry have been incorporated in many previous IITRI systems. These units have been used for transmitter

and local oscillator applications. The oscillator mounts have previously been of the split block metal waveguide type which contain a mode transition to the dielectric guide. Recently, an oscillator mount has been developed at IITRI where the diode is mounted directly into the dielectric waveguide.

7. Summary of MILIC Technology

Based on the above discussion, the significant aspects of the MILIC technology can be summarized as follows:

- MILIC is a truly planar hybrid integrated circuit technique with potential advantages in low cost and reliability.
- Insular circuit losses can be lower than in air-filled metal waveguide and image guide circuit losses are lower than any form of integrated circuit transmission line.
- Cross sectional dimensions are convenient without extreme dimensional tolerances at millimeter frequencies using alumina waveguides.
- Good isolation between guides can be achieved even though this is an open waveguide.
- Bandwidth is comparable to conventional metal waveguide bands.

The necessary technical know-how and experience for MILIC components/devices/systems at Ku-, Ka- and V-bands is available at IITRI. This technology was extensively used to design, fabricate, and test the Ku-band data bus system.

REFERENCES

1. Toullos, P. P., "Image Line Millimeter Integrated Circuits Directional Coupler Design," Proc. of the National Electronics Conference, Chicago, Illinois, December 1970.
2. Toullos, P. P., and R. M. Knox, "Image Line Integrated Circuits for System Applications at Millimeter Wavelengths," Final Report, Contract DAAB07-73-C-0217, U.S. Army Electronics Command Report ECOM-73-0217-F, July 1974.
3. Knox, R. M., and J. E. Kietzer, "Dielectric Waveguide Control System Data Bus System," Final Report, Contract F33615-73-C-0263, Air Force Flight Dynamics Laboratory, Wright-Patterson AFB, Ohio, January 1974.
4. Coale, F. S., "A Traveling-Wave Directional Filter," IRE Transactions on Microwave Theory and Techniques, Vol. MTT-4, October 1956, pp. 256-260.